ASSESSING WATER STRESS AND AFLATOXIN CONTAMINATION IN PEANUTS USING UAS-BASED CANOPY TEMPERATURE

by

SANDESH SHRESTHA

(Under the Direction of Lorena Nunes Lacerda)

ABSTRACT

In-season crop water stress monitoring is vital in peanuts (Arachis hypogaea L.) to optimize irrigation and reduce pre-harvest aflatoxin contamination risk. This study evaluated UAS-based thermal imagery for detecting spatial and temporal variability in water stress and its relation to pre-harvest aflatoxin risk. In 2025, empirical wet and dry baselines for the Crop Water Stress Index (CWSI) were developed across irrigation treatments in two experimental fields using UAS thermal data and ground physiological measurements. Stressed plants reached canopy temperatures up to 9°C above air temperature, while well-watered canopies were as low as 4°C below the air temperature. A second study across five commercial fields (2023–2024) showed positive correlations between thermal indices (ΔT, CWSI) and aflatoxin contamination levels, particularly under prolonged late-season stress, although overall aflatoxin levels for all fields in both years were below 4 ppb, considered low risk. Overall, UAS thermal sensing is validated as an effective technology for precise water-stress monitoring and shows great potential for pre-harvest aflatoxin contamination risk assessment in peanut fields.

INDEX WORDS: thermal imagery, crop water stress index, aflatoxin, peanuts, UAS

ASSESSING WATER STRESS AND AFLATOXIN CONTAMINATION IN PEANUTS USING UAV-BASED CANOPY TEMPERATURE

by

SANDESH SHRESTHA

BS, Agriculture and Forestry University, Nepal, 2021

A Thesis Submitted to the Graduate Faculty of The University of Georgia in Partial Fulfillment of the Requirements for the Degree

MASTER OF SCIENCE

ATHENS, GEORGIA

2025

ASSESSING WATER STRESS AND AFLATOXIN CONTAMINATION IN PEANUTS USING UAV-BASED CANOPY TEMPERATURE

by

SANDESH SHRESTHA

Major Professor: Lorena Nunes Lacerda

Committee: Wesley Porter
Cristiane Pilon

Electronic Version Approved:

Ron Walcott
Vice Provost for Graduate Education and Dean of the Graduate School
The University of Georgia
December 2025

ACKNOWLEDGEMENTS

I would like to express my gratitude to all who have supported and guided me throughout the journey of completing this thesis. This achievement would not have been possible without the invaluable contributions and unwavering support of individuals and organizations. I extend my deepest appreciation to my advisor, Dr. Lorena Lacerda. Your expertise, dedication, and relentless commitment to pushing me have been instrumental in shaping me and facilitating the completion of this project. Thank you for being an exceptional mentor and a constant source of encouragement. I am thankful to my committee members. Dr. Wesley Porter and Dr. Cristiane Pilon. Your insightful guidance and invaluable critiques have contributed significantly to my growth and the quality of this research.

I also want to thank my friends and colleagues at the University of Georgia for their team support and encouragement. My sincere gratitude also goes to all the staff and members of Stripling Irrigation Research Park (SIRP) and all the collaborating growers. Your support and technical assistance, and collaboration on this research were vital to its success. This research would not have been possible without the generous financial support from our funding agencies. I would like to acknowledge and thank the Peanut National Board, the US Peanut Federation, the Institute for Integrative Precision Agriculture (IIPA), and the USDA, Agricultural Research Service (ARS). Finally, to my parents and my sister, thank you for your boundless support from a distance. Your faith in me has been a constant driving force, and thank you from the bottom of my heart.

TABLE OF CONTENTS

Page

LIST OF TABLES

Page

LIST OF FIGURES

Page

CHAPTER 1

INTRODUCTION AND LITERATURE REVIEW

1.1. Introduction

Peanuts are a major global leguminous industrial and food crop native to tropical South America, highly valued for their significant oil (around 50%) and protein (25 %) content (Asibuo et al., 2008; Mingrou et al., 2022). It is used in a variety of food products, including peanut butter, peanut oil, and animal feed, and is a valuable crop for both farmers and consumers, providing a source of protein, fiber, and healthy fats (Arya et al., 2016). The United States (U.S) is the fourth largest peanut producing country behind China, India, and Nigeria, and is responsible for producing 6 percent of the total world peanut production (USDA, 2025). According to the latest USDA report, the U.S. peanut production in 2023 was estimated at approximately 3.367 million tons. Georgia accounts for around 54% of all the U.S. peanut production. The stability of this crucial crop, however, is increasingly threatened by water scarcity and droughts, particularly in arid and semi-arid regions (Wei et al., 2022a; Zhang et al., 2021). Effective water management is critical for ensuring both the quantity and quality of the peanut crops, as their growth and development are sensitive to climatic factors like temperature, precipitation, and sunlight (Sezen et al., 2022). Timely and accurate monitoring of crop water status is fundamental for implementing efficient irrigation practices and advancing water savings in agriculture.

Peanuts are sensitive to growth and development conditions, and their yield and quality are determined by climatic resources such as temperature, precipitation, and sunlight. Its production can be challenging, particularly in the face of water stress (Wei et al., 2022b). Water stress is a condition that occurs when water availability to the plants is not enough to meet their demands.

This can be caused by drought, salinity, or other factors. Water stress can reduce peanut yield and quality, and it can also make the plants more susceptible to pests and diseases (Puppala et al., 2023a). Peanuts are particularly sensitive to water stress during the flowering and pod-filling stages (Zeng et al., 2020). Irregular rainfall or extended drought periods can significantly affect yield. The evaluation and development of specific irrigation recommendations based on the crop's needs at these different growth stages can significantly improve peanut irrigation management and not only increase yield but also reduce the risk of aflatoxin contamination.

Aflatoxin is a group of mycotoxins produced by the fungus *Aspergillus flavous* and *A. parasiticus* (Payne & Brown, 1998) that can adversely affect crop performance and human health. Aflatoxin contamination poses a significant threat to peanut crops, making it a priority concern in peanut production. Aflatoxin is found to cause acute liver disease in humans and to be carcinogenic and teratogenic. It impairs protein formation, causes coagulation, weight gain, and reduces immunity in animals (Robens & Richard, 1992). The serious health concern imposed on humans and animals demands the detection and mitigation of aflatoxin contamination. One of the key factors influencing the development of aflatoxin in peanut pods is water status. When peanuts experience water stress, their susceptibility to aflatoxin contamination increases significantly (Hill et al., 1983). An adequate irrigation regime may be a mitigating factor for the increased risk of contamination.

Irrigation scheduling methods based on farmers' evaluations are very common but are subjective. Some examples include decision-making based on the visual inspection of crop condition or using a "feel of soil" to determine soil moisture level, and irrigation based on predetermined irrigation calendars, in which irrigation is applied at a set frequency. These methods

are not efficient approaches and have been found to significantly decrease yield (Chastain et al., 2016).

Traditional methods for monitoring crop water stress, including visual field and crop observations, the use of tensiometers, soil sampling, and leaf porometers, are characterized by their labor-intensive procedures (Ihuoma & Madramootoo, 2017). Moreover, some of these methods may offer delayed indications, allowing for the possibility of significant damage to crops occurring before visible signs of water stress manifest. In addition, crops have different water requirements at different stages of growth, and both below and above the optimum level of requirement may have a negative effect on the crop.

Recent advancements in sensing technologies have opened up new avenues for crop monitoring, particularly in areas such as water stress detection through the use of remote sensors that enable the collection of extensive information on crops through the analysis of radiation reflected in the form of image data (Ahmad et al., 2021). Notably, the emergence of unmanned aerial systems (UAS) technology is playing a transformative role in capturing this data in more robust and affordable ways. The utilization of UAS equipped with remote sensors allows for the acquisition of real-time information at higher spatial and temporal resolutions.

UAS-based thermal sensors can be used efficiently to monitor leaf/canopy temperature of crops, which serves as a water status indicator. Crop canopy temperature is a reliable indicator of water status because it is closely linked to transpiration rates. Water stress prompts stomatal closure, diminishing transpiration and resulting in elevated leaf and overall crop canopy temperatures (Jackson et al., 1981). The direct correlation between crop water status and canopy temperature allows for crop water monitoring and the potential of aflatoxin contamination assessment, overcoming the traditional labor-intensive, time-consuming, and destructive methods.

Hence, the main goal of this proposal is to use a UAS-based thermal camera to map crop water stress field variability, aiding in potential improvements in irrigation management, and to perform aflatoxin risk assessment in peanuts.

1.2. Literature Review

1.2.1. Peanut Production Overview

Peanut is a perennial, herbaceous plant with indeterminate growth that is cultivated as an annual crop (Stalker et al., 2016). In indeterminate plants, vegetative growth does not stop when the plant starts to produce flowers and fruits. This characteristic can be an advantage to the crop since it helps the plant to be more resilient to different stresses. Peanut production is concentrated in the semi-arid tropic regions under rainfed conditions (Rachaputi et al., 2020) and has an average growth cycle of 4 to 5 months. In these regions, drought during the crop cycle is common and can be a great constraint to peanut yield. Other factors such as row spacing, variety, soil moisture, temperature, and planting date can affect the growth rate of peanuts, especially if the crop is exposed to cooler air and soil temperatures during initial growth (Tubbs & Monfort, 2022).

In 2023, the overall world production was 50.46 million tons, with the five biggest producing countries being China, India, Nigeria, US, and Sudan (USDA, 2025). The U.S. contributed 6% of the world's total peanut production. In the U.S., peanut production is mostly concentrated in the south and southeast regions of the country due to the warmer climate (USDA, 2025. Georgia, Texas, Alabama, and Florida were the four biggest producers in 2025, with Georgia being responsible for more than half of the country's production.

1.2.2. Production in Georgia

Peanuts represent a $2 billion industry in the state of Georgia (GPC, 2025). The warm, humid, and sub-tropical regions of Georgia make the state the hub of peanut production, accounting for 54% of the total peanut production of the U.S. in 2024. In the same year, Georgia harvested approximately 342,035 hectares with a productivity of 4.69 tons per hectare. Four types of peanuts are grown as market types in the U.S.: Virginia, Runner, Spanish, and Valencia. In Georgia, the runner type is primarily grown for its uniform kernel size, allowing even roasting for making peanut butter (Monfort & Branch, 2022). Georgia-06G, Georgia-07W, Georgia-09B, Georgia 18RU, Georgia 12Y, Georgia-13M, and Georgia-14N are major runner-type peanuts grown in the state.

The state of Georgia usually receives regular precipitation at an annual average of about 1270 mm. Despite the regular precipitation, drought periods are not uncommon due to poor water-holding capacity and high temperatures during the summer (NIDIS, 2023). The record-breaking drought of 2006-2008 and 2010-2012, as well as the shorter drought in 2016 and 2019 impact on agriculture cannot be overlooked in peanut production.

Peanut yield can be limited by multiple abiotic stresses, such as extreme temperatures and drought, as well as by biotic stresses such as pests and diseases (Prasad et al., 2009). Among these stresses, drought is the most significant in causing a reduction of transpiration and photosynthesis, which reduces biomass accumulation and yield (Tardieu & Tuberosa, 2010). In addition, peanuts under drought stress are vulnerable to aflatoxin contamination due to infection caused by the fungus *Aspergillus* (Hamidou et al., 2014).

1.2.3. Water Requirements

Peanuts are relatively drought-tolerant, but there are critical stages of growth at which water deficit can limit the yield and quality of the crop (Wright et al., 2020). Based on research in the southeastern U.S., a peanut crop requires an average of 457 mm of water to achieve a satisfactory yield (Porter, 2022). Peanut water requirements change in different growth stages (Figure 1.1) and therefore have different responses to water deficit conditions at each one of these growth stages. The peanut growth cycle comprises three distinct stages: pre-bloom/bloom, flowering/pod set, and pod formation/maturity. At the initial stages during pre-bloom, peanuts require low amounts of water, while at pegging/pod set, water requirement is high. Peanut water requirements are at their highest around 10 weeks after planting, when the crop is in its reproductive stage. Water deficits during the early growth stage primarily impact vegetative growth and reduce the growth rate, while water stress during flowering can delay or completely inhibit flower formation (Rao et al., 1988). Inadequate soil moisture after flowering results in one-sided pods and lower calcium content in the seeds.

Sarma and Sivakumar (1989) studied the response of peanuts to water stress at different growth stages and found that peanuts showed high tolerance to drought at early stages of development and that they become more water sensitive during the flowering stage, impacting the seed yield and quality. Similarly, Jain et al. (1997) found that the limiting effect of water stress on yield is more prominent when peanuts are exposed to drought during the flowering and pod formation stages, when compared to the vegetative stage. According to Porter et al. (2021), the peak water requirements for peanuts occur around week 10 when the crop requires approximately 40 mm of water/week. Wright et al. (1991) found that treatments that were exposed to water deficit

during flowering and pod growth stages had a reduction of 17 to 25% in peanut yield compared to well-watered plants.

1.2.4. Peanut Physiological Responses to Water Stress

Water deficit poses a significant challenge to peanut production, adversely impacting many aspects of the physiology of plants, especially photosynthetic function (Osakabe et al., 2014). Excessive water above the crop water requirements and waterlogging conditions are also detrimental to the growth and final yield of peanuts, and the intensity of the effect increases with the increase in waterlogging period (Zeng et al., 2020). Potential Waterlogging conditions in the field can cause an anaerobic condition in the root zone, which deprives the roots of oxygen and may disturb necessary plant physiological processes essential for plant growth (Pan et al., 2021).

Photosynthesis

The assimilation of CO_2 in the presence of water and sunlight, a process known as photosynthesis, plays a major role in determining crop yield. Under water stress conditions, the photosynthetic process can be disrupted through multiple processes. One of the first drought stress defense mechanisms in plants is stomatal closure, which restricts CO_2 influx to conserve water (Carmo-Silva et al., 2012;; Pou et al., 2008). Pilon et al., (2018) reported significantly reduced photosynthesis and gas exchange due to stomatal closure in response to water stress conditions, directly affecting the electron transport chain. Disruptions in the photosynthetic process directly affect the products and by-products of photosynthesis. Glucose, the main photosynthetic product, can be severely reduced by the disruption of the carboxylation reaction in the Calvin cycle due to reduced CO_2 diffusion into the leaf. In addition, water deficit destabilizes the Ribulose 1,5-biphosphate carboxylase/oxygenase (Rubisco), which is a key enzyme in the metabolic apparatus (Wang et al., 2022).

Excess water will also have an impact on physiological processes in the plant. Waterlogging conditions restrict the peanut production by limiting the CO^2 assimilation rate and reducing the photosynthetic efficiency of leaves (Zeng et al., 2020). Sharma et al. (2022) studied the effect of waterlogging conditions on peanuts and found that waterlogging reduced the number of leaves, total leaf area, and plant dry matter. They also found that chlorophyll content decreased significantly due to waterlogging and observed complete wilting. Plants that were exposed to extended waterlogging conditions of 100 days all senesced.

Excess moisture during the growing season has also been shown to predispose crops to fungal diseases (Choppakatla et al., 2008). A higher incidence of pod rot associated with *Pythium spp.,* or *Pythium spp.,* and *Rhizoctonia spp.* was observed in wetter areas of irrigated fields. Moreover, peanut yield and quality are both limited by water deficit and waterlogging conditions, impacting various physiological processes such as photosynthesis, stomatal conductance, leaf development, chlorophyll content, and overall plant health (Neto et al., 2010; Pilon et al., 2018; Sharma et al., 2022).

Stomatal Conductance and Leaf Transpiration

Stomata, pores found in the epidermis of leaves, play a crucial role in facilitating the exchange of gases and water vapor between plants and the atmosphere, regulating the uptake of carbon dioxide (CO^2) for photosynthesis and the loss of water (H_2O) through transpiration (Zeiger, 1983). This balance between water loss and CO^2 uptake is essential for plant survival, particularly in hot and dry environments. Stomatal conductance, which refers to the opening and closing of stomatal pores, allows plants to adjust CO^2 uptake and water loss according to environmental conditions and the plant's physiological state. The pores are bordered by a pair of specialized cells called guard cells, responsible for the opening and closing of stomata.

Factors such as CO^2 concentration, leaf-to-air vapor pressure deficit (VPD), and plant water status influence stomatal conductance, ultimately optimizing water use efficiency (Haworth et al., 2018; Merilo et al., 2014; Ou et al., 2014). Under water stress, plants undergo physiological adjustments to cope with reduced water availability, and stomatal conductance serves as a key mechanism in this response (Wu et al., 2022). Water stress triggers a series of signaling pathways within the plant, leading to changes in stomatal aperture and conductance. One of the primary signals involved in this response is abscisic acid (ABA), a hormone that accumulates in response to reduced soil moisture (Hu et al., 2016; Munemasa et al., 2015; Saradadevi et al., 2017). Elevated levels of ABA prompt the closure of stomata, reducing water loss through transpiration. Additionally, efflux of potassium ions from guard cells decreases leaf turgor pressure, contributing to stomatal closure (Brodribb & Holbrook, 2003).

The impact of reduced stomatal conductance under water stress extends beyond water conservation, it also influences leaf and canopy temperature (Buckley, 2019). With fewer stomata open, transpiration cooling is reduced, leading to higher leaf temperatures. Due to the canopy temperature response to water stress, canopy temperature can be used as an indicator of water status and stress in plants.

1.2.5. Irrigation Management

About 90% of the human freshwater consumption is dedicated to irrigated agriculture, providing approximately 40% of the global food production (Rosa, 2022). Efficient irrigation management is crucial in agricultural production systems and even more when addressing changes posed by the changing climate and water scarcity. Irrigation management is a practice that consists of the application of the right amount of water at the right time of crop growth to maximize crop productivity (Lascano & Sojka, 2015). The first and most common irrigation approach was based

on the plant's visible wilting as an indicator of irrigation need, however, by the time wilting is apparent, significant potential yield is already reduced (Jones, 2004). Different irrigation scheduling methods have been used since an early age, but they have shortcomings that need to be addressed over time. Other approaches used are based on soil water measurement methods such as gravitational methods, tensiometers, electrical resistance blocks, and neutron probe, which offer valuable insights into soil water status and irrigation needs. Nonetheless, challenges such as soil heterogeneity and determining representative soil depth can affect the reliability of these measurements for irrigation scheduling (García-Tejera et al., 2021).

The soil water balance calculation is the prevalent irrigation scheduling approach, and relies on accurate estimations of evaporation, rainfall, and evapotranspiration, making it less precise than direct measurements (Andales et al., 2011). Emerging methods using plant response sensing provide a promising avenue for precision irrigation management (Alvino & Marino, 2017; Fernández, 2014; García-Tejero & Durán-Zuazo, 2022). Monitoring plant stress indicators, like stomatal conductance and leaf temperature, can offer timely insights for irrigation scheduling, surpassing visible wilting cues and direct soil water measurements (Katsoulas et al., 2016; Parkash & Singh, 2020).

1.2.6. Soil Moisture and Soil Moisture Sensor

Soil moisture and soil water potential are crucial indicators of soil health and water availability (Bianchi et al., 2017). Soil moisture content is an indicator of the water present in the soil, usually expressed as a percentage of the soil's weight or volume. Soil water potential, on the other hand, refers to the energy status of water in the soil and its ability to move within and between soil particles (Bittelli, 2010), determining the water availability to plants. The soil texture (sandy, loamy, and/or clay) significantly impacts moisture retention and distribution in a soil(Wang et al.,

2021). Sandy soils have a low water retention capacity and tend to dry quickly when compared to clay soils, which retain more water but present an increased risk of waterlogging. Understanding soil texture is crucial for effective irrigation, maintaining optimal moisture for healthy plant growth, and maximizing agricultural productivity.

The evolution of soil moisture sensors in the US has been marked by advancements in technology and a growing emphasis on precision agriculture (Yu et al., 2021). Early soil moisture sensing techniques were effective, but labor-intensive and time-consuming (Kashyap & Kumar, 2021). New developments of electronic soil moisture sensors have revolutionized soil moisture measurements and monitoring (Nieberding et al., 2023; Rasheed et al., 2022). Some examples include capacitance, time domain reflectometry (TDR), and frequency domain reflectometry (FDR) sensors. Capacitance sensors detect changes in electrical capacitance in the soil, providing real-time data on moisture levels (Domínguez-Niño et al., 2020; Li et al., 2022). TDR sensors analyze the travel time of electronic pulses in the soil back to the sensor to measure soil moisture content (Noborio, 2001). FDR sensors operate similarly but determine moisture levels by emitting electromagnetic waves at different frequencies and analyzing dielectric properties (Ojo et al., 2015).

1.2.7. Canopy Temperature

Canopy temperature represents the thermal behavior of a plant canopy (Still et al., 2021). It serves as a proxy for understanding various physiological processes within plants, especially in response to environmental stressors like water scarcity. Canopy temperature represents the average temperature of the entire canopy, considering the combined effect of leaf temperature, air temperature, and canopy architecture. Various methods have been developed to measure canopy temperature. Traditional techniques involve handheld infrared thermometers (Jackson et al., 1977)

or thermocouples (Ehrler, 1973) placed at different canopy heights. Most recently, advancements in remote sensing technologies have revolutionized canopy temperature measurement. Infrared thermography from UAVs allows for large-scale, non-destructive monitoring of canopy temperature and the spatial and temporal variations in canopy temperature with high resolution (Das et al., 2021).

Canopy temperature serves as a valuable indicator of plant water status, particularly under water-limited conditions (González-Dugo et al., 2006; Jackson et al., 1981). When plants experience water stress, higher canopy temperatures are observed due to reduced transpiration and impaired cooling mechanisms. Consequently, monitoring changes in canopy temperature can help with early detection of water stress, allowing for timely irrigation management (Bockhold et al., 2011).

Numerous studies have demonstrated the use of canopy temperature in assessing crop water stress across different agricultural systems. Van Zyl (2017) used canopy temperature to study the effect of different drying cycles on vines, and a strong linear correlation was observed between soil water content and canopy temperature in stressed plants. Canopy temperature of stressed vines was 1.16 to 1.62˚C higher than non-stressed vines. DeJonge et al., (2015) investigated canopy-based stress indices in sunflower under different levels of regulated deficit and revealed that canopy temperature reflects water stress, particularly when water is limited, and it responds to both the amount and timing of irrigation. Moreover, remote sensing-based approaches have been increasingly adopted for large-scale assessment of crop water stress using canopy temperature data. Recent work by Lacerda et al., (2022) utilized UAV-based thermal imagery to evaluate the water status of cotton. The results showed the potential of UAV-based thermal systems to monitor crop water status availability and to improve irrigation management decisions.

1.2.8. Remote Sensing

Remote sensing, as defined by Jensen (1996), involves acquiring and interpreting information from a distance using sensors without direct contact with the object of interest. It offers non-destructive methods for data collection, covering large geographical areas and inaccessible locations. Various satellite data types differ in techniques (active/passive, radiometer/scatterometer), spatial resolution (submeter to kilometer), spectral range, and viewing geometry. Remote sensing aids in various agricultural applications, including global crop mapping, localized monitoring, irrigation, disease detection, nutrient management, and yield prediction (Sishodia et al., 2020). It detects plant responses to environmental and water stress, enabling timely interventions to prevent crop damage.

Hyperspectral remote sensing offers detailed spectral information for discerning stress indicators, while multispectral and thermal remote sensing identify water stress signs such as reduced chlorophyll content and elevated temperatures (Marshall et al., 2016). LiDAR technology assists in canopy structure and biomass assessment related to water stress (Cao et al., 2019). Integration of these technologies optimizes irrigation strategies, enhances water resource management, and improves crop productivity and sustainability in agriculture.

Precision agriculture (PA) relies on remote sensing systems, categorized by sensor platform and type, to gather crucial data for site-specific management (Shafi et al., 2019). These systems include satellites, aerial platforms like aircraft and UAVs, and ground-based platforms, each offering distinct advantages. Passive and active sensors, including thermal infrared and microwave sensors, play key roles in assessing crop health, water stress, and soil moisture (Karmakar et al., 2023). The use of thermal sensors in agriculture is increasing. Thermal infrared sensors estimate the temperature of objects by measuring energy emitted. In crop sciences, this measurement can

be translated into estimation of crop water stress, evapotranspiration, and irrigation requirements (Zhou et al., 2021).

1.2.9. Thermal Imaging

Thermal imaging, also known as thermography, is a technique used to visualize and capture the infrared radiation emitted by objects (Usamentiaga et al., 2014). Thermal images can detect infrared radiation emitted by objects that have a temperature above absolute zero (-273.15 ºC or 0 Kelvin) and convert it into a visual image representing temperature variations. Several studies indicate that the thermal infrared part of the spectrum is more effective at identifying water stress compared to the visible, near infrared, or shortwave infrared wavelengths (Kim & Glenn, 2017; Möller et al., 2007; Zhou et al., 2021). This is due to the direct correlation between canopy temperature and plant water status. When plants experience water stress, their stomata close, reducing transpiration and causing the plant to heat up, consequently elevating canopy temperature. Water-stressed plants exhibit higher canopy temperature due to increased transpiration rates and reduced evaporative cooling. Several studies have explored the utility of thermal imaging in assessing crop canopy temperature and identifying water stress. Khorsandiet al. (2018) demonstrated the effectiveness of thermal imaging in monitoring crop water stress by comparing canopy temperature measurements with other physiological indicators. Their study highlighted the potential of thermal imaging as a non-destructive and rapid method for assessing water stress levels in crops. Similarly, in a study by Caruso et al. (2022), thermal imaging was employed to assess water status in olive orchards. The researchers observed significant differences in remotely sensed crop water stress between well-watered and water-stressed trees, demonstrating the effectiveness of thermal imaging in detecting water stress-induced temperature variations.

1.2.10. Crop Water Stress Index (CWSI)

Irrigation management is vital for enhancing water use efficiency and crop productivity, particularly in regions with limited water resources (Adeyemi et al., 2017). Precision irrigation systems play a crucial role in this context by enabling the precise application of water tailored to crop requirements, considering factors such as soil moisture, weather conditions, and crop growth stages(Liang et al., 2021) . Detecting crop water stress across different growing seasons is essential for predicting yield conditions and planning irrigation schedules. Various methods for detecting crop water stress exist, including soil water measurements, plant responses, and remote sensing techniques (Adeyemi et al., 2017).

In a study published in 1981 Idso et al. developed the Crop Water Stress Index (CWSI) based on canopy temperature and meteorological conditions.

$$CWSI = \frac{Tcanopy - Twet}{Tdry - Twet}$$

T_{canopy} is the canopy temperature, which can be captured using a UAV-based thermal infrared (TIR) system, T_{wet} and T_{dry} are the baseline temperatures representing a fully transpiring and a non-transpiring leaf, respectively. Various wet and dry baseline forms have been proposed and used for CWSI calculations. Cohen et al., (2017) have summarized the different methods that can be applied in the calculation of baseline temperature. In empirical methods, the baseline temperature can be derived by adding or subtracting a threshold value from the air temperature based on the data observation of canopy temperature. In the theoretical method, the energy balance equation is used, which involves accounting for the balance between incoming solar radiation and outgoing longwave radiation, as these are the primary drivers of temperature changes. Moreover, the temperature of the actual wet (non-stressed) and dry canopy surface (stressed) of crops can be used

to establish the baseline limit. Similarly, fabrics (cotton, polyester) have similar evaporative properties of the crops can be used as an artificial surface using the temperature of wet fabrics (T_{wet}) and dry fabrics (T_{dry}). Another approach to determining the wet baseline temperature is statistically, taking into account the coolest 5-10% of the canopy pixels as the temperature for the wet baseline.

1.2.11. Aflatoxin Contamination

Aflatoxin, produced primarily by the fungi *Aspergillus flavus* and *Aspergillus parasiticus*, represents a significant threat to food safety and public health worldwide (Shabeer et al., 2022; Speijers, 2003; Wilson et al., 2002). These mycotoxins are highly carcinogenic and can contaminate a variety of agricultural commodities, posing serious risks to human and animal health. Aflatoxin contamination severely impacts global agriculture economically. In developing nations, ensuring food safety is challenging, leading to widespread consumption of contaminated food due to food scarcity. The U.S. FDA sets a maximum limit of 20 ppb (parts per billion) for aflatoxin in food or feed, while the European Union mandates lower levels of 2 ppb for aflatoxin B1 and 4 ppb for total aflatoxins (Goldman & Osmani, 2007). Goods containing excessive aflatoxin levels are often discarded to comply with these limits.

Primary inoculum of *A. flavus* and *A. parasiticus* present as conidia or sclerotia in soil (Horn, 2017). Sclerotia survive harsh conditions, multiplying during hot and dry weather, germinating into mycelium, forming conidiophores and conidia. Aspergillus infects peanuts before and after harvest, with pre-harvest infections, particularly in semi-arid areas during last 20-40 days of drought, leading to significant aflatoxin contamination (Craufurd et al., 2006). According to Gnonlonfin et al., (2013), a complex interplay among these factors contributes significantly to the invasion of peanut seeds and subsequent aflatoxin production by these fungi. Specifically, the

combination of high soil temperatures and late-season drought stress plays a crucial role in promoting both pre-harvest infection and aflatoxin contamination in peanut seeds.

Conventionally, aflatoxin measurement typically involves extraction, purification, and quantification process. Traditionally, analytical methods like Thin Layer Chromatography (TLC), High-pressure Liquid Chromatography (HPLC), and gas chromatography, along with rapid immune assays (RIA) and Serum Assay (ELISA), have been in use for surveillance of the aflatoxin level in the commodities (Rahmani et al., 2009). Thermal imagery, a non-destructive technique utilizing thermal sensors, shows promise for potential early prediction of aflatoxin contamination risk in the field by measuring plant canopy temperature distribution (Chaitra & Suresh, 2016).

1.2.12. Water Stress and Aflatoxin

Various environmental factors, including nutrition, water, temperature, and pH, influence aflatoxin biosynthesis (Yu, 2012). Among these factors, water stress can be highlighted because it can aggravate aflatoxin contamination in crops. Drought or inadequate irrigation increases plant vulnerability to aflatoxigenic fungi. Authors have documented aflatoxin outbreaks in corn due to severe hot and dry weather (Jaime-Garcia, 2007; Sanders et al., 1983). Similarly, Hamidou et al. (2014) studied the relationship between drought intensity and aflatoxin contamination and found increased concentration of aflatoxin in seeds as drought stress intensity increased. Wilson & Stansell (1983) investigated the effect of different irrigation levels on the aflatoxin contamination of peanut pods and found significantly higher aflatoxin levels in treatments where the crop was left dry from 106 to 145 days and no significant aflatoxin contamination in treatments where irrigation was applied during the last 40 days of the season. They concluded that water stress during the last 40-75 days of the season contributes to aflatoxin contamination of pods. These fungi thrive in hot, dry conditions and can produce aflatoxins as a defense mechanism. Additionally, water

stress can weaken plant defenses, making them more susceptible to fungal invasion and subsequent aflatoxin production. Therefore, proper irrigation and water management are crucial in minimizing aflatoxin contamination in crops.

1.3 References

Adeyemi, O., Grove, I., Peets, S., & Norton, T. (2017). Advanced monitoring and management systems for improving sustainability in precision irrigation. In *Sustainability (Switzerland)* (Vol. 9, Issue 3). https://doi.org/10.3390/su9030353

Ahmad, U., Alvino, A., & Marino, S. (2021). A Review of Crop Water Stress Assessment Using Remote Sensing. *Remote Sensing*, *13*(20), 4155. https://doi.org/10.3390/rs13204155

Alvino, A., & Marino, S. (2017). Remote sensing for irrigation of horticultural crops. In *Horticulturae* (Vol. 3, Issue 2). https://doi.org/10.3390/horticulturae3020040

Andales, A. A., Chávez, J. L., & Bauder, T. A. (2011). Irrigation Scheduling: The Water Balance Approach. *Colorado State University Extension*, *4*, 1–6.

Arya, S. S., Salve, A. R., & Chauhan, & S. (2016). Peanuts as functional food: a review. *Journal of Food Science and Technology*, *53*(1), 31–41. https://doi.org/10.1007/s13197-015-2007-9

Asibuo, J., Akromah, R., Safo-Kantanka, O., Adu-Dapaah, H., Ohemeng-Dapaah, S., & Agyeman, A. (2008). Chemical composition of groundnut, Arachis hypogaea (L) landraces. *African Journal of Biotechnology*, *7*(13), 2203–2208. https://www.ajol.info/index.php/ajb/article/view/58950

Bianchi, A., Masseroni, D., Thalheimer, M., de Medici, L. O., & Facchi, A. (2017). Field irrigation management through soil water potential measurements: A review. In *Italian Journal of Agrometeorology* (Vol. 22, Issue 2). https://doi.org/10.19199/2017.2.2038-5625.025

Bittelli, M. (2010). Measuring soil water potential for water management in agriculture: A review. *Sustainability*, *2*(5). https://doi.org/10.3390/su2051226

Bockhold, D. L., Thompson, A. L., Sudduth, K. A., & Henggeler, J. C. (2011). Irrigation scheduling based on crop canopy temperature for humid environments. *Transactions of the ASABE*, *54*(6).

Brodribb, T. J., & Holbrook, N. M. (2003). Stomatal closure during leaf dehydration, correlation with other leaf physiological traits. *Plant Physiology*, *132*(4). https://doi.org/10.1104/pp.103.023879

Buckley, T. N. (2019). How do stomata respond to water status? *New Phytologist*, *224*(1), 21–36. https://doi.org/10.1111/NPH.15899

Cao, L., Coops, N. C., Sun, Y., Ruan, H., Wang, G., Dai, J., & She, G. (2019). Estimating canopy structure and biomass in bamboo forests using airborne LiDAR data. *ISPRS Journal of Photogrammetry and Remote Sensing*, *148*. https://doi.org/10.1016/j.isprsjprs.2018.12.006

Carmo-Silva, A. E., Gore, M. A., Andrade-Sanchez, P., French, A. N., Hunsaker, D. J., & Salvucci, M. E. (2012). Decreased CO 2 availability and inactivation of Rubisco limit

photosynthesis in cotton plants under heat and drought stress in the field. *Environmental and Experimental Botany*, *83*. https://doi.org/10.1016/j.envexpbot.2012.04.001

Caruso, G., Palai, G., Tozzini, L., & Gucci, R. (2022). Using Visible and Thermal Images by an Unmanned Aerial Vehicle to Monitor the Plant Water Status, Canopy Growth and Yield of Olive Trees (cvs. Frantoio and Leccino) under Different Irrigation Regimes. *Agronomy*, *12*(8). https://doi.org/10.3390/agronomy12081904

Chaitra, C., & Suresh, K. V. (2016). Identification and evaluation of technology for detection of aflatoxin contaminated peanut. Communications on Applied Electronics, 4(5), 46-50.

Chastain, D. R., Snider, J. L., Collins, G. D., Perry, C. D., Whitaker, J., Byrd, S. A., Oosterhuis, D. M., & Porter, W. M. (2016). Irrigation scheduling using predawn leaf water potential improves water productivity in drip-irrigated cotton. *Crop Science*, *56*(6), 3185–3195. https://doi.org/10.2135/CROPSCI2016.01.0009

Choppakatla, V., Wheeler, T. A., Schuster, G. L., Robinson, C., & Porter, D. O. (2008). Relationship of Soil Moisture With The Incidence of Pod Rot In Peanut in West Texas1. *Peanut Science*, *35*(2), 116–122. https://doi.org/10.3146/PS07-001.1

Cohen, Y., Alchanatis, V., Saranga, Y., Rosenberg, O., Sela, E., & Bosak, A. (2017). Mapping water status based on aerial thermal imagery: comparison of methodologies for upscaling from a single leaf to commercial fields. *Precision Agriculture*, *18*(5). https://doi.org/10.1007/s11119-016-9484-3

Cotty, P. J., & Jaime-Garcia, R. (2007). Influences of climate on aflatoxin producing fungi and aflatoxin contamination. *International Journal of Food Microbiology*, *119*(1–2). https://doi.org/10.1016/j.ijfoodmicro.2007.07.060

Craufurd, P. Q., Prasad, P. V. V., Waliyar, F., & Taheri, A. (2006). Drought, pod yield, pre-harvest Aspergillus infection and aflatoxin contamination on peanut in Niger. *Field Crops Research*, *98*(1), 20–29. https://doi.org/10.1016/J.FCR.2005.12.001

Das, S., Chapman, S., Christopher, J., Choudhury, M. R., Menzies, N. W., Apan, A., & Dang, Y. P. (2021). UAV-thermal imaging: A technological breakthrough for monitoring and quantifying crop abiotic stress to help sustain productivity on sodic soils – A case review on wheat. In *Remote Sensing Applications: Society and Environment* (Vol. 23). https://doi.org/10.1016/j.rsase.2021.100583

DeJonge, K. C., Taghvaeian, S., Trout, T. J., & Comas, L. H. (2015). Comparison of canopy temperature-based water stress indices for maize. *Agricultural Water Management*, *156*. https://doi.org/10.1016/j.agwat.2015.03.023

Domínguez-Niño, J. M., Oliver-Manera, J., Girona, J., & Casadesús, J. (2020). Differential irrigation scheduling by an automated algorithm of water balance tuned by capacitance-type soil moisture sensors. *Agricultural Water Management*, *228*. https://doi.org/10.1016/j.agwat.2019.105880

Ehrler, W. L. (1973). Cotton Leaf Temperatures as Related to Soil Water Depletion and Meteorological Factors 1 . *Agronomy Journal*, *65*(3), 404–409. https://doi.org/10.2134/agronj1973.00021962006500030016x

Fernández, J. E. (2014). Plant-based sensing to monitor water stress: Applicability to commercial orchards. In *Agricultural Water Management* (Vol. 142). https://doi.org/10.1016/j.agwat.2014.04.017

García-Tejera, O., López-Bernal, Á., Orgaz, F., Testi, L., & Villalobos, F. J. (2021). The pitfalls of water potential for irrigation scheduling. *Agricultural Water Management*, *243*. https://doi.org/10.1016/j.agwat.2020.106522

García-Tejero, I. F., & Durán-Zuazo, V. H. (2022). Plant Water Use Efficiency for a Sustainable Agricultural Development. In *Agronomy* (Vol. 12, Issue 8). https://doi.org/10.3390/agronomy12081806

Georgia Peanut Commission. (2025). Annual report 2024. Georgia Peanut Commission. http://www/gapeanuts.com

Gnonlonfin, G. J. B., Hell, K., Adjovi, Y., Fandohan, P., Koudande, D. O., Mensah, G. A., Sanni, A., & Brimer, L. (2013). A Review on Aflatoxin Contamination and Its Implications in the Developing World: A Sub-Saharan African Perspective. *Critical Reviews in Food Science and Nutrition*, *53*(4), 349–365. https://doi.org/10.1080/10408398.2010.535718

Goldman, G. H., & Osmani, S. A. (2007). The aspergilli: Genomics, medical aspects, biotechnology, and research methods. In *The Aspergilli: Genomics, Medical Aspects, Biotechnology, and Research Methods*. https://doi.org/10.1201/9781420008517

González-Dugo, M. P., Moran, M. S., Mateos, L., & Bryant, R. (2006). Canopy temperature variability as an indicator of crop water stress severity. *Irrigation Science*, *24*(4). https://doi.org/10.1007/s00271-005-0022-8

Hamidou, F., Halilou, O., & Vadez, V. (2013). Assessment of Groundnut under Combined Heat and Drought Stress. *Journal of Agronomy and Crop Science*, *199*(1), 1–11. https://doi.org/10.1111/j.1439-037X.2012.00518.x

Hamidou, F., Rathore, A., Waliyar, F., & Vadez, V. (2014). Although drought intensity increases aflatoxin contamination, drought tolerance does not lead to less aflatoxin contamination. *Field Crops Research*, *156*, 103–110. https://doi.org/10.1016/j.fcr.2013.10.019

Haworth, M., Marino, G., Cosentino, S. L., Brunetti, C., De Carlo, A., Avola, G., Riggi, E., Loreto, F., & Centritto, M. (2018). Increased free abscisic acid during drought enhances stomatal sensitivity and modifies stomatal behaviour in fast growing giant reed (Arundo donax L.). *Environmental and Experimental Botany*, *147*. https://doi.org/10.1016/j.envexpbot.2017.11.002

Hill, R. A., Blankenship, P. D., Cole, R. J., & Sanders, T. H. (1983). Effects of soil moisture and temperature on preharvest invasion of peanuts by the Aspergillus flavus group and

subsequent aflatoxin development. *Applied and Environmental Microbiology*, *45*(2), 628–633. https://doi.org/10.1128/aem.45.2.628-633.1983

Horn, B. W. (2017). Colonization of wounded peanut seeds by soil fungi: selectivity for species from Aspergillus section Flavi. https://doi.org/10.1080/15572536.2006.11832854

Hu, B., Cao, J., Ge, K., & Li, L. (2016). The site of water stress governs the pattern of ABA synthesis and transport in peanut. *Scientific Reports*, *6*. https://doi.org/10.1038/srep32143

Idso, S. B., Jackson, R. D., Pinter, P. J., Reginato, R. J., & Hatfield, J. L. (1981). Normalizing the stress-degree-day parameter for environmental variability. *Agricultural Meteorology*, *24*(C). https://doi.org/10.1016/0002-1571(81)90032-7

Ihuoma, S. O., & Madramootoo, C. A. (2017). Recent advances in crop water stress detection. In *Computers and Electronics in Agriculture* (Vol. 141). https://doi.org/10.1016/j.compag.2017.07.026

Jackson, R. D., Idso, S. B., Reginato, R. J., & Pinter, P. J. (1981). Canopy temperature as a crop water stress indicator. *Water Resources Research*, *17*(4), 1133–1138. https://doi.org/10.1029/WR017i004p01133

Jackson, R. D., Reginato, R. J., & Idso, S. B. (1977). Wheat canopy temperature: A practical tool for evaluating water requirements. *Water Resources Research*, *13*(3). https://doi.org/10.1029/WR013i003p00651

Jain, L. L., Panda, R. K., & Sharma, C. P. (1997). Water stress response function for groundnut (Arachis hypogaea L.). *Agricultural Water Management*, *32*(2). https://doi.org/10.1016/S0378-3774(96)01240-1

Jensen, J. R. (1996). Introductory digital image processing: a remote sensing perspective. Second edition. In *Introductory digital image processing: a remote sensing perspective. Second edition*.

Jones, H. G. (2004). Irrigation scheduling: Advantages and pitfalls of plant-based methods. *Journal of Experimental Botany*, *55*(407). https://doi.org/10.1093/jxb/erh213

Karmakar, P., Teng, S. W., Murshed, M., Pang, S., Li, Y., & Lin, H. (2023). Crop monitoring by multimodal remote sensing: A review. https://doi.org/10.1016/j.rsase.2023.101093

Kashyap, B., & Kumar, R. (2021). Sensing Methodologies in Agriculture for Soil Moisture and Nutrient Monitoring. *IEEE Access*, *9*. https://doi.org/10.1109/ACCESS.2021.3052478

Katsoulas, N., Elvanidi, A., Ferentinos, K. P., Kacira, M., Bartzanas, T., & Kittas, C. (2016). Crop reflectance monitoring as a tool for water stress detection in greenhouses: A review. In *Biosystems Engineering* (Vol. 151). https://doi.org/10.1016/j.biosystemseng.2016.10.003

Khorsandi, A., Hemmat, A., Mireei, S. A., Amirfattahi, R., & Ehsanzadeh, P. (2018). Plant temperature-based indices using infrared thermography for detecting water status in sesame

under greenhouse conditions. *Agricultural Water Management*, *204*. https://doi.org/10.1016/j.agwat.2018.04.012

Kim, J. Y., & Glenn, D. M. (2017). Multi-modal sensor system for plant water stress assessment. *Computers and Electronics in Agriculture*, *141*, 27–34. https://doi.org/10.1016/J.COMPAG.2017.07.009

Lacerda, L. N., Snider, J. L., Cohen, Y., Liakos, V., Gobbo, S., & Vellidis, G. (2022). Using UAV-based thermal imagery to detect crop water status variability in cotton. *Smart Agricultural Technology*, *2*, 100029. https://doi.org/10.1016/J.ATECH.2021.100029

Lascano, R. J., & Sojka, R. E. (2015). Irrigation of agricultural crops: Second Edition. In *Irrigation of Agricultural Crops*. https://doi.org/10.2134/agronmonogr30.2ed

Li, B., Wang, C., Ma, M., Li, L., Feng, Z., Ding, T., Li, X., Jiang, T., Li, X., & Zheng, X. (2022). Accuracy calibration and evaluation of capacitance-based soil moisture sensors for a variety of soil properties. *Agricultural Water Management*, *273*. https://doi.org/10.1016/j.agwat.2022.107913

Liang, Z., Liu, X., Xiao, J., & Liu, C. (2021). Review of conceptual and systematic progress of precision irrigation. *International Journal of Agricultural and Biological Engineering*, *14*(4). https://doi.org/10.25165/j.ijabe.20211404.5463

Marshall, M., Thenkabail, P., Biggs, T., & Post, K. (2016). Hyperspectral narrowband and multispectral broadband indices for remote sensing of crop evapotranspiration and its components (transpiration and soil evaporation). *Agricultural and Forest Meteorology*, *218–219*. https://doi.org/10.1016/j.agrformet.2015.12.025

Merilo, E., Jõesaar, I., Brosché, M., & Kollist, H. (2014). To open or to close: Species-specific stomatal responses to simultaneously applied opposing environmental factors. *New Phytologist*, *202*(2). https://doi.org/10.1111/nph.12667

Mingrou, L., Guo, S., Ho, C. T., & Bai, N. (2022). Review on chemical compositions and biological activities of peanut (Arachis hypogeae L.). *Journal of Food Biochemistry*, *46*(7), e14119. https://doi.org/10.1111/JFBC.14119

Möller, M., Alchanatis, V., Cohen, Y., Meron, M., Tsipris, J., Naor, A., Ostrovsky, V., Sprintsin, M., & Cohen, S. (2007). Use of thermal and visible imagery for estimating crop water status of irrigated grapevine. *Journal of Experimental Botany*, *58*(4). https://doi.org/10.1093/jxb/erl115

Monfort, S., & Branch, B. (2022). Peanut Varieties. *In:Peanut Production Guide*.

Munemasa, S., Hauser, F., Park, J., Waadt, R., Brandt, B., & Schroeder, J. I. (2015). Mechanisms of abscisic acid-mediated control of stomatal aperture. In *Current Opinion in Plant Biology* (Vol. 28). https://doi.org/10.1016/j.pbi.2015.10.010

Neto, A. D. A., Nogueira, R. J. M. C., Filho, P. A. M., & Santos, R. C. (2010). Physiological and biochemical responses of peanut genotypes to water deficit. *Journal of Plant Interactions*, *5*(1). https://doi.org/10.1080/17429140902999243

Nieberding, F., Huisman, J. A., Huebner, C., Schilling, B., Weuthen, A., & Bogena, H. R. (2023). Evaluation of Three Soil Moisture Profile Sensors Using Laboratory and Field Experiments. *Sensors*, *23*(14). https://doi.org/10.3390/s23146581

NOAA's National Integrated Drought Information System. (2023). *Drought in Georgia: Precipitation, drought risk, and water-holding capacity. https://www.drought.gov/states/georgia*

Noborio, K. (2001). Measurement of soil water content and electrical conductivity by time domain reflectometry: A review. *Computers and Electronics in Agriculture*, *31*(3). https://doi.org/10.1016/S0168-1699(00)00184-8

Ojo, E. R., Bullock, P. R., L'Heureux, J., Powers, J., McNairn, H., & Pacheco, A. (2015). Calibration and Evaluation of a Frequency Domain Reflectometry Sensor for Real-Time Soil Moisture Monitoring. *Vadose Zone Journal*, *14*(3). https://doi.org/10.2136/vzj2014.08.0114

Osakabe, Y., Osakabe, K., Shinozaki, K., & Tran, L. S. P. (2014). Response of plants to water stress. In *Frontiers in Plant Science* (Vol. 5, Issue MAR). https://doi.org/10.3389/fpls.2014.00086

Ou, X., Gan, Y., Chen, P., Qiu, M., Jiang, K., & Wang, G. (2014). Stomata prioritize their responses to multiple biotic and abiotic signal inputs. *PLoS ONE*, *9*(7). https://doi.org/10.1371/journal.pone.0101587

Pan, J., Sharif, R., Xu, X., & Chen, X. (2021). Mechanisms of Waterlogging Tolerance in Plants: Research Progress and Prospects. *Frontiers in Plant Science*, *11*. https://doi.org/10.3389/fpls.2020.627331

Parkash, V., & Singh, S. (2020). A review on potential plant-basedwater stress indicators for vegetable crops. In *Sustainability (Switzerland)* (Vol. 12, Issue 10). https://doi.org/10.3390/SU12103945

Payne, G. A., & Brown, M. P. (1998). Genetics and physiology of aflatoxin. *Annual Review of Phytopathology*, *36*(1), 329–362. https://doi.org/10.1146/annurev.phyto.36.1.329

Pilon, C., Snider, J. L., Sobolev, V., Chastain, D. R., Sorensen, R. B., Meeks, C. D., Massa, A. N., Walk, T., Singh, B., & Earl, H. J. (2018). Assessing stomatal and non-stomatal limitations to carbon assimilation under progressive drought in peanut (Arachis hypogaea L.). *Journal of Plant Physiology*, *231*. https://doi.org/10.1016/j.jplph.2018.09.007

Porter, W. (2021). Irrigation Reference Guide for Corn, Cotton, Peanuts and Soyabeans. In *University of Georgia Extension*. e University of Georgia in cooperation with Fort Valley State University, the U.S. Department of Agriculture.

Porter, W. M. (2022). Water Use and Relationship in Peanut Production. In Peanut Production Guide. University of Georgia Extension.

Pou, A., Flexas, J., Alsina, M. D. M., Bota, J., Carambula, C., De Herralde, F., Galmés, J., Lovisolo, C., Jiménez, M., Ribas-Carbó, M., Rusjan, D., Secchi, F., Tomàs, M., Zsófi, Z., & Medrano, H. (2008). Adjustments of water use efficiency by stomatal regulation during drought and recovery in the drought-adapted Vitis hybrid Richter-110 (V. berlandieri x V. rupestris). *Physiologia Plantarum*, *134*(2). https://doi.org/10.1111/j.1399-3054.2008.01138.x

Prasad, P. V., Kakani, V. G., & Upadhyaya, H. D. (2010). Growth and production of groundnut. UNESCO Encyclopedia, 1-26.

Puppala, N., Nayak, S. N., Sanz-Saez, A., Chen, C., Devi, M. J., Nivedita, N., Bao, Y., He, G., Traore, S. M., Wright, D. A., Pandey, M. K., & Sharma, V. (2023a). Sustaining yield and nutritional quality of peanuts in harsh environments: Physiological and molecular basis of drought and heat stress tolerance. *Frontiers in Genetics*, *14*. https://doi.org/10.3389/fgene.2023.1121462

Rachaputi, R., Chauhan, Y. S., & Wright, G. C. (2020). Peanut. *Crop Physiology Case Histories for Major Crops*, 360–382. https://doi.org/10.1016/B978-0-12-819194-1.00011-6

Rahmani, A., Jinap, S., & Soleimany, F. (2009). Qualitative and quantitative analysis of mycotoxins. *Comprehensive Reviews in Food Science and Food Safety*, *8*(3). https://doi.org/10.1111/j.1541-4337.2009.00079.x

Rao, R. C. N., Williams, J. H., Sivakumar, M. V. K., & Wadia, K. D. R. (1988). Effect of Water Deficit at Different Growth Phases of Peanut. II. Response to Drought During Preflowering Phase. *Agronomy Journal*, *80*(3), 431–438. https://doi.org/10.2134/AGRONJ1988.00021962008000030010X

Rasheed, M. W., Tang, J., Sarwar, A., Shah, S., Saddique, N., Khan, M. U., Imran Khan, M., Nawaz, S., Shamshiri, R. R., Aziz, M., & Sultan, M. (2022). Soil Moisture Measuring Techniques and Factors Affecting the Moisture Dynamics: A Comprehensive Review. In *Sustainability (Switzerland)* (Vol. 14, Issue 18). https://doi.org/10.3390/su141811538

Robens, J.F., Richard, J.L. (1992). Aflatoxins in Animal and Human Health. In: Ware, G.W. (eds) Reviews of Environmental Contamination and Toxicology. Reviews of Environmental Contamination and Toxicology, vol 127. Springer, New York, NY. https://doi.org/10.1007/978-1-4613-9751-9_3

Rosa, L. (2022). Adapting agriculture to climate change via sustainable irrigation: Biophysical potentials and feedbacks. In *Environmental Research Letters* (Vol. 17, Issue 6). https://doi.org/10.1088/1748-9326/ac7408

Sanders, T. H., Blankenship, P. D., Cole, R. J., & Hill, R. A. (1984). Effect of soil temperature and drought on peanut pod and stem temperatures relative to Aspergillus flavus invasion and aflatoxin contamination. *Mycopathologia*, *86*(1). https://doi.org/10.1007/BF00437229

Saradadevi, R., Palta, J. A., & Siddique, K. H. M. (2017). ABA-mediated stomatal response in regulating water use during the development of terminal drought in wheat. In *Frontiers in Plant Science* (Vol. 8). https://doi.org/10.3389/fpls.2017.01251

Sarma, P. S., & Sivakumar, M. V. K. (1989). Response of groundnut to drought stress in different growth phases. *Agricultural Water Management*, *15*(3). https://doi.org/10.1016/0378-3774(89)90022-X

Sezen, S. M., Ahmad, I., Habib-ur-Rahman, M., Amiri, E., Tekin, S., Oz, K. C., & Maambo, C. M. (2022). Growth and productivity assessments of peanut under different irrigation water management practices using CSM-CROPGRO-Peanut model in Eastern Mediterranean of Turkey. *Environmental Science and Pollution Research*, *29*(18), 26936–26949. https://doi.org/10.1007/s11356-021-17722-w

Shabeer, S., Asad, S., Jamal, A., & Ali, A. (2022). Aflatoxin Contamination, Its Impact and Management Strategies: An Updated Review. In *Toxins* (Vol. 14, Issue 5). https://doi.org/10.3390/toxins14050307

Shafi, U., Mumtaz, R., García-Nieto, J., Hassan, S. A., Zaidi, S. A. R., & Iqbal, N. (2019). Precision agriculture techniques and practices: From considerations to applications. In *Sensors (Switzerland)* (Vol. 19, Issue 17). https://doi.org/10.3390/s19173796

Sharma, S., Bhatt, U., Sharma, J., Darkalt, A., Mojski, J., & Soni, V. (2022). Effect of different waterlogging periods on biochemistry, growth, and chlorophyll a fluorescence of Arachis hypogaea L. *Frontiers in Plant Science*, *13*. https://doi.org/10.3389/fpls.2022.1006258

Sishodia, R. P., Ray, R. L., & Singh, S. K. (2020). Applications of remote sensing in precision agriculture: A review. *Remote Sensing*, *12*(19), 1–31. https://doi.org/10.3390/rs12193136

Speijers, D. G. (2003). Mycotoxins and Food Safety. *Trends in Food Science & Technology*, *14*(3). https://doi.org/10.1016/s0924-2244(03)00025-6

Stalker, H. T., Tallury, S. P., Seijo, G. R., & Leal-Bertioli, S. C. (2016). Biology, Speciation, and Utilization of Peanut Species. *Peanuts: Genetics, Processing, and Utilization*, 27–66. https://doi.org/10.1016/B978-1-63067-038-2.00002-2

Still, C. J., Rastogi, B., Page, G. F. M., Griffith, D. M., Sibley, A., Schulze, M., Hawkins, L., Pau, S., Detto, M., & Helliker, B. R. (2021). Imaging canopy temperature: shedding (thermal) light on ecosystem processes. In *New Phytologist* (Vol. 230, Issue 5). https://doi.org/10.1111/nph.17321

Tardieu, F., & Tuberosa, R. (2010). Dissection and modelling of abiotic stress tolerance in plants. *Current Opinion in Plant Biology*, *13*(2), 206–212. https://doi.org/10.1016/j.pbi.2009.12.012

Tubbs, R. S., & Monfort, W. S. (2022). *Chapter 9: Planting*. In Peanut Production Guide, University of Georgia Cooperative Extension, 72-75.

Usamentiaga, R., Venegas, P., Guerediaga, J., Vega, L., Molleda, J., & Bulnes, F. G. (2014). Infrared thermography for temperature measurement and non-destructive testing. In *Sensors (Switzerland)* (Vol. 14, Issue 7). https://doi.org/10.3390/s140712305

USDA-*Peanut Explorer*. (2025). Retrieved November 16, 2025, from https://ipad.fas.usda.gov/cropexplorer/cropview/commodityView.aspx?cropid=2221000

Van Zyl, J. L. (2017). Canopy Temperature as a Water Stress Indicator in Vines. *South African Journal of Enology & Viticulture*, *7*(2). https://doi.org/10.21548/7-2-2326

Wang, D., Wang, Z., Zhang, J., Zhou, B., Lv, T., & Li, W. (2021). Effects of soil texture on soil leaching and cotton (Gossypium hirsutum l.) growth under combined irrigation and drainage. *Water (Switzerland)*, *13*(24). https://doi.org/10.3390/w13243614

Wang, X., Liu, H., Zhang, D., Zou, D., Wang, J., Zheng, H., Jia, Y., Qu, Z., Sun, B., & Zhao, H. (2022). Photosynthetic Carbon Fixation and Sucrose Metabolism Supplemented by Weighted Gene Co-expression Network Analysis in Response to Water Stress in Rice With Overlapping Growth Stages. *Frontiers in Plant Science*, *13*. https://doi.org/10.3389/fpls.2022.864605

Wei, S., Li, K., Yang, Y., Wang, C., Liu, C., & Zhang, J. (2022). Comprehensive climatic suitability evaluation of peanut in Huang-Huai-Hai region under the background of climate change. *Scientific Reports*, *12*(1), 11350. https://doi.org/10.1038/s41598-022-15465-3

Wilson, D. M., & Stansell, J. R. (1983). Effect of Irrigation Regimes on Aflatoxin Contamination of Peanut Pods1. *Peanut Science*, *10*(2), 54–56. https://doi.org/10.3146/i0095-3679-10-2-2

Wilson, D. M., Mubatanhema, W., & Jurjevic, Z. (2002). Biology and ecology of mycotoxigenic Aspergillus species as related to economic and health concerns. *Advances in Experimental Medicine and Biology*, *504*. https://doi.org/10.1007/978-1-4615-0629-4_2

Wright, D. L., Tillman, B. L., Small, I. M., Pratap, D., Grabau, Z., Paula-Moraes, S., Carter, E., Ferrell, J. A., Mulvaney, M. J., Barrett, C., & DuFault, N. (2020). *Management and cultural practices for peanuts* (Publication SS-AGR-74). University of Florida Cooperative Extension Service, Institute of Food and Agricultural Sciences (UF/IFAS). Retrieved from https://nfrec.ifas.ufl.edu/media/nfrecifasufledu/docs/pdf/Peanut-Production-Guide-2020.pdf

Wright, G. C., Hubick, K. T., & Farquhar, G. D. (1991). Physiological analysis of peanut cultivar response to timing and duration of drought stress. *Australian Journal of Agricultural Research*, *42*(3), 453–470. https://doi.org/10.1071/AR9910453

Wu, J., Wang, J., Hui, W., Zhao, F., Wang, P., Su, C., & Gong, W. (2022). Physiology of Plant Responses to Water Stress and Related Genes: A Review. In *Forests* (Vol. 13, Issue 2). https://doi.org/10.3390/f13020324

Yu, J. (2012). Current understanding on aflatoxin biosynthesis and future perspectives in reducing aflatoxin contamination. In *Toxins* (Vol. 4, Issue 11). https://doi.org/10.3390/toxins4111024

Yu, L., Gao, W., Shamshiri, R. R., Tao, S., Ren, Y., Zhang, Y., & Su, G. (2021). Review of research progress on soil moisture sensor technology. *International Journal of Agricultural and Biological Engineering*, *14*(4). https://doi.org/10.25165/j.ijabe.20211404.6404

Zeiger, E. (1983). The Biology of Stomatal Guard Cells. *Annual Review of Plant Physiology*, *34*(1). https://doi.org/10.1146/annurev.pp.34.060183.002301

Zeng, R., Chen, L., Wang, X., Cao, J., Li, X., Xu, X., Xia, Q., Chen, T., & Zhang, L. (2020). Effect of Waterlogging Stress on Dry Matter Accumulation, Photosynthesis Characteristics, Yield, and Yield Components in Three Different Ecotypes of Peanut (Arachis hypogaea L.). *Agronomy*, *10*(9), 1244. https://doi.org/10.3390/agronomy10091244

Zhang, J., Wang, Q., Xia, G., Wu, Q., & Chi, D. (2021). Continuous regulated deficit irrigation enhances peanut water use efficiency and drought resistance. *Agricultural Water Management*, *255*. https://doi.org/10.1016/j.agwat.2021.106997

Zhou, Z., Majeed, Y., Diverres Naranjo, G., & Gambacorta, E. M. T. (2021). Assessment for crop water stress with infrared thermal imagery in precision agriculture: A review and future prospects for deep learning applications. *Computers and Electronics in Agriculture*, *182*, 106019. https://doi.org/10.1016/J.COMPAG.2021.106019

CHAPTER 2

ESTABLISHING WET AND DRY BASELINES FOR CROP WATER STRESS INDEX CALCULATION IN PEANUTS USING THERMAL IMAGERY [1]

[1]Shrestha, S., Lacerda, L.N., Pilon. C., Porter, W., Snider, J., Grubbs, H., and Kumar, M. To be submitted to the *Precision Agriculture Journal*

Abstract

Timely monitoring of water stress in peanuts is critical for obtaining satisfactory yield. Meeting stage-specific peanut water requirements is crucial, as water stress can reduce yield, affect plant physiological processes, and increase susceptibility to diseases. Canopy temperature is a reliable indicator for understanding various physiological status within plants, especially in response to water deficit. This study explored the potential of using an unmanned aerial system (UAS) to develop empirical baselines for crop water stress index (CWSI) calculation and assessed its performance in monitoring in-season peanut water stress. The study was conducted over two experimental fields (Field A and Field B) at the University of Georgia (UGA) Stripling Irrigation Research Park (SIRP), Georgia, USA. Treatments were used to drive variability in stomatal conductance (g_s) and CWSI. Field A was designed using a randomized complete block design with nine irrigation treatments based on different combinations of three soil water tension (SWT) irrigation trigger levels (20, 45, and 70 kPa) for critical growth stages, and two cultivars, Georgia-06G and Georgia-18RU. Field B used a split plot design with four irrigation treatments based on crop evapotranspiration and crop coefficient (100% ETc, 75 % ETc, 50% ETc and rainfed) with three cultivars Georgia-06G, Georgia-20VHO, and Tif Jumbo replicated four times within a treatment. Ground and aerial data were collected every two weeks, when the weather was sunny and cloud-free. The UAS-based thermal imagery was segmented using a two-step segmentation, 1) creating a binary mask based on RGB images and a random forest model to remove soil background, and 2) the focal statistics tool was used to remove edge mixed pixels. Comparison between empirical dry and wet baselines developed from UAS and handheld IR sensor showed that the wet baseline from the UAS was $\Delta T = -2.1\ VPD + 3.9$ and the dry baseline was 9 °C above air temperature, while for the handheld sensor, the wet baseline was $\Delta T = -3.2\ VPD + 6.4$ and the

dry baseline was 6.5 °C. CWSI calculated using empirical, Jones, Monteith, and theoretical methods increased with irrigation deficit and showed a strong positive linear relationship with g_s, with R^2 ranging from 0.72 to 0.87 during periods of pronounced stress. UAS-derived and handheld CWSI agreed closely (R^2 0.80–0.96) when pronounced stress was present, supporting that an UAS platform can be used as a reliable and scalable tool for field-scale stress assessment. These results establish sensor-specific baselines and a validated processing workflow for thermal imagery in peanuts, enabling reliable, field-scale water-stress monitoring and supporting the development of precision irrigation strategies.

Keywords: CWSI, Thermal Imagery, UAS, Peanuts, Water Stress.

2.1. Introduction

In the United States (U.S.), peanuts are mostly grown in the southeast region, with the six major producing states being Georgia, Texas, Florida, Alabama, North Carolina, and South Carolina (NASS, 2025). The state of Georgia contributes 55% of the total U.S. production. All the peanuts produced in Georgia are concentrated in the southern part of the state, below the Columbus-Augusta line, with very sandy soils (Brenneman, et al., 2022). Due to soil and weather conditions, more than half of peanut producers in the state use irrigation to supplement water during the season.

Peanut production requires 457 mm of water distributed uniformly throughout the season for optimum yield, with the highest water requirements occurring at 10-12 weeks after planting (Porter, 2022). Meeting growth stage-specific peanut water requirements is crucial, as water stress can reduce yield, affect plant physiological processes, and increase susceptibility to diseases (Puppala et al., 2023; Wei et al., 2022). Too much water also leads to unwanted effects with excessive vegetative growth and shallow root depth at early season (Brenneman, et al., 2022), and potential of pod rotting later in the season (Zeng et al., 2020). The detrimental effects of both water deficit and excess water in peanuts reinforces the need for efficient irrigation management practices to address the crop water demands (Porter et al., 2024).

There are several irrigation scheduling methods available for Georgia peanut growers, including soil moisture sensor-based irrigation, University of Georgia (UGA) EasyPan Irrigation Scheduler, and online scheduling tools such as Irrigator Pro and PeanutFARM. Among these, the most commonly used irrigation scheduling method in the state is the UGA Checkbook Method, which is based on historical water requirement averages. Although fitting for some years, the Checkbook method fails to take into account water needs in years that are either too wet or too dry

compared to the average. Studies testing these different methods have shown that irrigation based on Watermark soil moisture sensors using 45 kPa as an irrigation threshold performed successfully across years, by applying less water and achieving high yields (Porter et al., 2024). Nonetheless, these methods still fail to account for field spatial variability.

As technology has progressed and different sensors have been developed, real-time assessment of field conditions has been easier than before. Infrared sensors have emerged as an efficient approach for continuous and large-scale monitoring of water stress based on the canopy temperature (Bo et al., 2023; Luan et al., 2021). Canopy temperature is a reliable indicator for understanding various physiological status within plants, especially in response to water deficit (Guilioni et al., 2008). Crops can regulate their leaf temperature through the process of transpiration, in which loss of water occurs through leaf stomata. However, when plants experience water stress, one of their response mechanisms is to close their stomata, leading to an increase in leaf temperature.

Canopy temperature is an absolute value and varies throughout the day and across the growing season because of its dependency on the weather and the crop growth stages. To normalize the canopy temperature, Crop Water Stress Index (CWSI) was developed considering environmental factors (Idso et al., 1981; Jackson et al., 1981). The CWSI varies from 0 to 1, with 0 indicating there is no limiting water to the plant and 1 representing a severely stressed crop. The application of CWSI for irrigation management has been extensively studied across various crops, including wheat (*Triticum aestivum L.)* (Jackson et al., 1977), maize (*Zea* mays *L.*) (DeJonge et al., 2015; Pradawet et al., 2023), and cotton (*Gossypium hirsutum L.)* (Alchanatis et al., 2010; Lacerda et al., 2022). However, limited research has focused on establishing baseline temperature values for peanut crops, which are essential for accurate CWSI calculations. A study conducted by

Porter et al. (2015) used fixed canopy temperature sensors to develop a wet baseline for peanuts and found a linear relationship between vapor pressure deficit and differential temperature (canopy temperature – air temperature).

The determination of a robust lower baseline temperature is crucial, as it influences the precision of stress detection and the transferability of the method across different climatic conditions (Adeyemi et al., 2018). The baseline temperature can be obtained in multiple ways, including empirically and theoretically. Empirical approaches rely on field measurement of crop canopy temperature under stress conditions or dryland and crops under well-irrigated conditions. However, a theoretical approach has been proposed to overcome the empirical retrieval of the baseline needed in the CWSI calculation. The use of theoretical equations of CWSI is based on the energy balance equation (Jackson et al., 1988). Han et al. (2018) compared two different theoretical baseline methods with empirical calculations and found that the empirical method was more efficient in providing accurate stress prediction between growth stages but showed higher overall uncertainty when compared to theoretical methods.

Given the potential of CWSI as a reliable in-season water stress indicator, and the lack of information for wet and dry baseline temperatures for peanuts. This study aimed to develop a methodology to establish baseline temperature values for peanuts using a UAS-based thermal sensor for the calculation of an empirical CWSI. CWSI based on empirical baselines was compared to three different CWSI methods based on empirical and theoretical baselines, and compared to the same CWSI methods derived from a high-accuracy handheld infrared sensor. This study may impact future efforts using thermal images to aid in in-season crop water stress monitoring and irrigation scheduling.

2.2. Materials and Methods

2.2.1. Study Site and Experimental Design

Two studies were conducted during 2025 during two different experimental fields at the University of Georgia's Stripling Irrigation Research Park (SIRP) in Camilla, GA located in a semi-arid temperate region (Figure 2.1). Field A (31° 16'43" N, 84°17'49" W) was planted on May 8th, 2025, in an area of approximately 1 ha. A randomized complete block design was employed with nine irrigation threshold combinations and two cultivars crossed with each irrigation strategy, with all treatments being replicated three times (9 irrigation strategies × 2 cultivars× 3 replicates) for a total of 54 plots. Each plot consisted of 4 rows, 42.08 m in length. The two cultivars used were the Georgia-06G (Branch, 2007) and Georgia-18RU (Branch, 2019). Table 2.1 summarizes the irrigation treatments applied in the field, with treatment 1 through 9 representing different irrigation regimes based on soil water tension (SWT) measured in kilopascals (kPa) at three stages: early season (0-40 days after planting, DAP), mid-season (41-110 DAP), and late season (110-DAP to harvest). The early season corresponds to germination and early vegetative growth, the mid-season covers flowering and pegging, and the late season represents the pod maturation stage. Each of the nine irrigation regimes specifies the SWT thresholds (in kPa) at which irrigation was applied, representing the level of water stress imposed during these stages. A lower kPa threshold indicates more frequent irrigation, while a higher kPa threshold represents less frequent irrigation.

Field B (31°16'44" N, 84°17'42" W) was planted on May 16th, 2025, in an area of approximately 0.36 ha. The study was conducted using a split-plot design with 3 replications. Four irrigation treatments were implemented as the whole plot factor. Irrigation treatments were defined as dryland, 50% ET_c (T50), 75% ET_c (T75), and 100% ET_c (T100). The 100% ET_c (T100) treatment was considered the optimal irrigation, with supplemental irrigation being applied to meet

100% crop evapotranspiration. The FAO-56 Penman-Monteith equation (Allen et al., 1998) was used to calculate reference evapotranspiration (ET_0). Crop evapotranspiration (ET_c) was calculated by multiplying ET_0 by crop coefficient (K_c). Daily deficiency was then calculated as the difference between ET_c and irrigation + precipitation. Three different peanut genotypes were used as a subplot factor, Georgia-06G, TifJumbo, and Georgia-20VHO (Branch, 2021). There was a total of 48, 4 rows wide and 12.2 m-long plots.

2.2.2. Field Data Collection

Stomatal conductance (g_s) and leaf temperature were collected biweekly starting on June 24, 2025 (47 DAP in field 2025A and 39 DAP in field 2025B) (Table 2.2). A portable LI-600 porometer/fluorometer (LI-COR Inc., USA) was used to measure g_s (mmol $m^{-2}s^{-1}$). At 99 DAP, ground measurements on g_s and leaf temperature were not collected because of cloud coverage and time constraints. Measurements were collected during midday as close to 12 pm as possible from two random plants per plot. Measurements were collected from a healthy third fully expanded leaf. The leaf was clamped, and a measurement was taken after stabilization. Leaf temperature was measured using the Apogee Mi-210 (Apogee, USA) handheld infrared sensor at the same time as g_s measurements. Leaf temperature was collected from the proximity to the uppermost leaf. Two measurements per plot were made, and the average leaf temperature for each plot was used for the analysis.

Soil moisture data were collected on field 2025A with Watermark probes utilizing telemetry from RealmFive (Lincoln, NE, USA). The moisture probes had three sensors at 20, 40, and 60 cm depths and provided hourly measurements of SWT. The tension values were recorded in centibar (cb), equivalent to kilopascal (kPa). Although SWT is negative, tension values were presented using a positive scale for easy interpretation. A total of 18 sensors were installed, with

two sensors assigned to each irrigation treatment across different blocks. All probes were placed in plots planted with Georgia-06G cultivar. The irrigation was triggered based on different SWT weighted averages depending on estimated root growth at different growth stages (Table 2.4). During the early growth stage (0-40 DAP), the weighted average factors were 0.8, 0.2, and 0 for 10, 30, and 50 cm, respectively. From 41- 60 DAP, the weighting factors were 0.6, 0.3, and 0.1, and after 61 DAP, 0.4, 0.4, and 0.2 were used, respectively.

2.2.3. UAV Thermal Imagery Acquisition

Canopy temperature data were collected using the Matrice 300 RTK UAV (DJI, Shenzhen, China) equipped with the Wiris Pro Sc (Workswell, Prague, Czech Republic) thermal infrared (TIR) camera. The M300 UAV has the characteristics of stable flight and a long battery life of 55 minutes. The maximum take-off weight is 9 kg, and the maximum wind speed the UAV can withstand is 12 ms^{-1}. The Workswell WIRIS Pro Sc is an advanced system equipped with an RGB and a thermal sensor. The thermal camera uses an uncooled Vox microbolometer sensor to detect emitted heat on the 7.5 to 13.5 μm spectral range and has a camera resolution of 640 x 512. The camera has a temperature sensitivity of 30 mK and a temperature accuracy of ±2 °C.

UAS flights were conducted on the same dates as the physiological measurements, under clear sky conditions. Flights were carried out within two hours of solar noon. The thermal camera was turned on and left warming up for about 20 minutes before data collection to adapt to the environmental conditions. The flight was conducted at 50 m altitude, with 85% frontal and side overlap, at 3.3 ms^{-1} speed, with a spatial resolution of 6.54 cm in both fields.

2.2.4. Thermal Image Segmentation

The first step of image processing after flights was performed to the analysis of individual images using the Thermolab (Workswell, Prague, Czech Republic) software for the identification and removal of any problematic images before the image stitching process using Pix4Dmapper (Pix4D Sa, Lausanne, Switzerland). On Pix4Dmapper, ground control points (GCPs) were used to perform geometric correction. Resulting reflectance maps with temperature data per pixel were uploaded to ArcGIS Pro for further processing. Georeferenced GCPs were again used to align thermal reflectance maps to RGB orthomosaics, ensuring accurate alignment between RGB and thermal images. The georeferenced images were then imported into R Studio v. 2025.09.01 for further image processing.

Image segmentation is a very important process for UAV-based canopy temperature data extraction. Soil background and mixed pixels in the borders of crop canopy rows significantly affect temperature readings, skewing the canopy temperature (Tc) data to higher values (Jones and Sirault, 2014). It is crucial that soil and mixed pixels are removed from the image before canopy temperature extraction to ensure only pure canopy pixels are being used. A two-step approach was used to perform this task (Figure 2.2). The first step was performed in R Studio using the FIELDimageR and FIELDimageR.Extra packages. RGB images (~3 cm) collected simultaneously with the thermal images were used to create a binary mask, leveraging their higher spatial resolution as compared to the thermal images (~6 cm). Using the *fieldView* and *fieldSegment* functions from FieldimageR.Extra package, a Random Forest classification algorithm, was deployed to segment the image into canopy and soil pixels. After removing the soil pixels to create the binary mask, a second tool was used to remove pixels on the borders of peanut rows to remove mixed pixels. The focal statistics tool in ArcGIS Pro calculates pixel statistics by analyzing neighborhood pixels specified by a passing window size. The neighborhood type used was circle,

with a maximum focal statistic of 2 to 5, depending on crop development (2 for initial growth stages in which the canopy is sparse, and 5 for later growth stages in which the canopy is full). The circular passing window analyzed pixels by assigning values of 1 when the pixel was surrounded by other canopy pixels, and 0 to pixels that were surrounded by soil pixels (value 0). In this manner, edge pixels were removed, leaving only pixels in the center of the peanut rows. This final mask was then used to extract pura canopy pixels that were averaged for analysis.

2.2.5. Wet and Dry Baselines for CWSI Calculations

The baseline includes both non-stressed (wet reference) and fully stressed (dry reference). Empirical upper or dry baseline $(Tc\text{-}Ta)_U$ was determined by the differential between canopy temperature and air temperature of dryland plots. To select specific dates for baseline development analysis of precipitation, SWT, and g_s data were performed to confirm the crop water status. For the dry baseline, dryland plots from 81 and 127 DAP from field A and 73 and 119 DAP from field B were selected. On these dates, dryland plots were under severe water stress, with low g_s and SWT and recorded no rainfall for the preceding days before flight. Lower or wet baseline $(Tc\text{-}Ta)_L$ was determined as a linear regression between differential temperature (Tc-Ta) and VPD where Tc was collected from optimal irrigation plots (45-45-45 kPa) from field A and T100 plots from field B from the days showing higher g_s and lower SWT. From field A, 47, 81, 99,111, and 127 DAP, and from field B, 39 and 103 DAP were selected for wet baseline calculation.

The second method used to calculate baselines was the theoretical method based on the energy balance equation (Jones, 1992) represented by equation 2.1.

$$Tc - Ta = \frac{r_{HR} \times (r_{aW} + r_{lw}) \gamma R_{ni}}{\rho C_p [\gamma (r_{aW} + r_{lw}) + \Delta r_{HR}]} - \frac{r_{HR} \times VPD}{\gamma (r_{aW} + r_{lw}) + \Delta r_{HR}} \quad (2.1)$$

where Tc-Ta is the differential temperature between canopy temperature and air temperature, R_{ni} is the net solar radiation, γ is the psychrometric constant, ρ is the density of air, C_p is the specific heat capacity of air, Δ is the slope of saturated vapor pressure to temperature, r_{HR} is the parallel resistance to heat and radiative transfer and r_{aW} is the boundary layer resistance to water vapor.

The broken-down version of equation 2.1 is shown below. The upper limit of $(Tc\text{-}Ta)_U$ was calculated when r_c is allowed to increase to infinity, thus getting to Equation 2.1a. The lower limit of $(Tc\text{-}Ta)_L$ was established by assuming that the canopy resistance is equal to zero (i.e. $r_{cp} = 0$), where canopy transpiration is assumed to be equal to evaporation of a free water surface (Jackson et al., 1981a, 1988).

$$(Tc - Ta)_U = \frac{r_{HR} \times R_{ni}}{\rho C_p} \tag{2.1a}$$

$$(Tc - Ta)_L = \frac{r_{HR} \times r_{aW} \times \gamma \times R_{ni}}{\rho C_p [\gamma (ra_W) + \Delta r_{HR}]} - \frac{r_{HR} \times VPD}{\gamma\, r_{aW} + \Delta r_{HR}} \tag{2.1b}$$

The parallel resistance to heat and radiative transfer (r_{HR}) was calculated as the harmonic mean of boundary layer resistance to the radiative transfer and heat transfer.

$$r_{aR} = \frac{\gamma C_p}{4 \epsilon_c \sigma T^3} \tag{2.1c}$$

where, r_{aR} is boundary layer resistance to radiative transfer, ϵ_c is the emissivity of the vegetation and T is temperature (K).

$$r_{aH} = 100 \times \sqrt{\frac{d}{u}} \tag{2.1d}$$

where r_{aH} is the boundary layer resistance to heat transfer, d is the dimension of the leaf and u is the wind velocity.

$$r_{aw} = \frac{r_{aH}}{1.08}, \quad r_{HR} = \frac{r_{aR} \times r_{aH}}{r_{aR} + r_{aH}} \tag{2.1f}$$

2.2.6. Crop Water Stress Index

The canopy temperature collected with the UAS-based thermal camera and the handheld IR sensor were used to calculate four different CWSI methods based on the following equation by Idso, 1982.

$$CWSI = \frac{Tc - Twet}{Tdry - Twet} \tag{2.2.}$$

where Tc is canopy temperature, Twet and Tdry are baseline temperature representing dry baseline (temperature of fully transpiring leaf) and wet baseline (temperature of non-transpiring leaf).

The different CWSI methods were calculated on a combination of empirically and theoretically derived wet and dry baselines, as shown in Table 2.5. The CWSI_E was calculated by using both empirical dry and wet baselines from the well-watered plots from both fields (45-45-45 kPa for field A, and T100 for field B). The CWSI_th was calculated by using the theoretical wet and dry baselines as described in Equation 2.1. The CWSI_M and CWSI_J were calculated using a combination of the empirical dry baseline and the theoretical approach for the wet baseline. The theoretical approach for CWSI_J used the energy balance equation proposed by Jones (1999), while the CWSI_M used the energy balance equation proposed by Monteith (2013).

2.2.7. Data Analysis

A two-way mixed effect analysis of variance was performed to evaluate the effects of irrigation on g_s at different DAP. For significant main or interaction effects, post hoc pairwise comparison of least-squares means was used to identify the differences among treatments. A one-way ANOVA was used to assess the differences in CWSI values derived from four different methods. Linear regression analysis was performed to determine the relationship between CWSI and g_s. The strength and accuracy of these relationships were evaluated based on the coefficient of determination (R^2) (Equation 3) and root mean square error (RMSE) (Equation 4). The CWSI method with the highest R^2 and lowest RMSE was selected as a reliable approach for estimating plant water stress.

$$R^2 = 1 - \frac{\sum(\hat{X}_i - X_i)^2}{\sum(X_i - \bar{X}_i)^2} \tag{3}$$

$$RMSE = \sqrt{\frac{1}{n}\sum_{i=1}^{n}(X_i - \hat{X}_i)^2} \tag{4}$$

where $X_i$is the observed value, $\hat{X}_i$is the predicted value from the regression, $\bar{X}$is the mean of observed values, and $n$is the number of observations.

2.3 Results and Discussions

2.3.1 Weather and Irrigation

Minimum and maximum air temperatures, and precipitation during the 2025 growing season for both fields are represented in Figure 2.3. Total precipitation amount recorded for field A was 415.3 mm (Figure 2.3a), and 379.2 mm for field B. Rainfall was uniformly distributed until mid-season, but minimal rainfall was observed during the late season after 110 DAP. The minimum

peanut water requirement to achieve an acceptable yield is 457 mm, with low requirements during early vegetative growth and maximum during canopy development (Porter, 2022).

Table 2.3 summarizes the total irrigation applied for each irrigation treatment for fields A and B, total precipitation received, and total water (irrigation + rainfall). Even though the rainfall amount was short of the required season amount required by peanuts, irrigation and rainfall efficiency is not 100%. Water can be lost by deep percolation or runoff. In addition, rainfall timing did not always match with water use for all growth stages. Both these factors resulted in multiple irrigation events being required throughout the season. In field A, irrigation events ranged from seven times in 45-70-70 kPa treatment to seventeen times in 70-45-20 kPa treatment. More frequent irrigation events were required for treatments that used a 20 kPa irrigation triggering threshold at mid to late season than compared to early season, due to the higher water use during the full canopy development stage. For field 2025B, irrigation treatments were the same throughout all growth stages, with optimal irrigation based on crop evapotranspiration requiring 19 irrigation events.

2.3.2. Soil Water Tension (SWT) and Stomatal Conductance (g_s)

To select dates for the dry and wet baselines, the SWT and g_s data were used to ensure the crop was stressed for the dry baseline data extraction and well-watered for the wet baseline. SWT was used to trigger the irrigation in field 2025A. Figure 2.4 shows seasonal SWT trends for dryland and optimal irrigation (45-45-45 kPa) treatments along with the precipitation trend during the 2025 growing season for field A. The rainfed plot had higher SWT throughout the season. In contrast, the optimal irrigated plot (45-45-45 kPa) maintained SWT below 45 kPa, indicating the crop was well-irrigated and soil water was available for plant growth and development. Figure 2.5 shows the g_s averages by date for fields A and B. For field A, plots with the same SWT triggering level

were averaged together irrespective of irrigation treatment (Figure 2.5a). Canopy temperature from dryland plots at 81 and 127 DAP were selected for field A, due to the very low g_s of 0.05 and 0.03 mmol $m^{-2}s^{-1,}$ respectively, and high SWT, indicating the crop was stressed. Field B did not have soil moisture sensors, therefore, only precipitation and g_s data were used. Dryland plots at 73 (0.05 mmol $m^{-2}s^{-1}$) and 119 DAP (0.08 mmol $m^{-2}s^{-1}$) showed the lowest g_s values, and low precipitation was recorded on the days preceding data collection.

Overall g_s averages showed significant differences at different DAP due to the irrigation treatments in both fields (Figure 2.5). Significant differences were observed at 81, 111, and 127 DAP, with the highest values being observed for the 20 and 45 kPa triggering levels, and the lowest for dryland and 70 kPa (Figure 2.5a). For field B, irrigation treatments did not show any significant differences, only at 103 DAP due to a rainfall event before data collection. T100 and T75 only showed significant differences at the beginning of the season at 39 DAP.

The seasonal treatment g_s averages for both fields are shown in Figure 2.6. Field A used a combination of different SWT triggering levels at three critical peanut growth stages. Significant differences in g_s were only observed for plots 8 (45-70-70 kPa) and 9 (dryland) (Figure 2.6a). This indicates that allowing the soil to dry more with SWT values reaching 70kPa at later growth stages is detrimental to stomatal conductance. Seasonal averages for field B showed significant differences between irrigation treatments. Dryland had the lowest stomatal conductance values, and the T50 had the second-lowest seasonal averages. Applying 75% of crop evapotranspiration did not result in significant differences from T100. In both fields, plots with no irrigation or low and less frequent irrigation events had the lowest $g_{s,}$ evidence of the plant physiological defense mechanism of closing stomata to prevent water loss during water stress conditions (Pirasteh-Anosheh et al., 2016). According to these results, it is suggested that stomatal conductance is

significantly affected only after certain levels of water stress. Experiments conducted under an automated rainout shelter showed that no initial significant difference in g_s between irrigated and drought treatments was seen before or soon after drought (Pilon et al., 2018). A significant decline in g_s only occurred after a progressive drought was imposed.

2.3.3. Image Segmentation

An original thermal image and the distribution of canopy and soil pixel temperatures under four irrigation thresholds (20, 45 and 70 kPa and dryland) before and after segmentation is shown in Figure 2.7. The histograms for all treatments before segmentation are right skewed with a lower pixel frequency with high temperature values near 60 °C, which are coming from the soil background, since soil surfaces absorb and radiate heat more strongly than vegetation (Duveiller et al., 2018). Calculating the mean Tc, including soil or mixed pixels, increases the mean Tc values, leading to a misinterpretation of the crop water status. Removal of these pixels is pivotal for pure canopy pixel extraction. This process not only reduced the classification noise but also removed mixed emissivity signals that often occur between adjacent rows, where both soil and canopy surfaces contribute to intermediate temperature values.

The graph after segmentation, images showed a clear shift toward lower and more concentrated temperature values below 40 °C, with very low pixel frequency with values between 40 to 45 °C. Isolating pure canopy pixels enhances the sensitivity of thermal measurements of plant physiological responses such as g_s and transpiration. et al. (2019) demonstrated the use of visible bands to classify crop and non-crop components and create masks to obtain the crop region of interest from the thermal image. This masking approach effectively removed soil and shaded areas, resulting in temperature measurements that were more representative of the true crop canopy. Siegfried et al. (2024) also reported the importance of exclusion of soil background in

thermal imagery for the accurate estimation of canopy temperature. Nonetheless, there are challenges in mixed pixel extraction from thermal imagery when there is significant water stress variability. Plots that were severely stressed had a much lower biomass and canopy coverage. A much higher number of pixels is removed in this situation, since more mixed pixels are observed in these conditions. This is possible to observe in Figure 2.7d.

2.3.4. Wet and Dry Baselines

Pure canopy pixels extracted after the two-step segmentation were used to develop wet and dry baselines for peanuts using the thermal camera and the handheld IR sensor (Figure 2.8). The response of the Tc – Ta differential (ΔT) to VDP for the well-watered crop and water-deficient crop was first determined. Mean ΔT from well-watered and rainfed plots experiencing water stress was plotted against vapor pressure deficit (VPD), and a linear function was fitted to the data, which represented the well-watered baseline for peanuts. The relationship showed a strong linear relationship between VPD and ΔT. The intercept and slope of the derived wet baseline for the UAV thermal camera were 3.9 °C and – 2.1 °C kPa^{-1} (ΔT = -2.1 VPD + 3.9) and 6.4 °C and -3.2 °C kPa^{-1} (ΔT = -3.2 VPD + 6.4) for the handheld IR sensor.

Although the regression equations were different between sensors, well-watered peanut plants showed a similar Tc range of 0 to 4 °C below Ta. Higher VPD values indicate that the air is dry, requiring more evaporation, which will increase crop evapotranspiration, allowing the crop to cool its canopy relative to the air (Jones, 2013). This behavior is consistent with the established theory of crop energy balance and transpiration, and it is supported by earlier work. An experiment with irrigated peanuts conducted in 2015 showed that the non-stress baseline had a negative slope, ΔT = -1.56 VPD + 2.0 (Porter et al., 2015). This same relationship between ΔT and VPD shows a

decline in ΔT as VPD increases in other crops such as corn (*Zea mays L.)* (Liao et al., 2024), and bean (*Phaseolus vulgaris L.)* (Silveira et al., 2024).

For the dry baseline, a difference in ΔT values was observed between the UAV and the handheld sensor. The Tc values extracted from the thermal camera were overestimated by up to 2 °C. Stressed peanuts showed that Tc can achieve as high as 6 °C above the air temperature for temperatures collected with the high-accuracy handheld IR sensor, and up to 9 °C from temperatures extracted from the UAV-based thermal camera. The difference in temperature values is within the camera's limitations, which has a temperature accuracy of ±2 °C.

2.3.5 Crop water stress index (CWSI)

The empirical baselines developed from the UAS-based thermal camera and derived from the theoretical approaches were used to calculate different CWSIs (Table 2.5). Results from the ANOVA analysis showed significant differences in irrigation between the average CWSI values from the four different methods in both fields (Figure 2.9). For field A, the CWSI_E showed significantly lower averages for all treatments, while the CWSI_th showed consistently higher averages (Figure 2.9a). Both the CWSI_J and CWSI_M calculated with a combination of dry empirical baseline and theoretical wet baseline did not show significant differences from each other in any of the treatments in both fields. For field B, significant differences among the methods were only observed for the higher irrigation levels of T75 and T100 (Figure 2.9b), with the CWSI_th showing consistently higher averages, and CWSI_E consistently lower.

Overall CWSI_E values from both fields ranged from -0.2 to 1, while the CWSI_th, CWSI_J and CWSI_M ranged from 0 to 1.4. The empirical lower baseline was developedased on the average ΔT values of well-watered treatments. Plots showing ΔT below the average are expected to have negative CWSI, even though the normal CWSI range is from 0 to 1. Katimbo et

al. (2022) and DeJonge et al. (2015) also observed negative CWSI values calculated based on the empirical approach. The theoretical method, on the other hand, uses the energy balance equation, assuming a virtual leaf for baseline calculation. It requires an accurate estimate of aerodynamic resistance, canopy resistance, and solar radiation, since CWSI is sensitive to solar radiation and aerodynamic resistance (Agam et al., 2013). However, small errors in estimating these parameters for different crops can lower the dry baseline, yielding the CWSI above 1. Han et al. (2018) also observed the overestimation of stress with the theoretical approach.

The irrigation treatment effects on CWSI are shown in Figure 2.10, with selected CWSI from the empirical method. Results showed significant differences in CWSI_E in both fields A and B. Overall seasonal averages in field A showed that the optimal irrigation treatment (45-45-45 kPa) had significantly lower CWSI_E values than all the other treatments besides the 70-45-20 kPa (Figure 2.10a), while the dryland treatment resulted in significantly higher average values than six out of the nine treatment combinations. In field B, T100 and T75 had significantly lower seasonal CWSI_E values than T50 and dryland treatments, similarly to g_s results (Figure 2.10b). These results clearly demonstrate the water stress and canopy temperature relationship, which can be effectively quantified using the CWSI. This aligns with previous studies, showing canopy temperature and CWSI as reliable indicators of water status (Gonzalez-Dugo et al., 2014; Gu et al., 2024; Katimbo et al., 2022). From a management perspective, these findings highlight the practical value of integrating CWSI into irrigation scheduling. Because UAS-based thermal imagery allows for rapid, non-destructive mapping of canopy temperature across an entire field, CWSI maps with high spatial resolution can be generated and used for within-field crop water status variability. The adoption of thermal sensing and CWSI monitoring enables the ability to align water delivery with actual crop demand, thus minimizing the risks of both underwatering and

overwatering, which ultimately enhances water productivity and secures greater yield stability. (Gonzalez-Dugo et al., 2014)

2.3.6 Crop Water Stress Index (CWSI) and Stomatal Conductance (g_s)

Simple linear regressions between the four CWSI methods and g_s across multiple sampling dates in fields A and B are shown in Table 2.6. In field 2025 A, a strong relationship between CWSI and g_s was observed at 81 and 127 DAP with R^2 values ranging from 0.72 to 0.73 for all CWSI methods. In both dates, the lack of rain helped with field variability in water stress driven by the different irrigation levels. In days when treatment effect was masked by the rainfall and g_s variability was minimal, the relationship between CWSI and g_s was weak, with R^2 values of 0.02 in 111 DAP and 0.40 at 47 DAP. Overall RMSE values were relatively low, with errors varying from 0.05 to 0.1.

In field 2025 B, stronger relationships were found at 39 DAP and 73 DAP. At 39 DAP and 73, all CWSI methods exhibited a strong relationship with g_s, with R^2 values ranging from 0.76 to 0.78 at 39 DAP and 0.87 for all methods at 73 DAP. Similar to field 2025A, at 91 DAP regression model performance dropped sharply to 0.1 and below when the stomatal variability was minimal because of rainfall. Regression models for field B showed higher accuracy at 73 DAP with RMSE values of 0.03 for all methods, and lower accuracy at 39 DAP with RMSE values of 0.16. When treatment effects were significant, CWSI effectively explained most of the variation in g_s. Lower CWSI corresponded with higher g_s and higher CWSI with lower g_s, indicating that CWSI is able to sense the water stress and reduce stomatal closure to prevent water loss through transpiration. These support the findings that CWSI reflect stomatal closure and reduced transpiration cooling under stress from (Yu et al. 2015).

CWSI methods had a very similar performance in explaining g_s variability. R^2 values for all four methods were the same for most dates, while all methods resulted in the same accuracy on each date. The CWSI_th had a slightly higher R^2 value (0.41) than the other methods at 47 DAP for field A and at 39 DAP (0.78) and 91 DAP (0.10) for field B. Even though CWSI value ranges were different between the CWSI methods, as shown in Figure 2.9, with empirical baselines resulting in overall lower CWSI values and theoretical baselines resulting in consistently higher values, all methods performed similarly in explaining g_s variability. The higher CWSI_th values range may be associated with small errors in the calculation of the boundary resistance layer, as discussed in the previous section.

2.3.7 UAS-based CWSI Validation

The relationship between UAV and handheld-derived CWSI was evaluated across methods and sampling dates for fields A (Figure 2.11) and B (Figure 2.12). Strong agreement among all UAS-derived CWSI methods and handheld-based at 81 and 127 DAP was observed for field A, with R^2 values of 0.87 for CWSI_E, CWSI_J, and CWSI_M and 0.80 for CWSI_th and RMSE values ranging from 0.07 for CWSI_J and CWSI_th to 0.1 for CWSI_E (Figure 2.11). However, at 47, 99, and 127 DAP, agreement between the two sensors was very low, with the handheld sensor showing very little variation in CWSI values, while the camera yielded CWSI_E values ranging from 0 to 0.4, and all other methods yielded values between 0.2 and 0.6. The agreement among the CWSI method from both sensors for field B was higher when compared to field A. The R^2 for all methods at 39 and 73 DAP were 0.93 and 0.96, respectively. At 91 DAP, a smaller range in CWSI was observed, which led to a lower agreement between sensors with R^2 values ranging from 0.61 for the CWSI_E and CWSI_M, and 0.66 for the CWSI_th.

The close agreement between UAS and handheld-based IR sensors suggests that even though CWSI values are overestimated when derived from a UAS-based thermal camera, the variability in stress is still correctly represented. The discrepancies between handheld and UAS-derived CWSI values can be attributed to multiple factors, such as differences in measurement timing and duration, proximity to the crop, and lower temperature accuracy from thermal cameras as compared to handheld IR sensors. The handheld sensor, being closer to the canopy and less influenced by atmospheric and background effects, provides more stable temperature readings, whereas UAS-based systems are subject to additional sources of error, such as altitude, sensor drift, and environmental interference.

Temperature drift is a common issue with thermal cameras during UAS flights, and the non-uniformity correction (NUC) performed by the camera during the flight does not always correct all external effects on temperature measurements (Kelly et al., 2019). Variations in canopy temperature due to diurnal fluctuation in solar radiation, air temperature, and humidity can substantially affect CWSI measurements (Park et al., 2021). On days with minimal water stress and uniform canopy conditions, handheld sensors recorded low and stable CWSI values, while UAV-derived estimates showed higher variability, likely driven by environmental noise rather than physiological differences. This laid the foundation for the use of UAS-based thermal imaging for detecting water stress in the field.

2.4. Conclusions

This study aimed to develop empirical wet and dry baselines for CWSI calculations for peanuts and validate them with a high-accuracy handheld thermal IR sensor, and to compare the empirical CWSI with other methods. Results from this study confirmed the potential of UAS-based thermal sensing and CWSI as a reliable and scalable tool for in-season water stress

monitoring in peanuts. CWSI developed from UAS-based thermal cameras, showed satisfactory performance when variability in crop water status was observed. However, it underperformed when no stress or very low stress was present.

The implementation of the two-step segmentation process using RGB images and a random forest for soil background removal and the focal statistics tool proved to be effective in segmenting pure canopy pixels in peanuts. Empirical wet baselines for peanuts established using the thermal camera and the handheld sensor showed very similar ΔT temperature ranges, with only different slopes ($\Delta T = -2.1\ VPD + 3.9$ and $\Delta T = -3.2\ VPD + 6.4$ for camera and handheld sensor, respectively). Empirical dry baselines from the thermal camera showed that stressed peanut plants can show temperatures up to 9°C above Ta, while 6.5°C was observed for the handheld sensor, indicating that the camera is overestimating temperatures by 1.5°C.

All four methods of CWSI (empirical, Jones, Monteith, and theoretical) yielded similar patterns, showing water stress progressively increased with irrigation deficit. CWSI demonstrated great reliability in explaining crop water status by showing a strong positive relationship with g_s, with R^2 ranging from 0.72 to 0.87 in days in which the crop was stressed. Nonetheless, CWSI developed from the UAS-based thermal camera showed great limitations in capturing small g_s variations when the crop is well-watered. Furthermore, the close agreement between UAS and handheld sensor-based CWSI values, with R^2 values ranging from 0.80 to 0.96, validates the reliability of the UAS-based platform for large-scale assessment of water stress in the field. These results indicate that CWSI can be effectively used to aid in irrigation scheduling.

2.5 References

Adeyemi, O., Grove, I., Peets, S., Domun, Y., & Norton, T. (2018). Dynamic modelling of the baseline temperatures for computation of the crop water stress index (CWSI) of a greenhouse cultivated lettuce crop. *Computers and Electronics in Agriculture*, *153*, 102–114. https://doi.org/10.1016/J.COMPAG.2018.08.009

Agam, N., Cohen, Y., Alchanatis, V., & Ben-Gal, A. (2013). How sensitive is the CWSI to changes in solar radiation? *International Journal of Remote Sensing*, *34*(17), 6109–6120. https://doi.org/10.1080/01431161.2013.793873

Alchanatis, V., Cohen, Y., Cohen, S., Moller, M., Sprinstin, M., Meron, M., Tsipris, J., Saranga, Y., & Sela, E. (2010). Evaluation of different approaches for estimating and mapping crop water status in cotton with thermal imaging. *Precision Agriculture*, *11*(1). https://doi.org/10.1007/s11119-009-9111-7

Bo, L., Guan, H., & Mao, X. (2023). Diagnosing crop water status based on canopy temperature as a function of film mulching and deficit irrigation. *Field Crops Research*, *304*, 109154. https://doi.org/10.1016/J.FCR.2023.109154

Branch, W. D. (2007). Registration of 'Georgia-06G' Peanut. *Journal of Plant Registrations*, *1*(2), 120–120. https://doi.org/10.3198/JPR2006.12.0812CRC

Branch, W. D. (2019). Registration of 'Georgia-18RU' Peanut. *Journal of Plant Registrations*, *13*(3), 326–329. https://doi.org/10.3198/JPR2 018.11.0073CRC

Branch, W. D. (2021). Registration of 'Georgia-20VHO' Peanut. *Journal of Plant Registrations*, *15*(2), 290–293. https://doi.org/10.1002/PLR2.20127

Brenneman, T., Knox, P., Tubbs, R. S., Monfort, W. S., Pilon, C., & Harris, G. H. (2022). *Peanut production field guide (Bulletin B 1146)*. University of Georgia Cooperative Extension. Retrieved from https://fieldreport.caes.uga.edu/publications/B1146/

DeJonge, K. C., Taghvaeian, S., Trout, T. J., & Comas, L. H. (2015). Comparison of canopy temperature-based water stress indices for maize. *Agricultural Water Management*, *156*. https://doi.org/10.1016/j.agwat.2015.03.023

Duveiller, G., Hooker, J., & Cescatti, A. (2018). The mark of vegetation change on Earth's surface energy balance. *Nature Communications*, *9*(1). https://doi.org/10.1038/S41467-017-02810-8

Gonzalez-Dugo, V., Zarco-Tejada, P. J., & Fereres, E. (2014). Applicability and limitations of using the crop water stress index as an indicator of water deficits in citrus orchards. *Agricultural and Forest Meteorology*, *198–199*, 94–104. https://doi.org/10.1016/j.agrformet.2014.08.003

Gu, H., Mills, C., Ritchie, G. L., & Guo, W. (2024). Water Stress Assessment of Cotton Cultivars Using Unmanned Aerial System Images. *Remote Sensing*, *16*(14), 2609. https://doi.org/10.3390/rs16142609

Guilioni, L., Jones, H. G., Leinonen, I., & Lhomme, J. P. (2008). On the relationships between stomatal resistance and leaf temperatures in thermography. *Agricultural and Forest Meteorology*, *148*(11). https://doi.org/10.1016/j.agrformet.2008.07.009

Han, M., Zhang, H., DeJonge, K. C., Comas, L. H., & Gleason, S. (2018). Comparison of three crop water stress index models with sap flow measurements in maize. *Agricultural Water Management*, *203*, 366–375. https://doi.org/10.1016/J.AGWAT.2018.02.030

Holbrook, C. C., Clevenger, J., Ozias-Akins, P., Chu, Y., & Brenneman, T. B. (2024). Registration of 'TifJumbo' peanut. *Journal of Plant Registrations*, *18*(2), 279–284. https://doi.org/10.1002/PLR2.20285;SUBPAGE:STRING:FULL

Idso, S. B., Jackson, R. D., Pinter, P. J., Reginato, R. J., & Hatfield, J. L. (1981). Normalizing the stress-degree-day parameter for environmental variability. *Agricultural Meteorology*, *24*(C). https://doi.org/10.1016/0002-1571(81)90032-7

Idso, S. B. (1982). Non-water-stressed baselines: A key to measuring and interpreting plant water stress. *Agricultural Meteorology*, *27*(1–2). https://doi.org/10.1016/0002-1571(82)90020-6

Jackson, R. D., Idso, S. B., Reginato, R. J., & Pinter, P. J. (1981). Canopy temperature as a crop water stress indicator. *Water Resources Research*, *17*(4), 1133–1138. https://doi.org/10.1029/WR017i004p01133

Jackson, R. D., Reginato, R. J., & Idso, S. B. (1977). Wheat canopy temperature: A practical tool for evaluating water requirements. *Water Resources Research*, *13*(3). https://doi.org/10.1029/WR013i003p00651

Jackson, R. D., Kustas, W. P., & Choudhury, B. J. (1988). A reexamination of the crop water stress index. *Irrigation Science*, *9*(4), 309–317. https://doi.org/10.1007/BF00296705/METRICS

Jones, H. G. (1999). Use of infrared thermometry for estimation of stomatal conductance as a possible aid to irrigation scheduling. *Agricultural and Forest Meteorology*, *95*(3). https://doi.org/10.1016/S0168-1923(99)00030-1

Jones, H. (2013). Plants and microclimate, a quantitative approach to environmental plant physiology, Hamlyn G. Jones. Retrieved March 23, 2025, from https://www.academia.edu/18193900/Plants_and_microclimate_a_quantitative_approach_to_environmental_plant_physiology_Hamlyn_G_Jones

Jones, H. G., & Sirault, X. R. R. (2014). Scaling of Thermal Images at Different Spatial Resolution: The Mixed Pixel Problem. *Agronomy*, *4*(3), 380-396. https://doi.org/10.3390/agronomy4030380

Katimbo, A., Rudnick, D. R., DeJonge, K. C., Lo, T. H., Qiao, X., Franz, T. E., Nakabuye, H. N., & Duan, J. (2022). Crop water stress index computation approaches and their sensitivity to soil water dynamics. *Agricultural Water Management*, *266*. https://doi.org/10.1016/j.agwat.2022.107575

Kelly, J., Kljun, N., Olsson, P. O., Mihai, L., Liljeblad, B., Weslien, P., Klemedtsson, L., & Eklundh, L. (2019). Challenges and Best Practices for Deriving Temperature Data from an Uncalibrated UAV Thermal Infrared Camera. *Remote Sensing 2019, Vol. 11, Page 567*, *11*(5), 567. https://doi.org/10.3390/RS11050567

Lacerda, L. N., Snider, J. L., Cohen, Y., Liakos, V., Gobbo, S., & Vellidis, G. (2022). Using UAV-based thermal imagery to detect crop water status variability in cotton. *Smart Agricultural Technology*, *2*, 100029. https://doi.org/10.1016/J.ATECH.2021.100029

Liao, Q., Gu, S., Gao, S., Du, T., Kang, S., Tong, L., & Ding, R. (2024). Crop water stress index characterizes maize productivity under water and salt stress by using growth stage-specific non-water stress baselines. *Field Crops Research*, *317*, 109544. https://doi.org/10.1016/J.FCR.2024.109544

Luan, Y., Xu, J., Lv, Y., Liu, X., Wang, H., & Liu, S. (2021). Improving the performance in crop water deficit diagnosis with canopy temperature spatial distribution information measured by thermal imaging. *Agricultural Water Management*, *246*, 106699. https://doi.org/10.1016/J.AGWAT.2020.106699

Silveira, J. M. D. C., Góes, J. D. A., Prado, D. F., Pires, R. C. D. M., & Chiorato, A. F. (2024). Baselines for Calculating Crop Water Stress Index in Bean Cultivation. The International Archives of the Photogrammetry, Remote Sensing and Spatial Information Sciences, 48, 501-506.

Matias, F. I., Caraza-Harter, M. V., & Endelman, J. B. (2020). FIELDimageR: An R package to analyze orthomosaic images from agricultural field trials. The Plant Phenome Journal, 3(1), e20005.

Monteith, J. L. . (2013). *Principles of environmental physics*. https://books.google.com/books/about/Principles_of_Environmental_Physics.html?id=EhLtk6hkLogC

Park, S., Ryu, D., Fuentes, S., Chung, H., O'connell, M., & Kim, J. (2021). Dependence of CWSI-Based Plant Water Stress Estimation with Diurnal Acquisition Times in a Nectarine Orchard. *Remote Sensing 2021, Vol. 13, Page 2775*, *13*(14), 2775. https://doi.org/10.3390/RS13142775

Pawar, P. S., & Matias, F. I. (2023). FIELDimageR. Extra: Advancing user experience and computational efficiency for analysis of orthomosaic from agricultural field trials. The Plant Phenome Journal, 6(1), e20083.

Pilon, C., Snider, J. L., Sobolev, V., Chastain, D. R., Sorensen, R. B., Meeks, C. D., Massa, A. N., Walk, T., Singh, B., & Earl, H. J. (2018). Assessing stomatal and non-stomatal limitations to carbon assimilation under progressive drought in peanut (Arachis hypogaea L.). *Journal of Plant Physiology*, *231*. https://doi.org/10.1016/j.jplph.2018.09.007

Pirasteh-Anosheh, H., Saed-Moucheshi, A., Pakniyat, H., & Pessarakli, M. (2016). Stomatal responses to drought stress. *Water Stress and Crop Plants: A Sustainable Approach*, *1–2*, 24–40. https://doi.org/10.1002/9781119054450.CH3

Porter, W. M., Snider, J. L., Perry, C. D., Monfort, W. S., & Vellidis, G. (2015). SmartCrop® Sensors for Predicting Irrigation Requirements for Peanut in the Southeast. *American Society of Agricultural and Biological Engineers Annual International Meeting 2015*, *3*, 1-. https://doi.org/10.13031/AIM.20152188627

Porter, W. M. (2022). Water Use and Relationship in Peanut Production in Peanut Production Guide. University of Georgia Extension.

Pradawet, C., Khongdee, N., Pansak, W., Spreer, W., Hilger, T., & Cadisch, G. (2023). Thermal imaging for assessment of maize water stress and yield prediction under drought conditions. *Journal of Agronomy and Crop Science*, *209*(1), 56–70. https://doi.org/10.1111/JAC.12582

Puppala, N., Nayak, S. N., Sanz-Saez, A., Chen, C., Devi, M. J., Nivedita, N., Bao, Y., He, G., Traore, S. M., Wright, D. A., Pandey, M. K., & Sharma, V. (2023). Sustaining yield and nutritional quality of peanuts in harsh environments: Physiological and molecular basis of drought and heat stress tolerance. *Frontiers in Genetics*, *14*, 1121462. https://doi.org/10.3389/FGENE.2023.1121462

Siegfried, J., Rajan, N., Adams, C. B., Neely, H., Hague, S., Hardin, R., Schnell, R., Han, X., & Thomasson, A. (2024). High-accuracy infrared thermography of cotton canopy temperature by unmanned aerial systems (UAS): Evaluating in-season prediction of yield. *Smart Agricultural Technology*, *7*, 100393. https://doi.org/10.1016/J.ATECH.2023.100393

USDA-National Agricultural Statistics Service (NASS). https://quickstats.nass.usda.gov/results/A05CCC03-9F8D-3916-BCA6-04ED4778208C (accessed October 21)

Wei, S., Li, K., Yang, Y., Wang, C., Liu, C., & Zhang, J. (2022). Comprehensive climatic suitability evaluation of peanut in Huang-Huai-Hai region under the background of climate change. *Scientific Reports*, *12*(1), 11350. https://doi.org/10.1038/s41598-022-15465-3

Yu, M. H., Ding, G. D., Gao, G. L., Zhao, Y. Y., Yan, L., & Sai, K. (2015). Using Plant Temperature to Evaluate the Response of Stomatal Conductance to Soil Moisture Deficit. *Forests 2015, Vol. 6, Pages 3748-3762*, *6*(10), 3748–3762. https://doi.org/10.3390/F6103748

TABLES AND FIGURES

Table 2.1. Different Irrigation threshold combinations applied in field A. Each irrigation treatment consisted of a combination of three soil water tension (kPa) thresholds used to trigger irrigation at three critical stages (Early Season (0-40 DAP) – Mid-Season (41-110 DAP) - Late Season (110 to harvest).

	Early Season (0-40 DAP)	**Mid-Season (41-110 DAP)**	**Late Season (110 to harvest)**
Irrigation regimes		**SWT (kPa)**	
1	45	45	45
2	70	45	70
3	70	45	45
4	70	45	20
5	45	45	70
6	70	20	45
7	20	70	45
8	45	70	70
9		Dryland	

Table 2.2. Data collection schedule (days after planting, DAP) for stomatal conductance (g_s), leaf temperature and UAV-based thermal imaging in fields A and B. The checkmark (✓) indicates data collected on that date, while a cross (×) indicates data not collected due to time constraints and/or weather conditions.

Field 2025 A				**Field 2025 B**			
DAP	**Stomatal Conductance**	**Leaf Temperature**	**UAV Flight**	**DAP**	**Stomatal Conductance**	**Leaf Temperature**	**UAV Flight**
47	✓	✓	✓	**39**	✓	✓	✓
81	✓	✓	✓	**73**	✓	✓	✓
99	×	×	✓	**91**	✓	✓	✓
111	✓	✓	✓	**103**	✓	✓	✓
127	✓	✓	✓	**118**	✓	✓	✓

Table 2.3. Irrigation, rainfall and total water applied in fields A and B in Camilla, GA during the 2025 growing seasons.

Field	Treatment	Irrigation Events	Irrigation (mm)	Rainfall (mm)	Total Water (mm)
2025A	**45-45-45**	11	217.2	415.3	632.5
	70-45-70	12	236.2	415.3	651.5
	70-45-45	15	285.8	415.3	701.1
	70-45-20	17	304.8	415.3	720.1
	45-45-70	12	228.6	415.3	643.9
	70-20-45	16	304.8	415.3	720.1
	20-70-45	9	179.1	415.3	594.4
	45-70-70	7	141.0	415.3	556.3
	Dryland	1	19.0	415.3	434.3
2025B	**T100**	19	369.6	379.2	748.8
	T75	13	236.2	379.2	615.4
	T50	10	198.1	379.2	577.3
	Dryland	-	-	379.2	379.2

Table 2.4. Weighting factors applied to soil water tension (SWT) at different depths for irrigation scheduling across growth stages

	0-40 DAP	41-60 DAP	60-110 DAP
Depth (cm)		**Weightage**	
10	0.8	0.6	0.4
30	0.2	0.3	0.4
50	0.1	0.1	0.2

Table 2.5 Summary of wet and dry baselines used for different crop water stress index (CWSI) approaches.

CWSI approach		Baselines	Remarks
CWSI _E (Empirical)	**Wet**	Ta + aVPD + b where (aVPD +B) empirical estimate dependent on VPD	Differential temperature between Tc from the well-irrigated plots (45-45-45 kPa) in field 2025A and T100 in field 2025B, and Ta was plotted against the VPD
	Dry	Ta + X °C	X is an empirical estimate calculated based on the differential temperature in rainfed plots
CWSI_th (Theoretical)	**Wet**	Temperature calculated using energy balance equation (Jones 1992)	
	Dry	Temperature calculated using energy balance equation (Jones 1992)	
CWSI_M (Monteith)	**Wet**	Temperature calculated using energy balance equation (Monteith and Unsworth 1990)	
	Dry	Using empirical dry baseline (Ta + X °C)	
CWSI_J (Jones)	**Wet**	Use the theoretical baseline	
	Dry	Using empirical dry baseline (Ta + X °C)	

Table 2.6. Linear regression models between CWSI calculated using UAV-based thermal sensor and stomatal conductance (g_s) in fields A and B.

Field	DAP	CWSI Method	Equation	R^2	RMSE
2025 A	47	CWSI _E	y = 0.394 + 0.217x	0.40	0.05
		CWSI_J	y = 0.317 + 0.293x	0.40	0.05
		CWSI_M	y = 0.342 + 0.269x	0.40	0.05
		CWSI_th	y = 0.321 + 0.276x	0.41	0.05
	81	CWSI _E	y = 0.329 - 0.321x	0.73	0.05
		CWSI_J	y = 0.460 - 0.45x	0.72	0.05
		CWSI_M	y = 0.407 - 0.398x	0.73	0.05
		CWSI_th	y = 0.452 - 0.36x	0.73	0.05
	111	CWSI _E	y = 0.584 - 0.108x	0.02	0.10
		CWSI_J	y = 0.640 - 0.163x	0.02	0.10
		CWSI_M	y = 0.631 - 0.155x	0.02	0.10
		CWSI_th	y = 0.638 - 0.15x	0.02	0.10
	127	CWSI _E	y = 0.403 - 0.423x	0.73	0.07
		CWSI_J	y = 0.623 - 0.643x	0.73	0.07
		CWSI_M	y = 0.551 - 0.571x	0.73	0.07
		CWSI_th	y = 0.605 - 0.484x	0.73	0.07
2025 B	39	CWSI _E	y = 0.639 - 2.194x	0.76	0.16
		CWSI_J	y = 1.454 - 2.978x	0.77	0.16
		CWSI_M	y = 1.105 - 2.66x	0.76	0.16
		CWSI_th	y = 1.434 - 3.06x	0.78	0.16
	73	CWSI _E	y = 0.173 - 0.229x	0.87	0.03
		CWSI_J	y = 0.282 - 0.338x	0.87	0.03
		CWSI_M	y = 0.232 - 0.288x	0.87	0.03
		CWSI_th	y = 0.275 - 0.289x	0.87	0.03
	91	CWSI _E	y = 0.323 - 0.297x	0.09	0.10
		CWSI_J	y = 0.504 - 0.477x	0.09	0.10
		CWSI_M	y = 0.441 - 0.416x	0.09	0.10
		CWSI_th	y = 0.492 - 0.456x	0.10	0.10

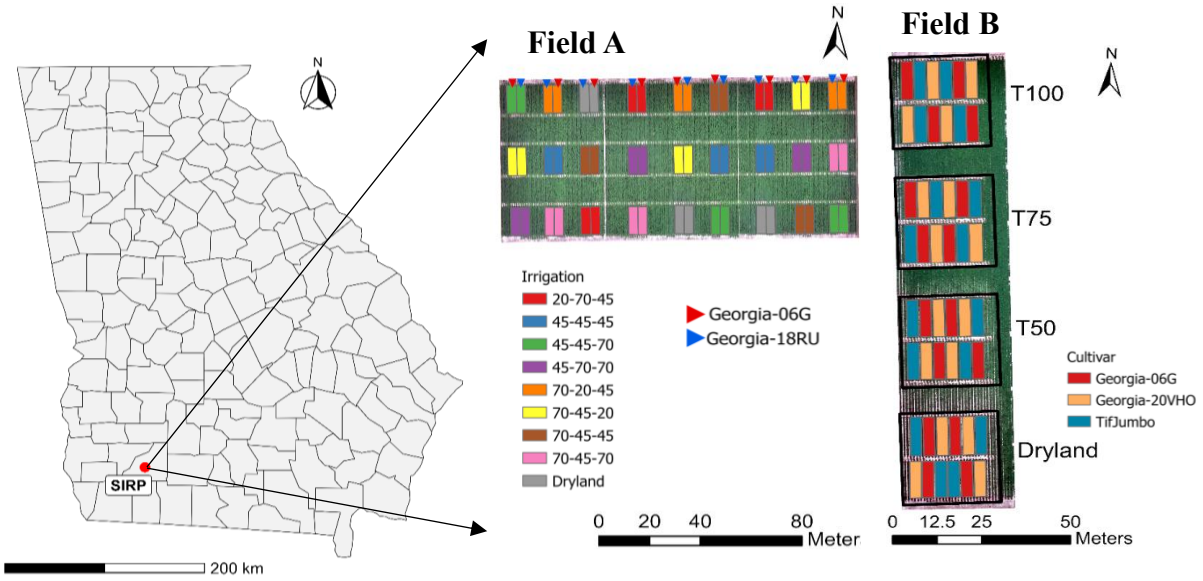

Figure 2.1. Layout of fields in 2025. Irrigation treatments are shown in different colors. Field A had 9 different combinations of irrigation triggering levels (20, 45, and 70 kPa) at three critical peanut growth stages (0-40 DAP, 41-110 DAP, and 111 DAP to harvest), including one dryland treatment throughout the season and two cultivars, Georgia-06 (red triangle rows) and Georgia-RU (blue triangle rows). Field B had 4 different irrigation levels (T100, T75, T50, and dryland) based on the crop evapotranspiration and three cultivars (Georgia-06g, Georgia-20VHO, and Tif Jumbo).

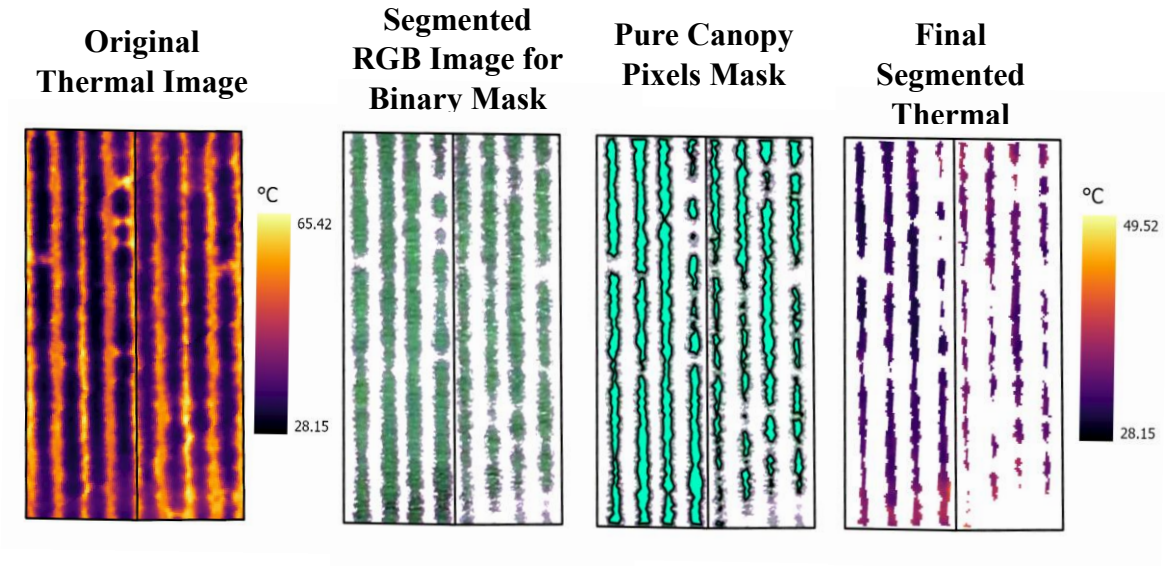

Figure 2.2. Workflow of the two-step image segmentation process to isolate pure canopy pixels from soil background.

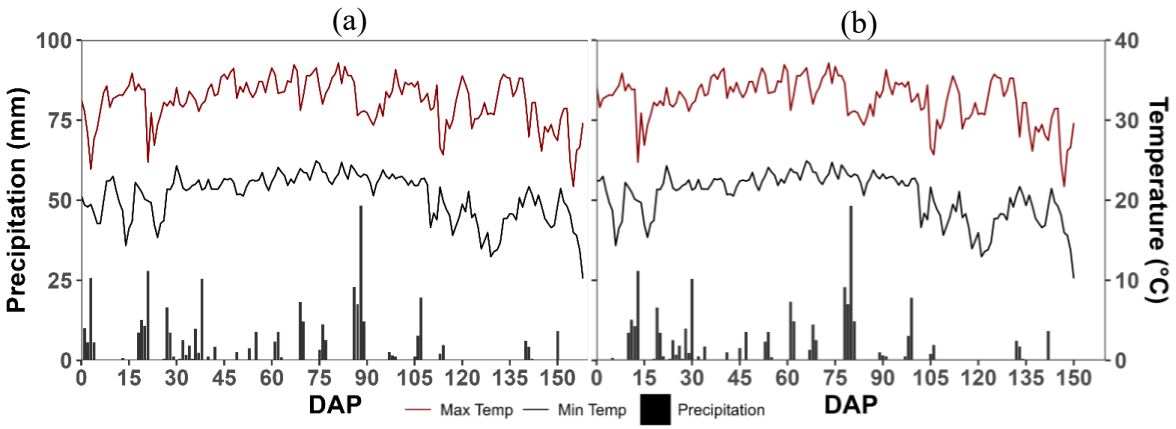

Figure 2.3. Daily Precipitation (mm), and maximum and minimum temperatures (°C) for fields A (a) and B (b) during the 2025 peanut growing season. Red lines indicate maximum daily temperature (°C), black lines indicate minimum daily temperature (°C), and black bars represent daily precipitation (mm).

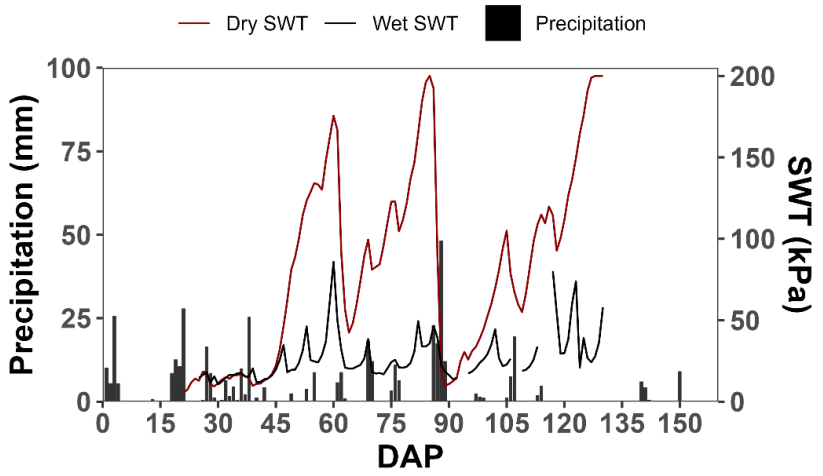

Figure 2.4. Soil water tension (SWT, kPa) for optimal irrigation treatment (45-45-45) and dryland at different days after planting (DAP), and precipitation (mm) for field A. Red line represents the dryland SWT and black line represent the SWT for optimal irrigation treatment (45-45-45 kPa).

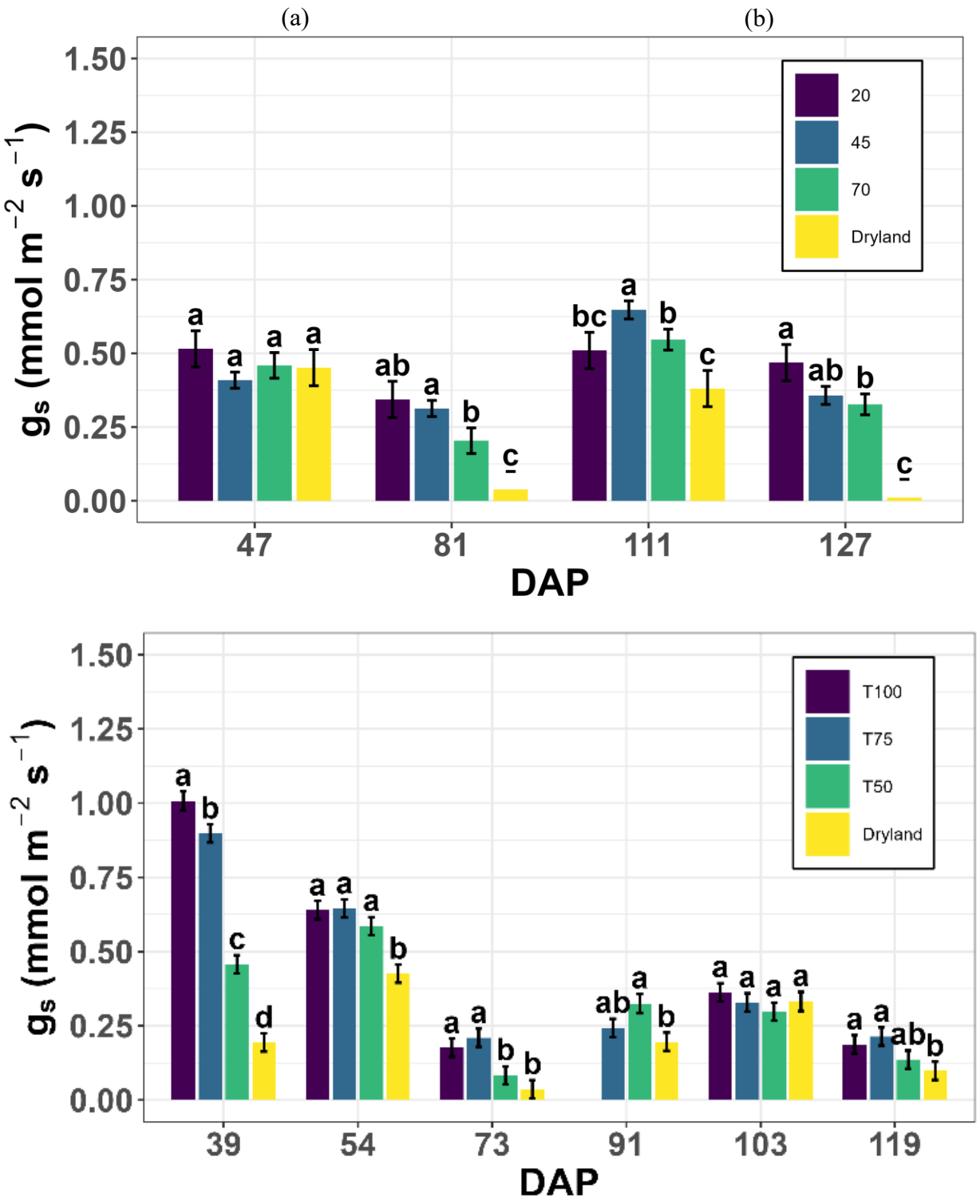

Figure 2.5. Stomatal conductance (g_s) response to different irrigation levels at different days after planting (DAP) in fields A (a) and B (b). In field A, irrigation levels were triggered at different levels of soil water tension (20, 45 and 75 kPa) including rainfed (dryland). In field B, irrigation levels were applied based on evapotranspiration (ET) and crop coefficient (K_c)-100% ETc, 75% ETc, 50% ETc and dryland.

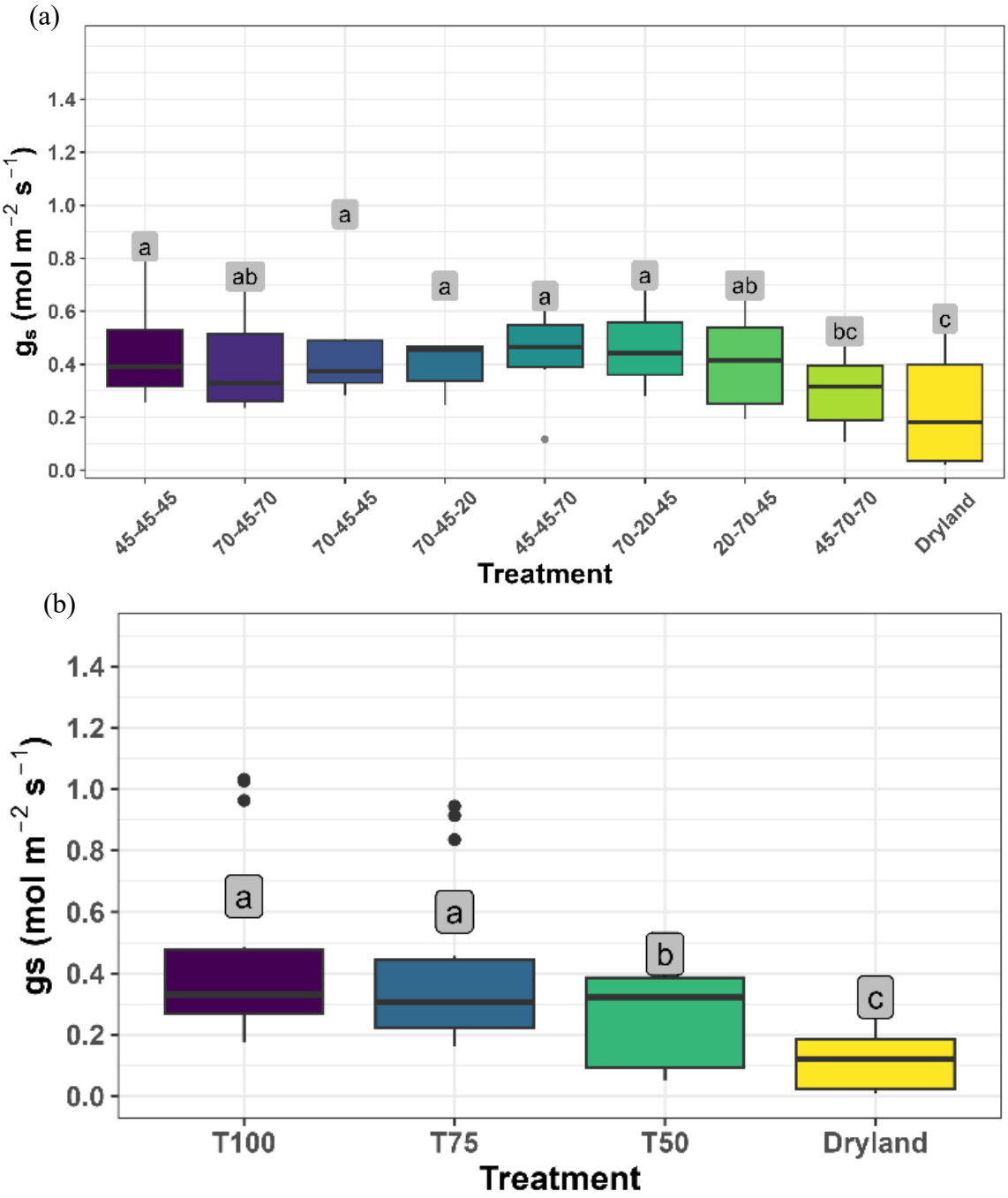

Figure 2.6. Stomatal conductance (g_s) response to different irrigation treatments at different days after planting (DAP) in fields A (a) and B (b). In field A, irrigation treatment was triggered at different levels of soil water tension (20, 45 and 75 kPa) including rainfed (dryland). In field B, irrigation treatments were applied based on evapotranspiration (ET) and crop coefficient (K_c)100% ETc, 75% ETc, 50% ETc and dryland.

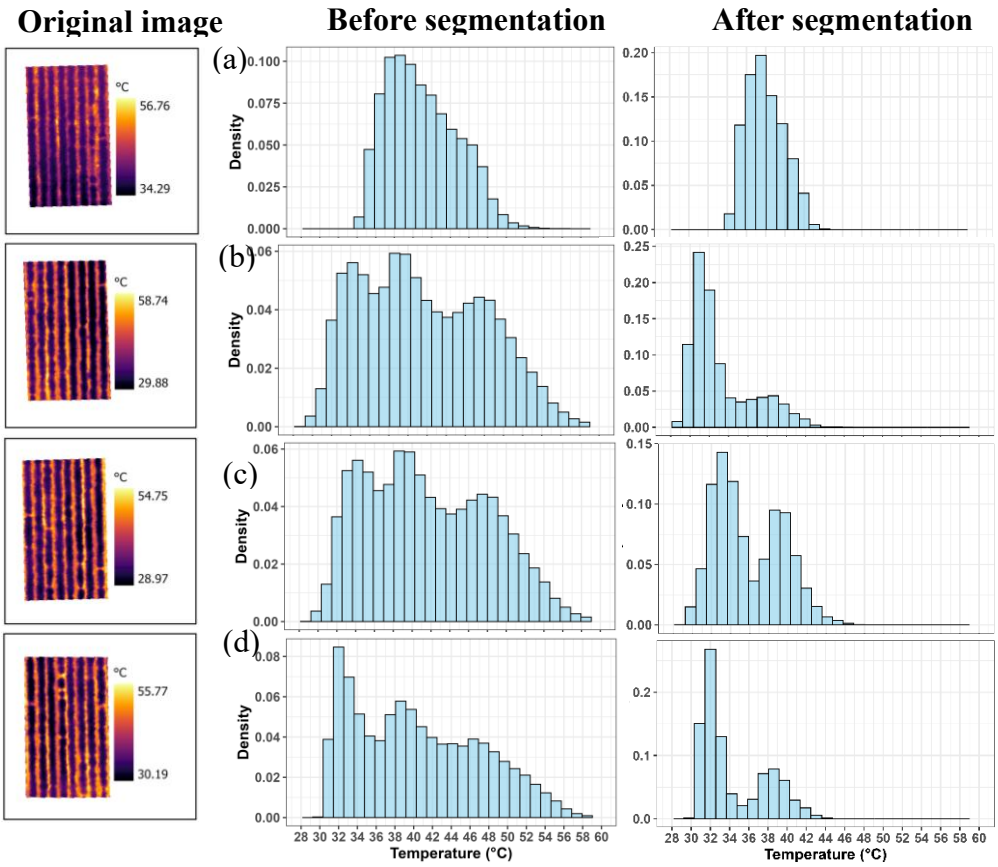

Figure 2.7. Histogram of canopy and soil pixels temperature distribution for SWT triggering levels of 20 kPa (a), 45 kPa (b), 70 kPa (c) and dryland (d) before and after segmentation.

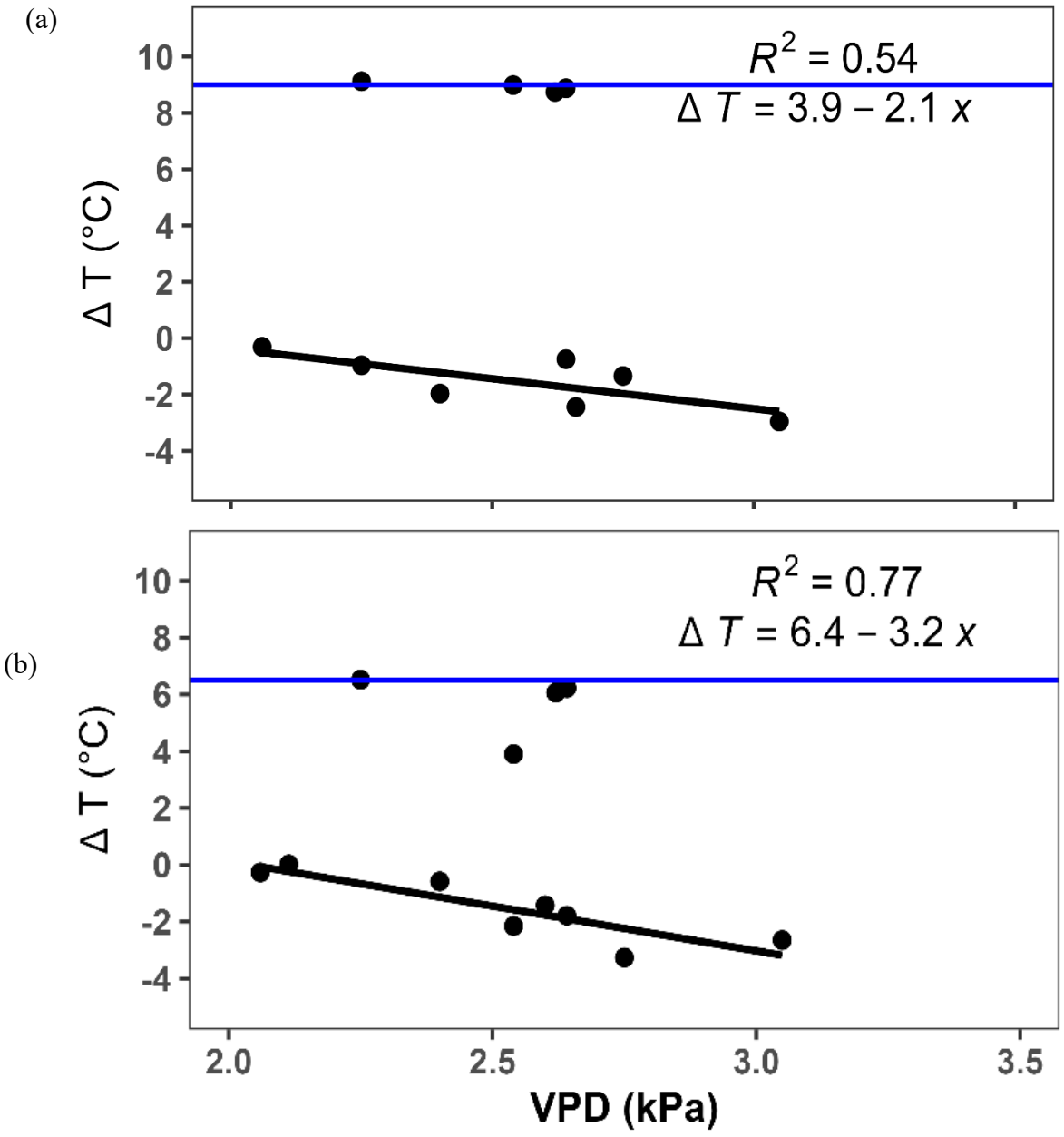

Figure 2.8. Canopy to air temperature differential (ΔT, °C) versus vapor pressure deficit (VPD) for well-watered and rainfed plots calculated based on UAV-based thermal sensor (a) and handheld infrared sensor (b). The blue line represents the dry baseline $(Tc\text{-}Ta)_U$, and the black line represents the wet baseline $(Tc\text{-}Ta)_L$. Only dates with solar radiation greater than 600 W m^{-2} were included. The wet baseline points correspond to the mean Tc of the 45-45-45 kPa treatment plots in Field A and the T100 (100% ETc) treatment plots in Field B.

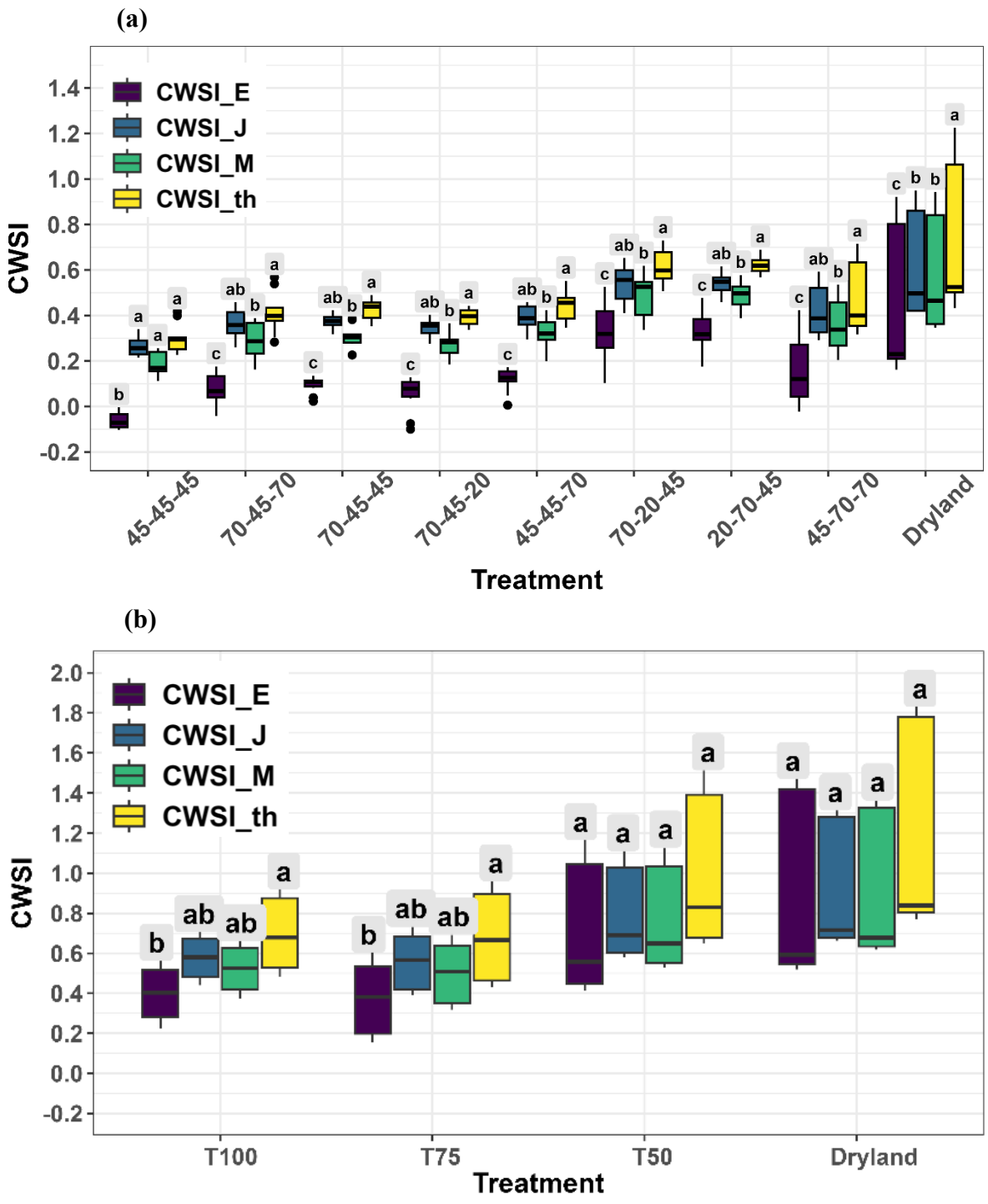

Figure 2.9. Crop water stress index (CWSI) based on four different methods (empirical, Jones, Monteith, and theoretical) across irrigation treatments in field A (a) and B (b). The canopy temperature was measured by a UAV-based thermal sensor. The letters indicate the difference among CWSI methods within each treatment at α= 0.05, using a least-squares means post hoc analysis.

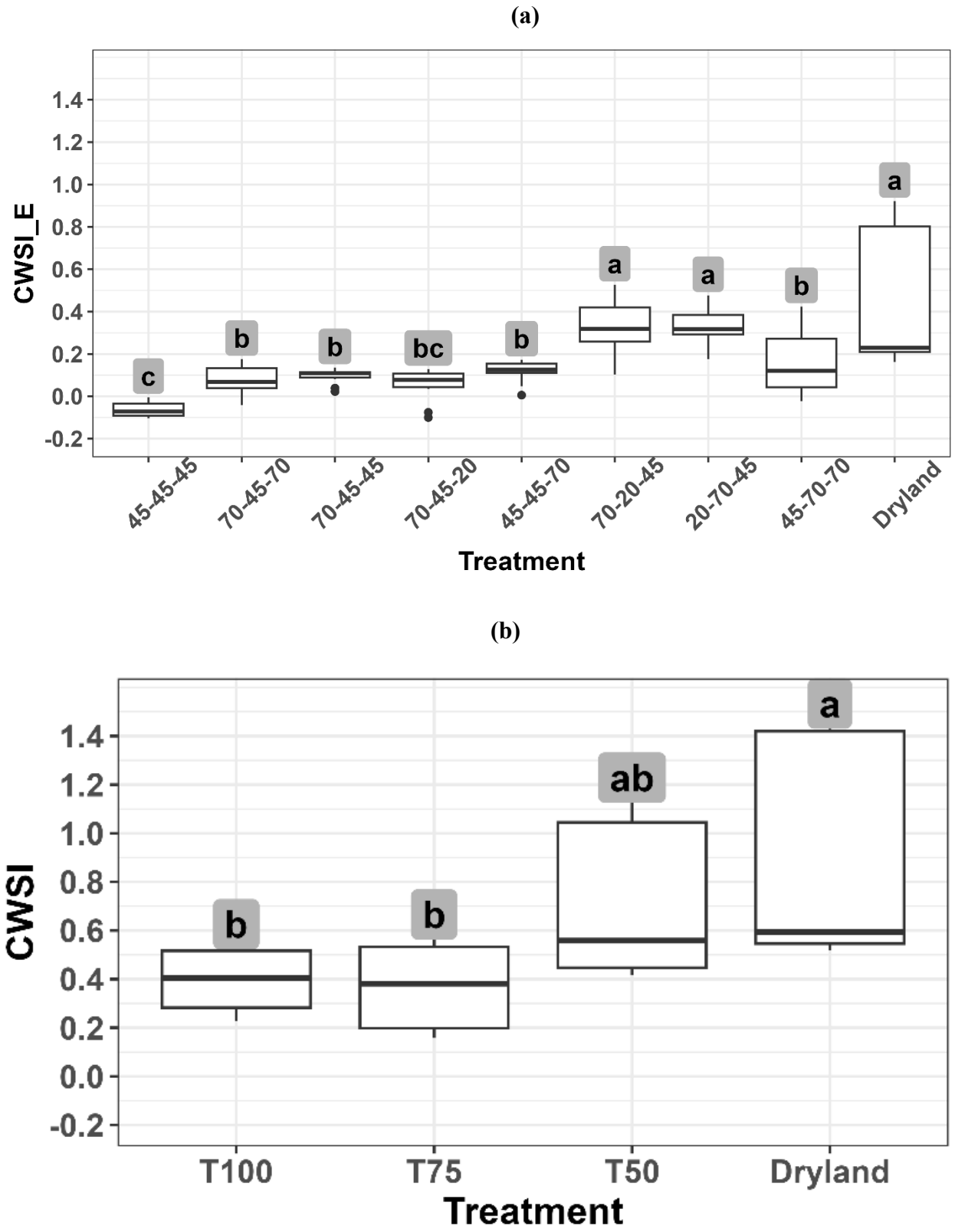

Figure 2.10. Crop water stress index (CWSI) based on empirical method across irrigation treatments in field A (a) and B (b). The canopy temperature was measured by a UAV-based thermal sensor. The letters indicate the difference among CWSI_E values between treatments at $\alpha = 0.05$, using a least-squares means post hoc analysis.

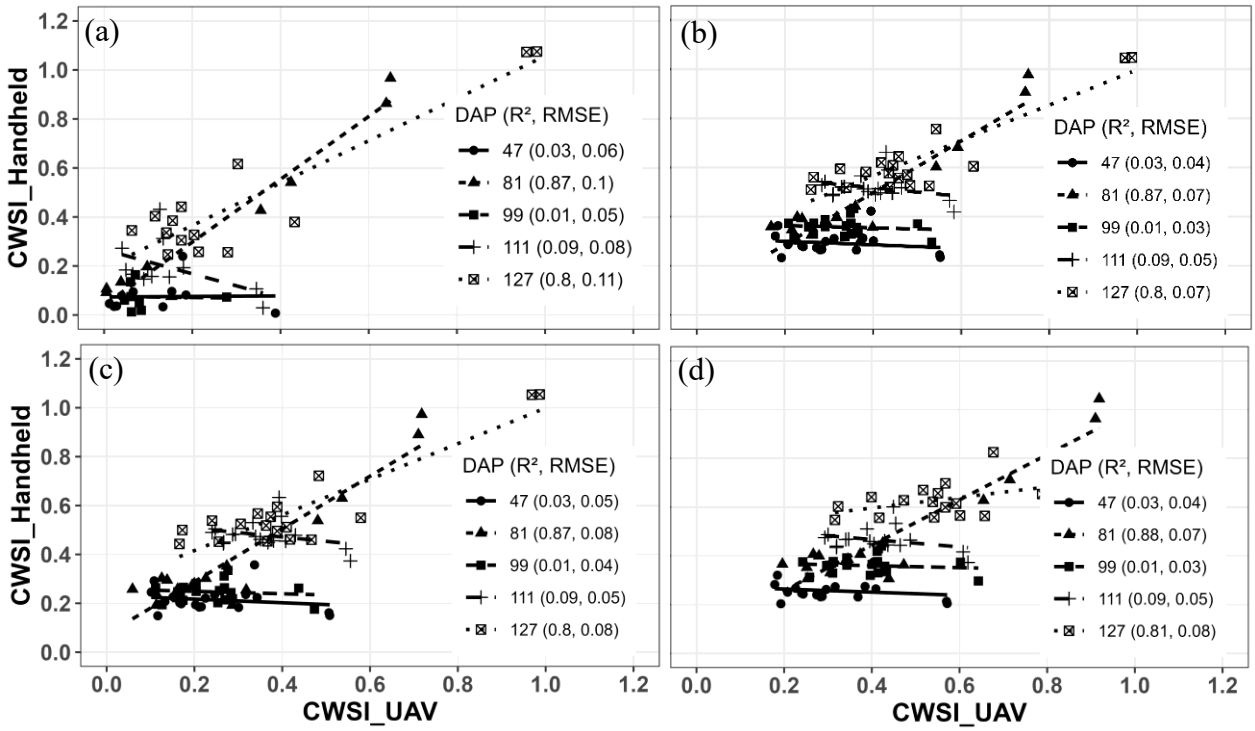

Figure 2.11. Relationship between UAV-derived and handheld CWSI calculated using four different methods (CWSI_E (a), CWSI_J (b), CWSI_M (c) and CWSI_th (d)) for field A.

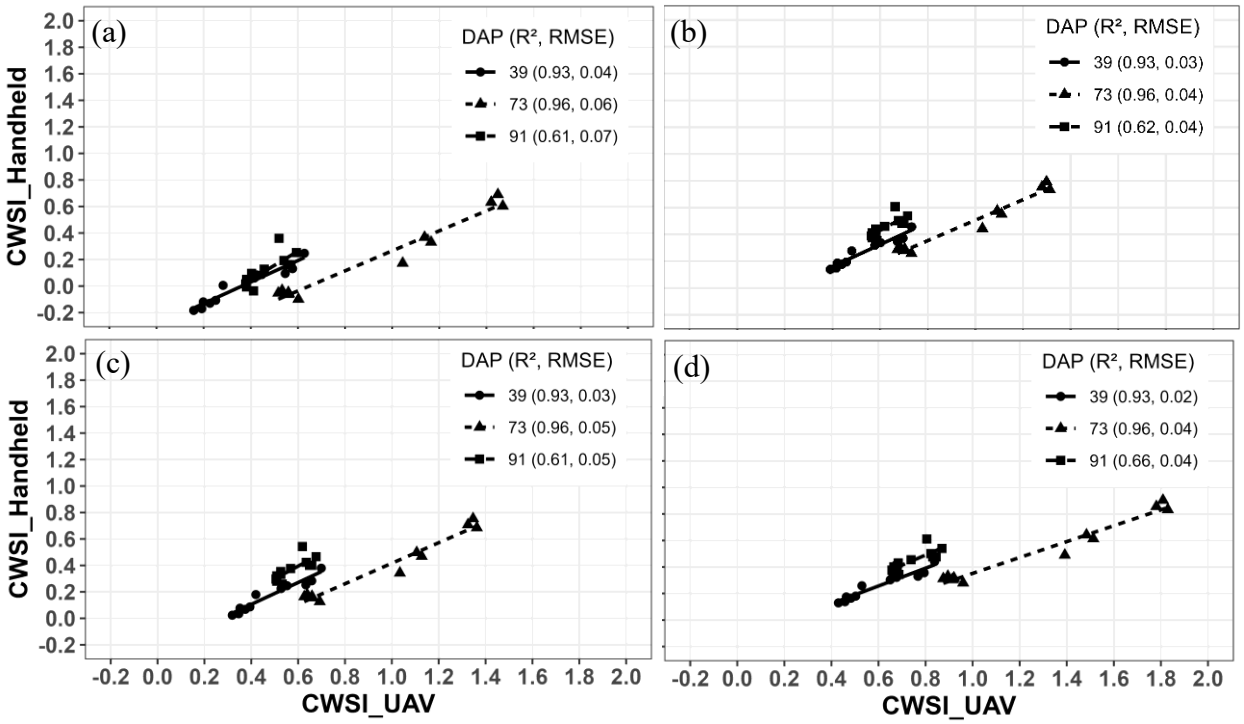

Figure 2.12. Relationship between UAV-derived and handheld CWSI calculated using four different methods (CWSI_E (a), CWSI_J (b), CWSI_M (c) and CWSI_th (d)) for field B.

CHAPTER 3

ASSESSING AFLATOXIN RISK IN PEANUT FIELDS USING UAS-BASED CROP CANOPY TEMPERATURE

Shrestha, S., Lacerda, L.N., Pilon, C., Vellidis, G., Maktabi, S., and Sysskind, M. To be submitted to the *Precision Agriculture Journal*

Abstract

Aflatoxin, a carcinogenic compound primarily produced by the fungus *Aspergillus flavus* and *A. parasiticus,* is a serious threat to the peanut industry, food safety, and overall economy. This study explored the potential of using an unmanned aerial system (UAS)-based Crop Water Stress Index (CWSI) to map aflatoxin risk in commercial peanut fields. The study was conducted over five fields during the 2023 and 2024 peanut growing seasons in collaboration with growers in Georgia, USA. Canopy temperature derived from thermal imagery was used to calculate differential temperature (ΔT) and CWSI using the energy balance equation model for wet and dry baselines. All five fields were divided into plots of approximately 0.5 ha. Soil moisture sensors were installed to measure soil water tension (SWT) across the growing season, crop physiological responses, such as stomatal conductance (g_s), were measured at different growth stages, and peanut samples for aflatoxin concentration analysis were conducted starting at 90 DAP. Results showed that higher canopy temperature and CWSI resonated with higher aflatoxin levels, with the highest R^2 (0.65) achieved in field 2. A positive correlation between late-season CWSI and aflatoxin suggests that terminal drought is critical in aflatoxin contamination. Correlation analysis between CWSI and aflatoxin suggests that fields experiencing drought during the season may predispose the crop to contamination. However, drought needs to be severe and extended to lead to contamination values considered moderate to high. Results also showed that higher correlations between CWSI were seen with aflatoxin contamination levels from late-season samples, near harvest.

3.1. Introduction

Aflatoxins are a group of highly toxic and carcinogenic mycotoxins primarily produced by the fungi *Aspergillus flavus* and *A. parasiticus*, posing a critical threat to agricultural production, food safety, and public health (Alameri et al., 2023; Shabeer et al., 2022). These toxins, which contaminate 25% of global food crops (Eskola et al., 2020), can cause acute liver disease, a weak immune system, and significant trade losses to strict regulatory limits (20 ppb in the U.S., 2 ppb in the EU (EC, 2021; APC, 2020). The peanut production in the United States (US) is concentrated in the warm southeast region, with Georgia being the leading producer. In 2019, it was estimated that 30% of the peanuts produced in the southeast failed to meet the USDA limit of permitted aflatoxin concentration (Butts et al., 2023).

Aflatoxin contamination in peanuts can occur pre- and post-harvest. A variety of toxin-producing fungi can be found in the soil, which enables contamination when the crop is still in the field (Horn, 2005) Pre-harvest contamination is exacerbated by environmental stressors, with drought-induced water stress identified as a key driver of fungal proliferation and aflatoxin biosynthesis (Puppala et al., 2023; Yu, 2012). Field studies have consistently shown that moderate to severe drought, particularly during the critical last 40–75 days before harvest, significantly increases aflatoxin contamination in peanut pods (Hamidou et al., 2014; Martins et al., 2023). Hot and dry conditions prevalent in semi-arid peanut-growing regions are conducive to the survival and growth of *Aspergillus* species (Nji et al., 2023).

Post-harvest contamination, on the other hand, may be affected by the contact of contaminated lots with healthy seeds and pods after harvest, mechanical damage of seeds during harvest, and improper storage conditions (Torres et al., 2014). Peanuts contaminated in the field contain spores and mycelia, which can lead to further contamination of other peanut seeds if proper

post-harvest management is not correctly applied. Peanut seeds with visible mold should be segregated and stored separately from peanuts with no contamination or with contamination levels below the legal limits. It is commonly accepted that peanut moisture levels above 10% are optimal for aflatoxin. Therefore, keeping low moisture levels during storage is essential to mitigate further contamination (Lavkor et al., 2017).

Monitoring and identifying aflatoxin contamination risk areas in the field may help mitigate pre-harvest and post-harvest contamination. However, traditional aflatoxin monitoring methods, such as Thin Layer Chromatography (TLC), High-Pressure Liquid Chromatography (HPLC), and ELISA (Enzyme Linked Immunosorbent Assay), are precise but destructive, expensive, and time-consuming (Rahmani et al., 2009). Emerging remote sensing technologies, particularly thermal imagery, offer a proactive solution by quantifying crop water stress through canopy temperature (Tc) measurements and the Crop Water Stress Index (CWSI), a normalized metric derived from canopy and ambient temperature differentials (Ihuoma & Madramootoo, 2017; Khorsandi et al., 2018; Stutsel et al., 2021). Thermal cameras detect water stress based on the Tc difference that is directly associated with plant physiological processes such as transpiration rates and stomatal conductance (Kim & Glenn, 2017; Usamentiaga et al., 2014).

The CWSI, derived from thermal infrared imagery, is used to quantify the degree of water stress by normalizing Tc against reference temperatures of fully transpiring and non-transpiring crops (Idso et al., 1982; Jackson et al., 1981). CWSI is a spatially explicit and scalable indicator of water stress in the field, enabling precision irrigation and reducing the risk of aflatoxin contamination (Adeyemi et al., 2017; Caruso et al., 2022). This study aims to explore the potential of thermal imagery-derived Tc and CWSI as a tool for mapping pre-harvest aflatoxin risk in peanut fields. This goal will be achieved through two primary objectives: 1) evaluate the correlation

between UAS-based thermal indices and aflatoxin contamination levels in peanuts, and 2) explore the potential of CWSI as a tool to map the spatial distribution of aflatoxin contamination risk within the fields. By establishing this relationship between water stress patterns and aflatoxin contamination, this study offers a foundation for the development of pre-harvest aflatoxin contamination risk areas to help growers mitigate aflatoxin development in irrigated fields and improve harvest logistics to prevent cross-contamination during harvest.

3.2.Materials and Methods

3.2.1. Study Sites

The study was conducted during 2023 and 2024, across five commercial peanut fields growing Georgia-06G cultivar located in southern Georgia, USA (Figure 3.1). The region is characterized by an arid subtropical climate with hot summers and mild winters. Table 3.2 summarizes the monthly rainfall and maximum air temperature recorded across five peanut fields during the 2023 growing season. Rainfall and temperature patterns followed typical regional trends, with higher rainfall during June and July and reduced precipitation toward the end of the season. Maximum air temperatures generally ranged between 32 °C and 41 °C, peaking in June and July across all sites before gradually declining through September and October. While total rainfall varied considerably among fields, temperature patterns remained consistent, indicating similar atmospheric conditions across locations during the growing period. The predominant soil type across all sites was sandy loam, typical of the region and well-suited for peanut cultivation. Each field was managed according to the respective grower's standard practices, following conventional production methods commonly used in the region.

Peanut planting dates for each field are presented in Table 3.3. Fields were planted between late April and early May during the 2023 and 2024 growing seasons. The fields were divided into

approximately 0.5-hectare plots that served as an experimental unit for data collection. Sampling points were established at the beginning of the study, where soil moisture sensors were also installed, and all plant sampling and physiological measurements were conducted around each sampling point.

3.2.2. Aflatoxin Mapping

To assess aflatoxin contamination levels at different stages during the season, plant samples were collected every two weeks starting at approximately 90 DAP until harvest. Three clusters of three to four plants, including roots and pods, were randomly collected around the georeferenced center points in each grid within the study fields during the pod development stage, which is critical for aflatoxin accumulation. Plant samples were subsequently taken to the laboratory, where pods were separated from vines, shelled, and sent to a laboratory for aflatoxin concentration analysis using the ELISA kit method (Kolosova et al., 2006). Aflatoxin sampling was done at four different dates in each field in both the 2023 and 2024 seasons.

The aflatoxin levels of sampling points were used to create interpolated aflatoxin risk maps. The interpolated maps were used only to represent the spatial distribution of potential areas of higher and lower aflatoxin risk, since actual aflatoxin contamination levels could not be analyzed in the entire field. Aflatoxin level was interpolated using ordinary kriging to create the interpolated aflatoxin risk map.

3.2.3. Physiological Measurements

Physiological measurements were conducted biweekly using a LI-600 porometer/fluorometer (LI-COR, Lincoln, NE, USA), coinciding with UAV flight dates to align ground-based and remotely sensed observations (Figure 3.2). Two peanut plants were selected per

plot around the sampling for physiological measurement. The LI-COR-600 mainly records stomatal conductance (g_s), photosystem II efficiency (Fv/Fm), electron transport rate (ETR), and leaf vapor pressure deficit (VPD). Measurements were made following the manufacturer's guidelines to ensure accuracy and consistency. Leaves were measured during midday as close to solar noon as possible in their original orientation under consistent ambient light (1000-2500 $\mu molm^{-2}s^{-1}$). Major leaf veins were avoided during the data collection process to ensure the instrument aperture was properly sealed and the reading was correct.

3.2.4. Soil Moisture Monitoring

Soil water status was continuously monitored using the UGA Smart Sensor Array system (UGA SSA), which records soil water tension (in kPa) at three depths: 10 cm, 20 cm, and 40 cm (Figure 3.3). Although soil water tension is negative, SWT values are shown on a positive scale to facilitate the interpretation of SWT response curves. The UGA SSA is a wireless soil moisture sensing system that also records soil temperature at 15-minute intervals, providing high-resolution temporal data (Vellidis et. al., 2013). This setup enabled the evaluation of soil water availability and thermal conditions, which are critical factors influencing plant physiological responses and aflatoxin development.

To analyze correlations between SWT and crop responses, the average SWT values per plot were calculated using three different timings: 1) average SWT values of the day before data collection, 2) average SWT from midnight to 6 am of the day of data collection, and 3) average SWT values during the period of data collection (flight time duration). Correlations between the average SWT values calculated based on the three different timings and stomatal conductance were analyzed to identify at which period leading to the canopy temperature data collection, the soil moisture would be most relevant.

3.2.5. Thermal Imagery Collection and Processing

Thermal and RGB images were simultaneously acquired using a DJI Matrice 300 RTK unmanned aerial vehicle (UAV) equipped with a Workswell WIRIS Pro SC thermal camera (Workswell, Prague, Czech Republic). The WIRIS Pro SC camera has a scientific grade radiometric thermal sensor with a thermal sensitivity of 30 millikelvin (mK) or 0.03° C, a thermal accuracy of ±2° C or ±2%, an infrared (IR) resolution of 640 x 512 pixels, a spectral range between 7.5 to 13.5 µm, and provides an average of 13 to 16 cm/pixel spatial resolution when flown at a 100 to 120-meter altitude (Table 3.1). The integrated RGB camera had a resolution of 1920 x 1080 pixels in full HD.

Flight plans settings for each field, such as altitude, speed, and course angle, were based on the thermal sensor specifications, and driven by field size, drone battery flight time, and duration of the flight to minimize temperature drift commonly seen in uncooled thermal cameras when flown for long periods. All flights were conducted on clear days, within 2 hours of solar noon (between 11:00 AM and 3:00 PM Eastern Standard Time) to minimize variability in thermal readings caused by diurnal changes, and used the same overlap of 85% to ensure higher quality on the stitching process. Before each flight, the camera was left on for an average of 20 minutes to allow for temperature stabilization with the environment and increased measurement accuracy (FLIR, 2020). UAV flights targeted frequency was every two weeks throughout the growing season, starting at 90 DAP, allowing for monitoring of temporal dynamics in Tc and water stress conditions. In some cases, flight frequency had to be changed due to weather conditions.

An initial analysis of individual thermal images captured during each flight was conducted using Thermolab (Workswell, Prague, Czech Republic) for the detection of any anomalies, such as blurry images, and sudden significant changes in Tc from images taken immediately after each

other. Subsequently, these images were stitched using Pix4Dmapper software (Pix4D Sa, Lausanne, Switzerland) to create a final reflectance map with pixel temperature data. The resulting reflectance maps were exported for further analysis in ArcGIS Pro (ESRI, Redlands, CA, USA) and R Studio (V.2025.05.1). Thermal reflectance maps were subjected to a supervised segmentation of UAV-derived RGB imagery to separate canopy and soil pixels using the Support Vector Machine (SVM) algorithm under the Image Classification Wizard function in ArcGIS Pro. Representative training samples of plant canopy and soil pixels were manually selected to train a random forest classifier. The resulting classified images were converted into binary vegetation masks, with canopy pixels assigned to a value of zero and non-canopy pixels to a value of one. These masks were co-registered with corresponding thermal images and applied to segment Tc by excluding background soil pixels (Figure 3.4). Mean Tc values were then extracted at the plot level using geo-referenced plot boundaries and within a 10-meter radius area around each sampling point (Figure 3.1).

3.2.6. Crop Water Stress

Peanut water stress was assessed in two different ways. The first approach was to use the differential temperature (ΔT), which is calculated by subtracting air temperature (Tair) from Tc at the time of the flight. Tair is used as a reference to represent crop water stress. If ΔT is positive, it means that the crop Tc is higher than Tair, and the crop is experiencing some level of water stress. Conversely, if ΔT is negative, it means that the crop canopy is cooler than the air temperature, indicating no water stress (Henson et al., 2006; Payares et al., 2025). The second approach is to calculate CWSI. Segmented images were used to compute the both the ΔT and CWSI following Idso (1982),

$$CWSI = \frac{T_c - T_{wet}}{T_{dry} - T_{wet}} \quad 1$$

where, Tc is the observed canopy temperature, T_{wet} is the temperature of a fully transpiring (non-stressed) canopy, and T_{dry} is the temperature of a non-transpiring (fully stressed) canopy. Because empirical wet and dry baselines have not been developed for peanuts, a theoretical approach to calculate the baselines was used. The theoretical CWSI was calculated based on the energy balance equation (H. Jones, 1992):

$$Tc - Ta = \frac{r_{HR} \times (r_{aW} + r_{lw}) \gamma R_{ni}}{\rho C_p [\gamma (r_{aW} + r_{lw}) + \Delta r_{HR}]} - \frac{r_{HR} \times VPD}{\gamma (r_{aW} + r_{lw}) + \Delta r_{HR}} \quad (2a)$$

where Tc-Ta is the differential temperature between canopy temperature and air temperature, R_{ni} is the net solar radiation, γ is the psychrometric constant, ρ is the density of air, C_p is the specific heat capacity of air, Δ is the slope of saturated vapor pressure to temperature, r_{HR} is the parallel resistance to heat and radiative transfer and r_{aw} is the boundary layer resistance to water vapor.

The upper limit of (Tc-Ta) was calculated when r_c is allowed to increase to infinity or without bound thus getting to Eq. (2b). The lower limit of (Tc-Ta) was established by assuming that the canopy resistance is equal to zero (i.e. $r_{cp} = 0$), where canopy transpiration is assumed to be equal to evaporation of a free water surface (Jackson et al., 1981, 1988).

$$(Tc - Ta)_U = \frac{r_{HR} \times R_{ni}}{\rho C_p} \quad (2b)$$

$$(Tc - Ta)_L = \frac{r_{HR} \times r_{aW} \times \gamma \times R_{ni}}{\rho C_p [\gamma (ra_W) + \Delta r_{HR}]} - \frac{r_{HR} \times VPD}{\gamma\, r_{aW} + \Delta r_{HR}} \quad (2c)$$

The parallel resistance to heat and radiative transfer (r_{HR}) was calculated as the harmonic mean of boundary layer resistance to the radiative transfer and heat transfer.

$$r_{aR} = \frac{\gamma C_p}{4\epsilon_c \sigma T^3} \quad (2d)$$

where, r_{aR} is boundary layer resistance to radiative transfer, ϵ_c is the emissivity of the vegetation and T is temperature (K)

$$r_{aH} = 100 \times \sqrt{\frac{d}{u}} \quad (2e)$$

where r_{aH} is the boundary layer resistance to heat transfer, d is the dimension of the leaf and u is the wind velocity.

$$r_{aw} = \frac{r_{aH}}{1.08} \quad (2f)$$

$$r_{HR} = \frac{r_{aR} \times r_{aH}}{r_{aR} + r_{aH}} \quad (2g)$$

3.2.7. Data Analysis

Exploratory data analysis were performed using Boxplot to visualize distribution and variability of data in each field. The approach was selected to evaluate and compare how soil moisture and crop physiological responses varied between fields, and to identify potential outliers. Correlations were analyzed using Spearman's correlation coefficient to assess correlations between CWSI, SWT, ΔT, and aflatoxin levels by field in each sampling date. Subsequently, regression models were developed between plot averages of selected SWT and CWSI and ΔT for dates in which correlations were higher. Coefficient of determination (R^2) (Equation 2), and root mean square error (RMSE) (Equation 3), were calculated to assess the relationship between crop responses and aflatoxin levels for plot averages.

$$R^2 = 1 - \frac{\sum(\hat{X}_i - X_i)^2}{\sum(X_i - \bar{X}_i)^2} \quad (2)$$

$$RMSE = \left[n^{-1} \sum_{i=1}^{n} (X_i - \bar{X}_i)^2 \right]^{1/2} \quad (3)$$

3.3. Results and Discussion

3.3.1. Weather Data

Weather variables were observed daily using in-field ATMOS41 weather stations and precipitation, maximum and minimum temperature trends for all fields during the 2023 and 2024 growing seasons (May – October) are shown in Figure 3.5. Cumulative rainfall exhibited substantial variation among fields, ranging from 492.54 mm in Field 1 to 860.1 mm in Field 4 (Table 3.2). According to the peanut production guide for Georgia, peanuts require an average of 457 mm of water (rainfall + irrigation) to achieve an acceptable yield (Porter, 2022). Both the 2023 and 2024 growing seasons were considered wet, with all fields receiving more than 457 mm of rainfall. However, rainfall was not uniform throughout the season, and short episodic drought events were observed in some fields, particularly due to the highly sandy soil with low water holding capacity observed in the Coastal Plains region (Pisani et al., 2020), in which fields are located. Rainfall for Field 1 was the most unevenly distributed throughout the season receiving 82.08 mm at early stage (before 40 DAP), and only 44.89 mm at late season (after 110 DAP). Fields 2 and 3 also received lower precipitation early in the season with 72.39 and 2.91 mm, respectively, but mid and late season rainfall amounts were greater. Fields 4 and 5 showed a more uniform rainfall distribution across the season with all critical stages receiving at least 190 mm of rain.

Since the fields are rainfed, the total rainfall and distribution are critical for crop water availability, particularly at periods of high temperatures. Inadequate or uneven rainfall induces periods of water stress. Fluctuation in air temperature further affects atmospheric water demand via vapor pressure deficit (VPD), influencing evapotranspiration. High daily temperatures increase VPD, which speeds up the loss of water from plants and soil, while cooler conditions lower water demand (Grossiord et al., 2020).

Aflatoxin contamination in peanuts is closely associated with hot and dry conditions close to the harvesting period (Bowen & Hagan, 2015). The growth of *Aspergillus* fungus and aflatoxin biosynthesis by the fungus is promoted by drought and elevated temperature during the pod development stage (Cotty & Jaime-Garcia, 2007). The extended period of dry spells during late season (90-130 DAP) is likely to increase aflatoxin risk.

3.3.2. Field Exploratory Analysis

The effect of different precipitation amounts and frequency between the 2023 and 2024 growing seasons was evident on the crop responses (Figure 3.6). Fields 1, 2, and 3 showed a lower variability in g_s values, but all fields exhibited conductance below 0.9 mol $m^{-2}s^{-1}$, while Fields 4 and 5 in 2024 had a higher variability with averages ranging from 0.01 to 2.36 mol $m^{-2}s^{-1}$ (Figure 3.6a). The lowest g_s values for all fields in 2023 were observed at late season after 110 DAP, while in the 2024 season, the lowest averages for fields 4 and 5 were observed from 50 to 70 DAP, after which the crop showed g_s averages above 1.0 mol $m^{-2}s^{-1}$. A similar trend was observed for the CWSI (Figure 3.6b) and the ΔT (Figure 3.6c). Fields in the 2023 growing season showed higher CWSI values and positive ΔT, indicating that the peanut canopy had higher temperature than the air temperature during data collection due to the plant being exposed to different levels of water stress (Jackson et al., 1981; Jones, 2004). Conversely, fields with low or negative ΔT values

indicate well-watered conditions and active transpiration. This can be observed in Fields 4 and 5 during the 2024 growing season. The strong correspondence between the two indices reinforces their effectiveness as complementary indicators of canopy water status and stress intensity under variable field conditions.

Despite some level of water stress being observed at different times during the growing season, the stress might not have been prolonged or severe enough to lead to higher in-field aflatoxin contamination (Figure 3.6d). An early work evaluated the correlation between stress duration and pre-harvest aflatoxin contamination and showed that an extensive water stress period of between 20 to 50 days at late season was needed for higher aflatoxin contamination (Sanders et al., 1985). Figure 3.6d shows the variability in aflatoxin across fields, and the temporal variation across sampling dates for each field shows that in both years, aflatoxin levels were relatively low across all sites (<3.5 ppb). According to the American Peanut Council, the limit in aflatoxin concentration in edible peanuts in the U.S. is 20 ppb, while in the European Union is 4 ppb (APC, 2020). Although the pre-harvest aflatoxin concentrations observed in these fields were considered low, depending on storage conditions such as moisture content, temperature, and relative humidity, contaminated peanuts may show increased concentration levels (Mbata et al., 2024) above legal limits.

3.3.3. Soil Water Tension and Stomatal Conductance

The relationships between the three SWT datasets using different timings to calculate plot average values, and g_s were analyzed across all five fields, as shown in Figure 3.7. The g_s values served as a physiological indicator of plant water status at the time of sampling. The results revealed a non-linear relationship, showing that g_s decreased as SWT tension increased. This decline represents a stomatal regulatory response to water stress, in which plants limit transpiration

to conserve water (Brodribb & Holbrook, 2003; Buckley, 2019; Pilon et al., 2018). When comparing the SWT average values calculated at different timings (whole day average of the previous day, midnight to 6 am of the sampling date, and during the sampling period), g_s values had a slightly stronger relationship with SWT at the time of data collection than the SWT previous day and the midnight to early morning averages. Physiologically, stomatal aperture responds rapidly to fluctuations in plant water status and atmospheric demand. Because the soil–plant–atmosphere continuum operates as a hydraulically integrated system, changes in soil water potential are transmitted to the leaves within minutes, leading to corresponding adjustments in leaf water potential and g_s. Experimental studies have shown that reductions in root-zone water potential can signal the plant shoot within 3 minutes, inducing changes in stomatal closure within 1.5 hours, with a complete closure achieved after 6 hours when soil water potential reached -0.8MPa (Christmann et al., 2007).

Georgia Coastal Plain soils can be highly variable, but they tend to be very sandy. Coarse-textured soils such as the Coastal Plain have low water retention and tend to dry rapidly after rainfall (Hanson et al., 2000), which may cause SWT fluctuations over short periods, especially under high evaporative demand. Consequently, in some situations, SWT measured concurrently with leaf gas exchange captures the most relevant hydraulic state affecting stomatal regulation at that moment compared to the SWT observations one day earlier or at early morning.

In addition, when soil was wet or at field capacity, g_s values showed little sensitivity to changes in SWT (Figure 3.7). The average SWT for Coastal Plain soils at field capacity ranges from 10 to 33 kPa (Hanson et al., 2000). These results can be seen in all fields, in which a higher variability in g_s values is observed when SWT is close to or below 33 kPA. In Field 4, very low g_s values were observed even in wet conditions. Soil moisture conditions in this field were wet

throughout the season, with an accumulated precipitation of around 860 mm and maintained near field-capacity moisture conditions. One possible explanation is that this field experienced waterlogging, creating reduced oxygen availability around the roots, which in turn lowered stomatal conductance even though the soil was not dry. This pattern is supported by research conducted by Zeng et al. (2020), which found the reduced g_s in leaves under waterlogging stress. As the soil began to dry, a decline in g_s occurred, as evidenced in the other fields. This reduction in g_s is due to the crop response mechanism to reduce water loss under stress conditions (Buckley, 2019; Comstock, 2002).

3.3.4. Soil Water Tension and Canopy Temperature

The sensitivity of CWSI and differential temperature (ΔT) to SWT was evaluated by fitting quadratic regression models, as well as assessing how the degree of water stress influenced the strength and direction of the relationship. Under conditions where average SWT remained below 50 kPa, the fitted quadratic regressions indicated very weak relationships ($R^2 = 0.19$ in Field 4 and $R^2 = 0.12$ in Field 5) (Figure 3.8). This suggests that UAS-based CWSI is largely unaffected by changes in SWT when soil moisture is non-limiting. This response is expected near or below field capacity, which typically corresponds to values of approximately 10-33 kPa in sandy to loamy soils of the southeastern US (Lena et al., 2021). Under this condition, changes in CWSI are more likely driven by microclimatic variability, wind speed, rather than true soil moisture availability. Previous studies have shown that high wind speeds (>6 ms^{-1}) can reduce stomatal conductance and transpiration even when soil water is sufficient, resulting in elevated canopy temperatures and artificially high CWSI values (Han et al., 2018; King et al., 2021).Han In contrast, stronger relationships were observed in Fields 2 and 3 ($R^2 = 0.71$ and 0.56, respectively), where SWT values extended well beyond 50 kPa. Excluding field 1, CWSI tended to increase with increased SWT,

indicating that as soil water availability declined, canopy temperature increased in response to stomatal closure and reduced transpiration (Jones, 1999; Katimbo et al., 2022).

Although similar relationships were observed between ΔT and SWT (Figure 3.9), the relationship between these two variables was not as strong as CWSI. Fields 1, 2, and 3 had R^2 values of 0.25, 0.13, and 0.47, respectively, while in 2024, fields 4 and 5 had R^2 values of 0.18 and 0.19, respectively. Field ΔT values were more scattered around the line of best fit than CWSI. These results are most likely associated with the use of meteorological data such as solar radiation, wind speed, and air humidity in the calculation and normalization of CWSI (Gonzalez-Dugo et al., 2024; Liu et al., 2024), which is not considered in the calculation of ΔT. Overall, these results show that while CWSI effectively captures crop water stress under moderate to severe soil drying, it is not reliable when the soil is well watered, when other factors have a stronger effect than soil water status.

3.3.5. Correlations Between Thermal Indices and Aflatoxin

The correlation matrices between aflatoxin concentration and thermal indices are presented in Figure 3.10. Overall, aflatoxin levels tended to show moderate positive correlation with canopy temperature indicators (CWSI and ΔT), though the strength of these correlations varied among fields and sampling dates. The correlation coefficients between aflatoxin concentration and CWSI and ΔT were the same for the same dates, indicating that the inclusion of weather variables in the calculation and normalization of CWSI did not affect how well CWSI correlated with aflatoxin compared to ΔT.

Two UAS flights were conducted in Field 1 at 99 and 131 DAP, both during a period of low precipitation. From 80 to 105 DAP, minimal rainfall was recorded. After 105 DAP, no rainfall

was recorded until 118 DAP. The highest correlations were observed between ΔT and CWSI collected at 131 DAP and aflatoxin at 126 DAP (r = 0.58), indicating that canopy temperature during the late pod-filling stage can serve as an indication of aflatoxin contamination (Figure 3.10a). In Field 2, two UAS flights were conducted at 98 and 112 DAP. The field experienced drought from 97 to 115 DAP and continued to have drought conditions with low rainfall at a later stage of growth, conducive to the fungal invasion and aflatoxin contamination. The highest correlation was observed between both ΔT and CWSI measured during the onset of drought (98 DAP) and aflatoxin levels close to harvest (139 DAP), with an r value of 0.79 (Figure 3.10b). Field 3 exhibited a similar pattern, with the highest correlation between ΔT and CWSI at 108 DAP and aflatoxin level at 155 DAP (r = 0.63), followed by CWSI and ΔT collected at 127 DAP and aflatoxin concentration at 125 DAP (r = 0.51) (Figure 3.10c). Among the three UAS flights in these fields, only the flight at 108 DAP was conducted during a period of prolonged drought from 96 to 110 DAP, which may explain the higher correlation with aflatoxin concentration. Rain was consistent before the first flight, which affected the representation of stress in the field, while for the third flight, rain was received a couple of days prior to data collection, but the rain accumulation was lower.

In contrast, Fields 4 and 5 experienced a more uniformly distributed rainfall (Figure 3.5), resulting in weaker ΔT and CWSI and aflatoxin correlations, particularly because the crop did not experience stress throughout the season, and was not exhibiting stress during the thermal data collection (Figures 3.10d-e). The highest correlation observed in Field 4 was between CWSI and ΔT collected at 137 DAP and aflatoxin level at 124 DAP (r = 0.38), while in Field 5, negative correlations were observed between crop water stress indicators and aflatoxin. Although correlation coefficients between aflatoxin concentration at the end of the season and UAV-based

data at 120 DAP were high (r=-0.63), the high negative correlation can be attributed to the low number of data points available in this field, and to the low overall aflatoxin concentrations ranging from 0 to 2 ppb. CWSI values ranged between 0.10 and 0.20, with only one plot with a value higher than 0.2 (Figure 3.11). These factors led to a higher negative correlation, which most likely does not represent the true correlation between aflatoxin concentration and crop water stress, as observed in most of the other fields.

Drought at later stages of peanut growth not only reduces yield components but also enhances susceptibility of pods to *Aspergillus* invasion (Wotton & Strange, 1987). Aminou et al. (2024) reported up to a 55% increase in aflatoxin contamination under late-season water deficit. Martins et al. (2023) evaluated the effects of harvest timing on pre-harvest aflatoxin concentration in peanuts exposed to water stress. Results from this study demonstrated that when water deficit persisted during the late stage of pod development and maturation, aflatoxin level increased substantially. However, harvesting the crop at least two weeks earlier helped keep contamination at lower levels than peanuts harvested at an ideal time. These studies highlight that terminal drought increases pre-harvest aflatoxin risk. It is worth highlighting that, compared to other studies, pre-harvest aflatoxin levels in the fields used in this study were very low. The discrepancy in correlation strength and direction across fields may arise from environmental factors besides moisture stress. Plant samples within each plot were randomly collected around the sampling point, which most likely caused the variation in aflatoxin levels from plot to plot. Furthermore, the research was conducted in farmers' fields, and no artificial inoculation of *Aspergillus* was performed in any field. Despite having some period of drought near harvesting time that favors the fungus growth, and aflatoxin contamination was observed in some fields, the stress was not severe or prolonged enough to lead to the development of higher contamination levels. The low levels

could also be attributed to the random sampling of plants from a 10 m buffer area potentially leading to sampling plants that were not representative of the highest aflatoxin contamination levels.

3.3.6. Spatial Variability of Interpolated Aflatoxin and Crop Water Stress Maps

Regression models between CWSI and aflatoxin concentration values were developed for fields and dates that showed the highest correlations (Figure 3.11). Despite CWSI and ΔT values showing similar correlation values with aflatoxin, CWSI was ultimately selected due to its stronger relationship with SWT. Fields 1 to 4 showed a positive relationship between aflatoxin and CWSI, in which aflatoxin concentration increased with increases in water stress. Field 5 showed an opposite relationship, with aflatoxin contamination decreasing with increased CWSI, with an R^2 of 0.83. However, as aforementioned, this field had a very low number of points available for analysis. The observed negative relationship between aflatoxin and CWSI is largely driven by a single data point. For the remaining fields, Field 2 showed the strongest relationship with a R^2 value of 0.65, followed by Fields 4 (R^2= 0.35), 3, and 1 (R^2= 0.33).

The relationship between aflatoxin levels and CWSI in all 5 fields combined is shown in Figure 3.11-f. Although CWSI explained only 37% of the aflatoxin level variability, the positive relationship between the two variables is evident. This positive relationship has been reported by recent work conducted on peanuts in 2024 (Aminou et al., 2024). Similarly, Martins et al. (2023) also found increased aflatoxin levels in peanuts, from 42 $\mu g kg^{-1}$ in no stress conditions to 316 $\mu g\ kg^{-1}$ (moderate) and 696 $\mu g\ kg^{-1}$(severe) in a greenhouse setting. Increased aflatoxin contamination due to drought stress was also reported in corn (Kebede et al., 2012). Sibakwe et al. (2017) found that a prolonged drought of four weeks significantly increased aflatoxin contamination (22.0 ppb) and fungus population as compared to non-stressed conditions (1.5 ppb).

The low coefficient of determination achieved in this study can be attributed to the overall low aflatoxin contamination levels observed in the two growing seasons. However, under higher inoculum pressure and prolonged drought conditions, it is expected that CWSI can show a stronger relationship with aflatoxin contamination levels. Furthermore, the low range of aflatoxin levels prevented the classification of CWSI ranges to represent low, moderate, and high aflatoxin risk. Nonetheless, interpolated aflatoxin risk maps based on the point aflatoxin contamination values were developed using ordinary kriging and compared to CWSI maps (Figure 3.12). Interpolated aflatoxin and CWSI maps were created for Fields 1 and 2. Field 4 had a very low range in CWSI values, all below 0.4, while Field 3 showed a very small variability in aflatoxin levels. Therefore, maps were not generated for these two fields. It is possible to observe that the overall spatial variability in CWSI was similar to how aflatoxin risk variability changed across the field, with higher aflatoxin risk observed in areas in which the crop showed higher stress.

3.4. Conclusions

This study investigated the potential of using UAS-based thermal images to assess the field spatial variability of crop water status and to compare it to the variability in pre-harvest aflatoxin contamination in commercial peanut fields. Results showed that higher canopy temperature and CWSI resonated with higher aflatoxin levels, with the highest R^2 (0.65) achieved in field 2. When comparing ΔT and CWSI, the latter showed a stronger relationship with soil moisture, since it takes into account weather conditions at the time of data collection, such as wind speed, relative humidity, and radiation. The highest R^2 between CWSI and SWT was observed for field 2 with a value of 0.71, followed by field 3 with an R^2 of 0.56. Correlation analysis between CWSI and aflatoxin suggests that fields experiencing drought during the season may predispose the crop to contamination; however, drought needs to be severe and extended to lead to contamination values

considered moderate to high. Results also showed that higher correlations between CWSI were observed with aflatoxin contamination levels from late-season samples, near harvest.

Despite aflatoxin contamination and CWSI being correlated, and that CWSI can explain some of the variability in preharvest aflatoxin, higher contamination levels are needed for the identification of thresholds for low, moderate, and high-risk areas and for the delineation of risk zones. Overall, this study shows that UAV-based thermal imagery collected during drought periods can be used to represent potential areas of aflatoxin risk. This approach demonstrates the potential to identify aflatoxin risk zones using a rapid nondestructive method, provided higher contamination levels can be observed.

3.5. References

Adeyemi, O., Grove, I., Peets, S., & Norton, T. (2017). Advanced monitoring and management systems for improving sustainability in precision irrigation. In *Sustainability (Switzerland)* (Vol. 9, Issue 3). MDPI. https://doi.org/10.3390/su9030353

Alameri, M. M., Kong, A. S. Y., Aljaafari, M. N., Ali, H. Al, Eid, K., Sallagi, M. Al, Cheng, W. H., Abushelaibi, A., Lim, S. H. E., Loh, J. Y., & Lai, K. S. (2023). Aflatoxin Contamination: An Overview on Health Issues, Detection and Management Strategies. *Toxins 2023, Vol. 15, Page 246*, *15*(4), 246. https://doi.org/10.3390/TOXINS15040246

Aminou, M. M., Falalou, H., Abdou, H., & Mendu, V. (2024). Aflatoxin B1 Contamination Association with the Seed Coat Biochemical Marker Polyphenol in Peanuts Under Intermittent Drought. *Journal of Fungi*, *10*(12), 850. https://doi.org/10.3390/JOF10120850/S1

APC. 2020. Aflatoxin limits in peanuts and peanut products as of April 15, 2020. American Peanut Council

Bowen, K. L., & Hagan, A. K. (2015). Temperature and Moisture Conditions That Affect Aflatoxin Contamination of Peanuts. *Peanut Science*, *42*(2), 121–127. https://doi.org/10.3146/0095-3679-42.2.121

Brodribb, T. J., & Holbrook, N. M. (2003). Stomatal closure during leaf dehydration, correlation with other leaf physiological traits. *Plant Physiology*, *132*(4). https://doi.org/10.1104/pp.103.023879

Buckley, T. N. (2019). How do stomata respond to water status? *New Phytologist*, *224*(1), 21–36. https://doi.org/10.1111/NPH.15899

Butts, C. L. & Lamb, M. & Zimmer, K. & Santos, R. & Hoisington, D. & Adams, J. & Cowart, D. & Tillman, B. & Kemerait, R. & Marshall, J. & Jackson, M. & Davis, J. & Sterling, S. & Elder, J., (2023) "U.S. Peanut Quality: Industry Priorities to Mitigate Aflatoxin Risk from Farm to Consumer", *Peanut Science* 50(1), p.29-40. doi: https://doi.org/10.3146/0095-3679-501-PS22-15

Caruso, G., Palai, G., Tozzini, L., & Gucci, R. (2022). Using Visible and Thermal Images by an Unmanned Aerial Vehicle to Monitor the Plant Water Status, Canopy Growth and Yield of Olive Trees (cvs. Frantoio and Leccino) under Different Irrigation Regimes. *Agronomy*, *12*(8). https://doi.org/10.3390/agronomy12081904

Christmann, A., Weiler, E. W., Steudle, E., & Grill, E. (2007). A hydraulic signal in root-to-shoot signalling of water shortage. *The Plant Journal*, *52*(1), 167–174. https://doi.org/10.1111/J.1365-313X.2007.03234.X

Comstock, J. P. (2002). Hydraulic and chemical signalling in the control of stomatal conductance and transpiration. *Journal of Experimental Botany*, *53*(367), 195–200. https://doi.org/10.1093/JEXBOT/53.367.195

Cotty, P. J., & Jaime-Garcia, R. (2007). Influences of climate on aflatoxin producing fungi and aflatoxin contamination. *International Journal of Food Microbiology*, *119*(1–2). https://doi.org/10.1016/j.ijfoodmicro.2007.07.060

Eskola, M., Kos, G., Elliott, C. T., Hajšlová, J., Mayar, S., & Krska, R. (2020). Worldwide contamination of food-crops with mycotoxins: Validity of the widely cited 'FAO estimate' of 25%. *Critical Reviews in Food Science and Nutrition*, *60*(16), 2773–2789. https://doi.org/10.1080/10408398.2019.1658570

European Commission. (2021). Aflatoxins - Food safety, Retrieved October 10, 2025, from https://food.ec.europa.eu/food-safety/chemical-safety/contaminants/catalogue/aflatoxins_en

Gonzalez-Dugo, V., & Zarco-Tejada, P. J. (2024). Assessing the impact of measurement errors in the calculation of CWSI for characterizing the water status of several crop species. *Irrigation Science*, *42*(3), 431–443. https://doi.org/10.1007/s00271-022-00819-6

Grossiord, C., Buckley, T. N., Cernusak, L. A., Novick, K. A., Poulter, B., Siegwolf, R. T. W., Sperry, J. S., & McDowell, N. G. (2020). Plant responses to rising vapor pressure deficit. *New Phytologist*, *226*(6), 1550–1566. https://doi.org/10.1111/NPH.16485

Hamidou, F., Rathore, A., Waliyar, F., & Vadez, V. (2014). Although drought intensity increases aflatoxin contamination, drought tolerance does not lead to less aflatoxin contamination. *Field Crops Research*, *156*, 103–110. https://doi.org/10.1016/j.fcr.2013.10.019

Han, M., Zhang, H., DeJonge, K. C., Comas, L. H., & Gleason, S. (2018). Comparison of three crop water stress index models with sap flow measurements in maize. *Agricultural Water Management*, *203*, 366–375. https://doi.org/10.1016/J.AGWAT.2018.02.030

Hanson, B. R., Orloff, S., & Peters, D. (2000). Monitoring soil moisture helps refine irrigation management. *California Agriculture*, *54*(3), 38–42. https://doi.org/10.3733/CA.V054N03P38

Henson, D. Y., Newman, S. E., & Hartley, D. E. (2006). Performance of Selected Herbaceous Annual Ornamentals Grown at Decreasing Levels of Irrigation. *HortScience*, *41*(6), 1481–1486. https://doi.org/10.21273/HORTSCI.41.6.1481

Horn, B. W. (2005). Colonization of wounded peanut seeds by soil fungi: selectivity for species from Aspergillus section Flavi. *Mycologia*, *97*(1), 202–217. https://doi.org/10.3852/MYCOLOGIA.97.1.202

Idso, S. B., Idso, & B., S. (1982). Non-water-stressed baselines: A key to measuring and interpreting plant water stress. *AgMet*, *27*(1), 59–70. https://doi.org/10.1016/0002-1571(82)90020-6

Ihuoma, S. O., & Madramootoo, C. A. (2017). Recent advances in crop water stress detection. In *Computers and Electronics in Agriculture* (Vol. 141, pp. 267–275). Elsevier B.V. https://doi.org/10.1016/j.compag.2017.07.026

Jackson, R. D., Idso, S. B., Reginato, R. J., & Pinter, P. J. (1981). Canopy temperature as a crop water stress indicator. *Water Resources Research*, *17*(4), 1133–1138. https://doi.org/10.1029/WR017i004p01133

Jackson, R. D., Kustas, W. P., & Choudhury, B. J. (1988). A reexamination of the crop water stress index. *Irrigation Science*, *9*(4), 309–317. https://doi.org/10.1007/BF00296705/METRICS

Jones, H. (1992). *Plants and microclimate, a quantitative approach to environmental plant physiology, Hamlyn G. Jones*. Retrieved March 23, 2025, from https://www.academia.edu/18193900/Plants_and_microclimate_a_quantitative_approach_to_environmental_plant_physiology_Hamlyn_G_Jones

Jones, H. G. (1999). Use of infrared thermometry for estimation of stomatal conductance as a possible aid to irrigation scheduling. *Agricultural and Forest Meteorology*, *95*(3). https://doi.org/10.1016/S0168-1923(99)00030-1

Jones, H. G. (2004). Irrigation scheduling: Advantages and pitfalls of plant-based methods. *Journal of Experimental Botany*, *55*(407). https://doi.org/10.1093/jxb/erh213

Katimbo, A., Rudnick, D. R., DeJonge, K. C., Lo, T. H., Qiao, X., Franz, T. E., Nakabuye, H. N., & Duan, J. (2022). Crop water stress index computation approaches and their sensitivity to soil water dynamics. *Agricultural Water Management*, *266*. https://doi.org/10.1016/j.agwat.2022.107575

Kebede, H., Abbas, H. K., Fisher, D. K., & Bellaloui, N. (2012). Relationship between aflatoxin contamination and physiological responses of corn plants under drought and heat stress. *Toxins*, *4*(11), 1385–1403. https://doi.org/10.3390/toxins4111385

Khorsandi, A., Hemmat, A., Mireei, S. A., Amirfattahi, R., & Ehsanzadeh, P. (2018). Plant temperature-based indices using infrared thermography for detecting water status in sesame under greenhouse conditions. *Agricultural Water Management*, *204*, 222–233. https://doi.org/10.1016/j.agwat.2018.04.012

Kim, J. Y., & Glenn, D. M. (2017). Multi-modal sensor system for plant water stress assessment. *Computers and Electronics in Agriculture*, *141*, 27–34. https://doi.org/10.1016/J.COMPAG.2017.07.009

King, B. A., Tarkalson, D. D., Sharma, V., & Bjorneberg, D. L. (2021). Thermal Crop Water Stress Index Base Line Temperatures for Sugarbeet in Arid Western U.S. *Agricultural Water Management*, *243*. https://doi.org/10.1016/j.agwat.2020.106459

Kolosova, A. Y., Shim, W. B., Yang, Z. Y., Eremin, S. A., & Chung, D. H. (2006). Direct competitive ELISA based on a monoclonal antibody for detection of aflatoxin B1. Stabilization of ELISA kit components and application to grain samples. *Analytical and Bioanalytical Chemistry*, *384*(1), 286–294. https://doi.org/10.1007/S00216-005-0103-9,

Lavkor, I., & Var, I. (2017). The control of aflatoxin contamination at harvest, drying, pre-storage and storage periods in peanut: The new approach. Aflatoxin-control, analysis, detection and health risks, 45-64.

Lena, B., Bondesan, L., Ortiz, B., Morata, G., Kumar, H. (2021). Irrigation scheduling using soil water tension sensors - *Alabama Cooperative Extension System*. Retrieved November 18, 2025, from https://www.aces.edu/blog/topics/crop-production/irrigation-scheduling-using-soil-water-tension-sensors

Liu, H., Song, W., Lv, J., Gui, R., Shi, Y., Lu, Y., Li, M., Chen, L., & Chen, X. (2024). Precise Drought Threshold Monitoring in Winter Wheat Using the Unmanned Aerial Vehicle Thermal Method. *Remote Sensing 2024, Vol. 16, Page 710*, *16*(4), 710. https://doi.org/10.3390/RS16040710

Martins, L. M., Bragagnolo, N., Calori, M. A., Iamanaka, B. T., Alves, M. C., da Silva, J. J., de Godoy, I. J., & Taniwaki, M. H. (2023). Assessment of early harvest in the prevention of aflatoxins in peanuts during drought stress conditions. *International Journal of Food Microbiology*, *405*. https://doi.org/10.1016/j.ijfoodmicro.2023.110336

Mbata, G.N., Danso J.K., Holton, R.L. Peanut aflatoxin: Impact of postharvest insect infestation and storage systems. Insects. 2024 Oct 25;15(11):836. doi: 10.3390/insects15110836

Nji, Q. N., Babalola, O. O., & Mwanza, M. (2023). Soil Aspergillus Species, Pathogenicity and Control Perspectives. *Journal of Fungi*, *9*(7), 766. https://doi.org/10.3390/JOF9070766

Payares, L. K. A., Gomez-Del-Campo, M., Tarquis, A. M., & García, M. (2025). *Thermal imaging from UAS for estimating crop water status in a Merlot vineyard in semi-arid conditions*. *43*, 87–103. https://doi.org/10.1007/s00271-024-00955-1

Pilon, C., Snider, J. L., Sobolev, V., Chastain, D. R., Sorensen, R. B., Meeks, C. D., Massa, A. N., Walk, T., Singh, B., & Earl, H. J. (2018). Assessing stomatal and non-stomatal limitations to carbon assimilation under progressive drought in peanut (Arachis hypogaea L.). *Journal of Plant Physiology*, *231*. https://doi.org/10.1016/j.jplph.2018.09.007

Pisani, O., Liebert, D., Bosch, D. D., Coffin, A. W., Endale, D. M., Potter, T. L., & Strickland, T. C. (2020). Element losses from fields in conventional and conservation tillage in the Atlantic Coastal Plain, Georgia, United States. *Journal of Soil and Water Conservation*, *75*(3), 376–386. https://doi.org/10.2489/JSWC.75.3.376

Porter, W. M. (2022). *Water Use and Relationship in Peanut Production in Peanut Production Guide*. University of Georgia Extension.

Puppala, N., Nayak, S. N., Sanz-Saez, A., Chen, C., Devi, M. J., Nivedita, N., Bao, Y., He, G., Traore, S. M., Wright, D. A., Pandey, M. K., & Sharma, V. (2023). Sustaining yield and nutritional quality of peanuts in harsh environments: Physiological and molecular basis of drought and heat stress tolerance. *Frontiers in Genetics*, *14*, 1121462. https://doi.org/10.3389/FGENE.2023.1121462

Rahmani, A., Jinap, S., & Soleimany, F. (2009). Qualitative and quantitative analysis of mycotoxins. *Comprehensive Reviews in Food Science and Food Safety*, *8*(3). https://doi.org/10.1111/j.1541-4337.2009.00079.x

Sanders, T. H., Cole1, R. J., Blankenship', P. D., & Hill2, R. A. (1985). Relation of Environmental Stress Duration to Aspergillus flavus Invasion and Aflatoxin Production in Preharvest Peanuts. *Peanut Science*, *12*(2), 90–93. https://doi.org/10.3146/PNUT.12.2.0011

Shabeer, S., Asad, S., Jamal, A., & Ali, A. (2022). Aflatoxin Contamination, Its Impact and Management Strategies: An Updated Review. In *Toxins* (Vol. 14, Issue 5). https://doi.org/10.3390/toxins14050307

Sibakwe, C. B., Kasambara-Donga, T., Njoroge, S. M. C., Msuku, W. A. B., Mhango, W. G., Brandenburg, R. L., & Jordan, D. L. (2017). The Role of Drought Stress on Aflatoxin Contamination in Groundnuts (Arachis hypogea L.) and Aspergillus flavus Population in the Soil. *Modern Agricultural Science and Technology*, *3*(3), 22–29. https://doi.org/10.15341/mast(2375-9402)/03.03.2017/005

Stutsel, B., Johansen, K., Malbéteau, Y. M., & McCabe, M. F. (2021). Detecting Plant Stress Using Thermal and Optical Imagery From an Unoccupied Aerial Vehicle. *Frontiers in Plant Science*, *12*, 734944. https://doi.org/10.3389/FPLS.2021.734944/FULL

Torres, A. M., Barros, G. G., Palacios, S. A., Chulze, S. N., & Battilani, P. (2014). Review on pre- and post-harvest management of peanuts to minimize aflatoxin contamination. *Food Research International*, *62*, 11–19. https://doi.org/10.1016/J.FOODRES.2014.02.023

Usamentiaga, R., Venegas, P., Guerediaga, J., Vega, L., Molleda, J., & Bulnes, F. G. (2014). Infrared thermography for temperature measurement and non-destructive testing. In *Sensors (Switzerland)* (Vol. 14, Issue 7). https://doi.org/10.3390/s140712305

Vellidis, G., Tucker, M., Perry, C., Reckford, D., Butts, C., Henry, H., ... & Edwards, W. (2013). A soil moisture sensor-based variable rate irrigation scheduling system. In Precision agriculture'13 (pp. 713-720). Wageningen Academic.

Wotton, H. R., & Strange, R. N. (1987). Increased susceptibility and reduced phytoalexin accumulation in drought-stressed peanut kernels challenged with Aspergillus flavus. *Applied and Environmental Microbiology*, *53*(2), 270–273. https://doi.org/10.1128/AEM.53.2.270-273.1987

Yu, J. (2012). Current understanding on aflatoxin biosynthesis and future perspective in reducing aflatoxin contamination. In *Toxins* (Vol. 4, Issue 11). https://doi.org/10.3390/toxins4111024

Zeng, R., Chen, L., Wang, X., Cao, J., Li, X., Xu, X., Xia, Q., Chen, T., & Zhang, L. (2020). Effect of Waterlogging Stress on Dry Matter Accumulation, Photosynthesis Characteristics, Yield, and Yield Components in Three Different Ecotypes of Peanut (Arachis hypogaea L.). *Agronomy*, *10*(9), 1244. https://doi.org/10.3390/agronomy10091244

TABLES AND FIGURES

Table 3.1. UAV flight specifications for peanut fields in years 2023 and 2024.

Flight specifications	**Sites**				
	Field 1	**Field 2**	**Field 3**	**Field 4**	**Field 5**
Altitude (m)	120	120	100	120	100
GSD (cm/pixel)	15.69	15.69	13.08	15.69	13.08
Takeoff speed (m/s)	10	8.3	10	10	10
Speed (m/s)	7.9	8	6.6	8	6.6
Course Angle	75 º	181º	88 º	1 º	177 º
Side overlap (%)	85	85	85	85	85
Frontal Overlap (%)	85	85	85	85	85

Table 3.2 Total precipitation, at different peanut growth stages (early season: emergency -40 DAP, mid-season: 40-110 DAP, and late season: 110-harvest) of five fields across 2023 and 2024.

	Precipitation (mm)			
Site	**Early Season**	**Mid-Season**	**Late Season**	**Total**
Field 1	82.08	365.57	44.89	492.54
Field 2	72.39	372.51	285.61	730.51
Field 3	2.91	335.30	308.20	646.41
Field 4	246.92	355.69	257.52	860.13
Field 5	192.11	232.41	279.35	703.87

Table 3.3. Planting dates of peanut fields during 2023 and 2024 growing seasons.

Year	**Field**	**Planting Date**
2023	Field 1	May 4. 2023
	Field 2	May 4, 2023
	Field 3	May 9, 2023
2024	Field 4	May 3, 2024
	Field 5	April 29, 2024

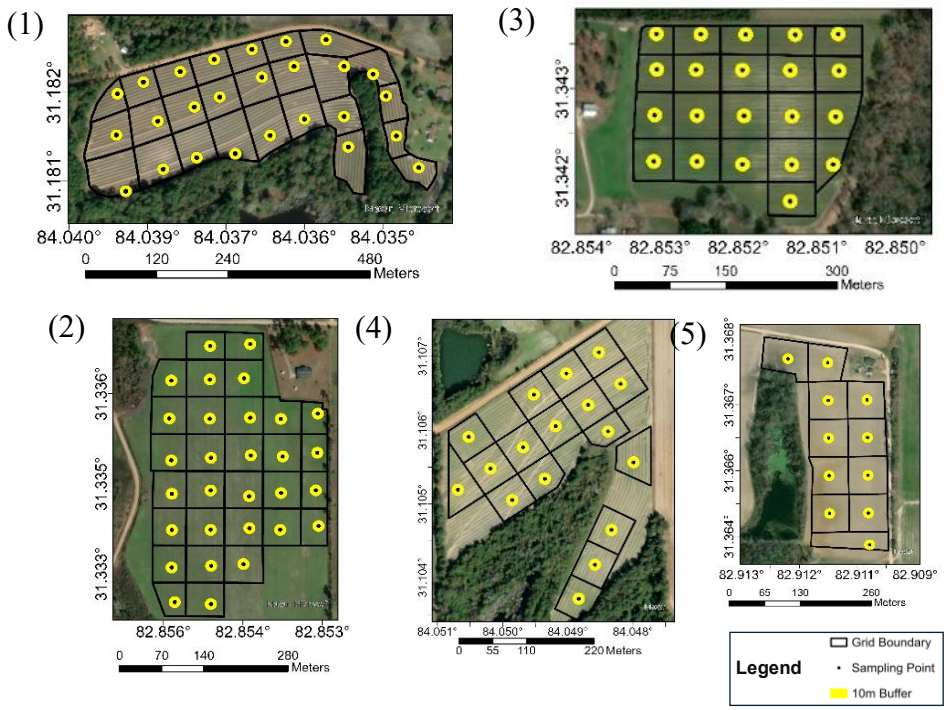

Figure 3.2. Commercial peanut fields for 2023 (Fields 1-3) and 2024 (Fields 4-5). The rectangular boxes in the field indicate grid boundaries, black dots mark sampling points, and the yellow circles denote a 10-meter buffer area around each sampling point.

Figure 3.2. Measurement of physiological parameters of peanut using LI-600 porometer/fluorometer.

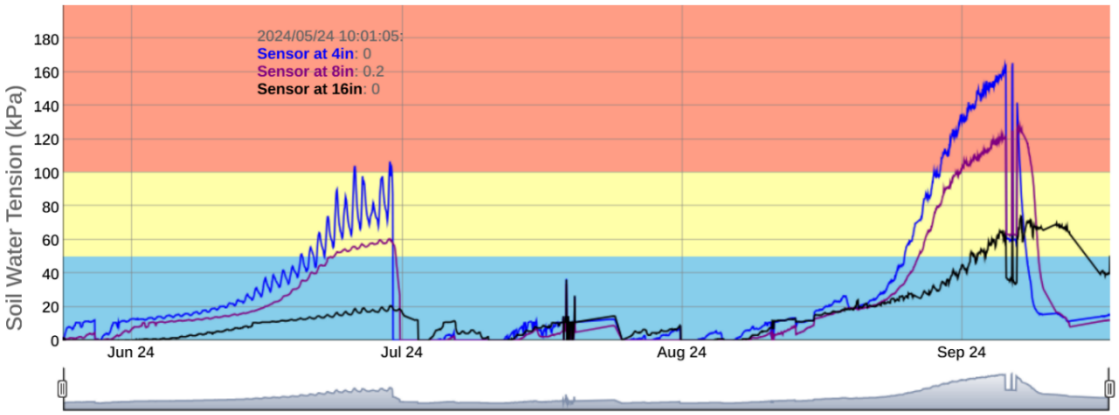

Figure 3.3. Soil Water Tension response curve from one selected plot throughout the 2024 growing season.

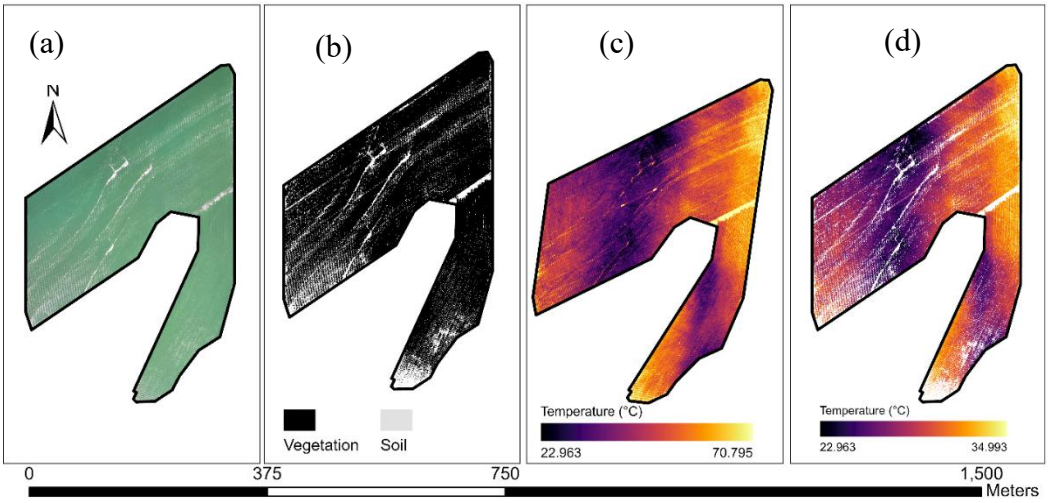

Figure 3.4. Image segmentation for canopy temperature extraction, with the original UAV-derived RGB image (a), binary vegetation mask generated via supervised classification to distinguish plant canopy from soil (b), original UAV-derived Thermal image (c) and segmented thermal image showing canopy temperature after applying the vegetation mask (d).

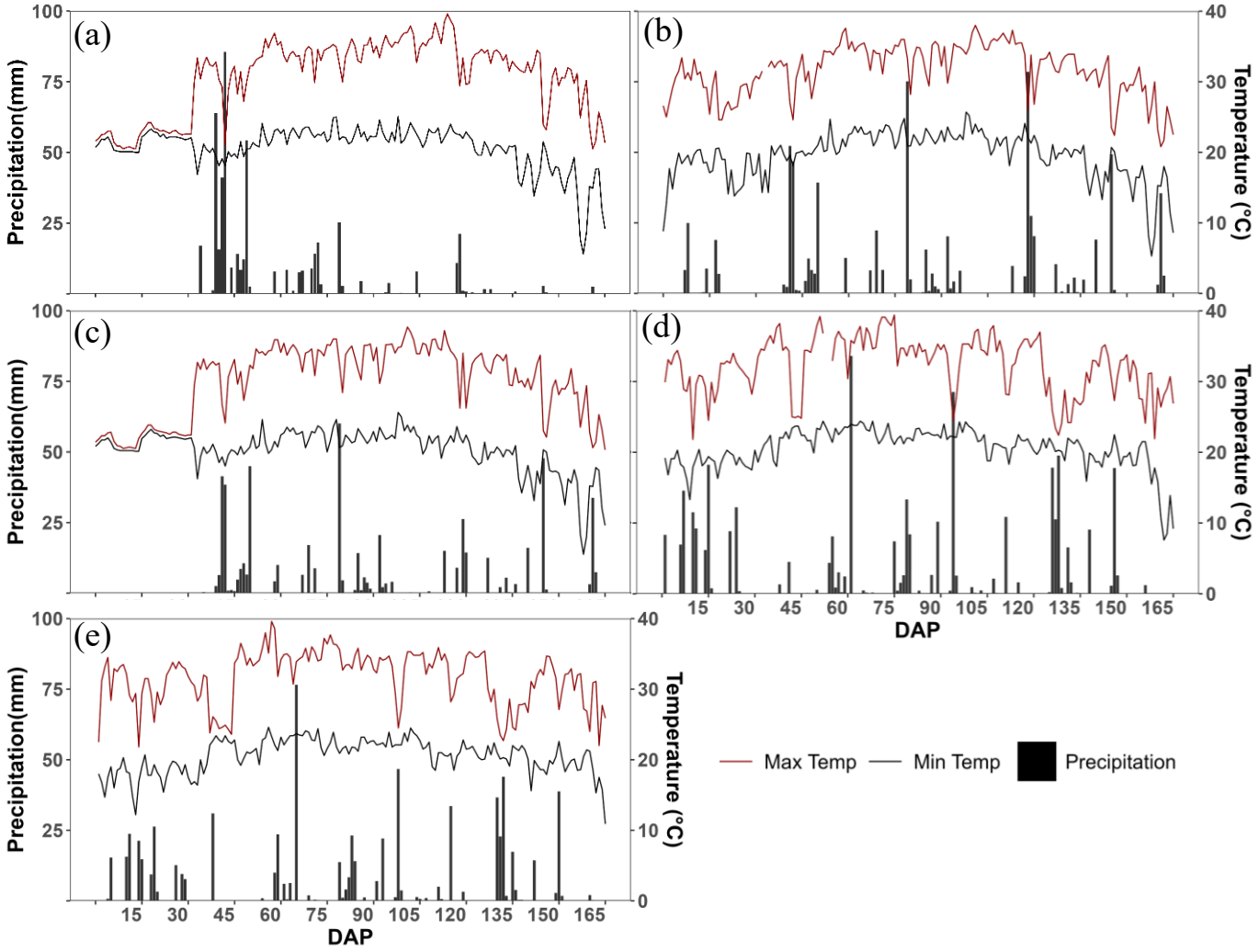

Figure 3.5. Weather variables during the peanut growing season across fields 1 (a), 2 (b) and 3 (c) in 2023 and 4 (d) and 5 (e) in 2024. Red lines indicate maximum daily temperature (°C), black lines indicate minimum daily temperature (°C), and black bars represent daily precipitation (mm).

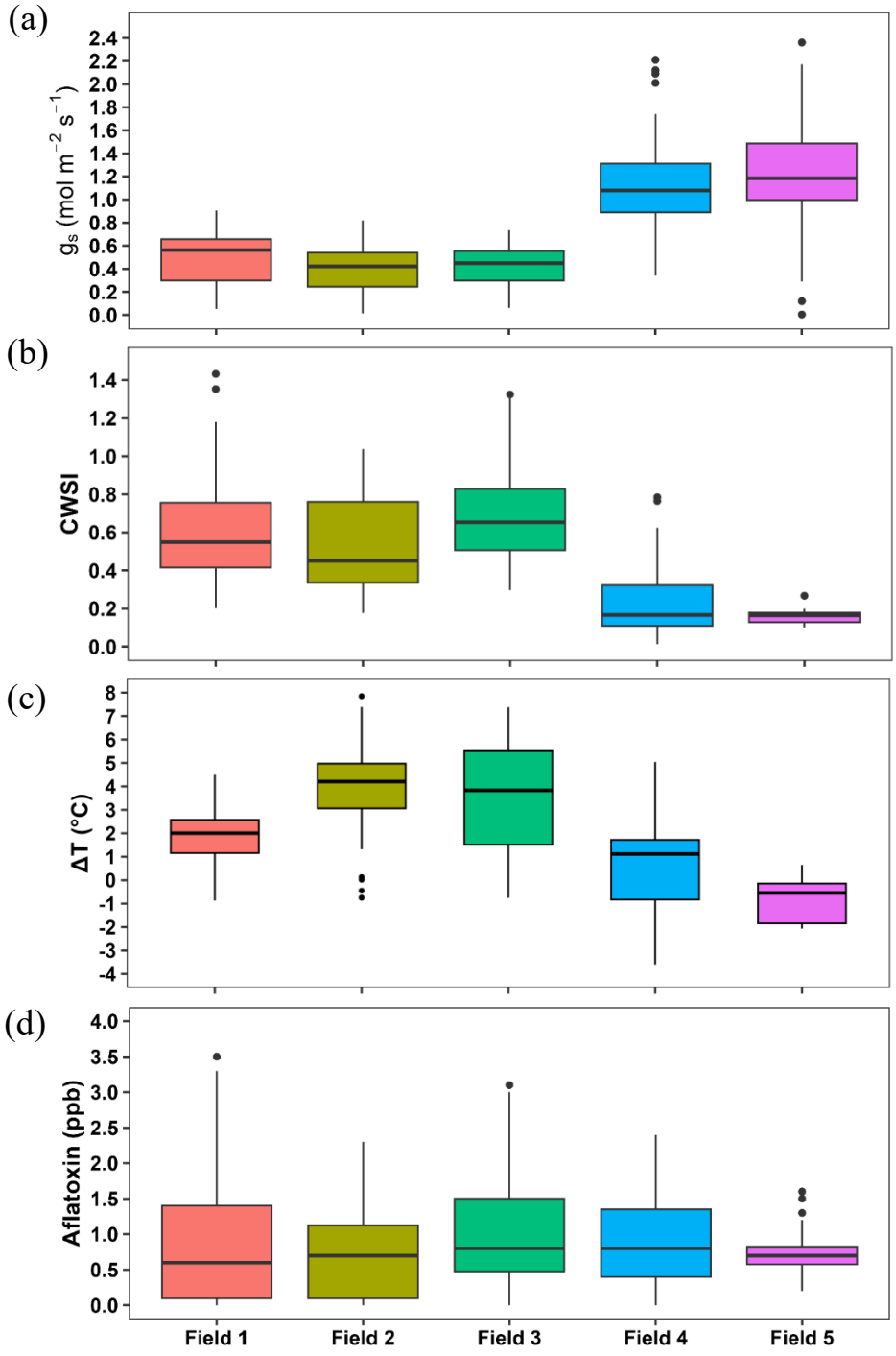

Figure 3.6. Boxplots showing the distribution of stomatal conductance (g_s; mol $m^{-2}s^{-1}$) (a), Crop Water Stress Index (CWSI) (b), differential temperature (ΔT) (d), and Soil Water Tension (SWT) (e) across fields 1, 2 and 3 in 2023 and 4 and 5 in 2024.

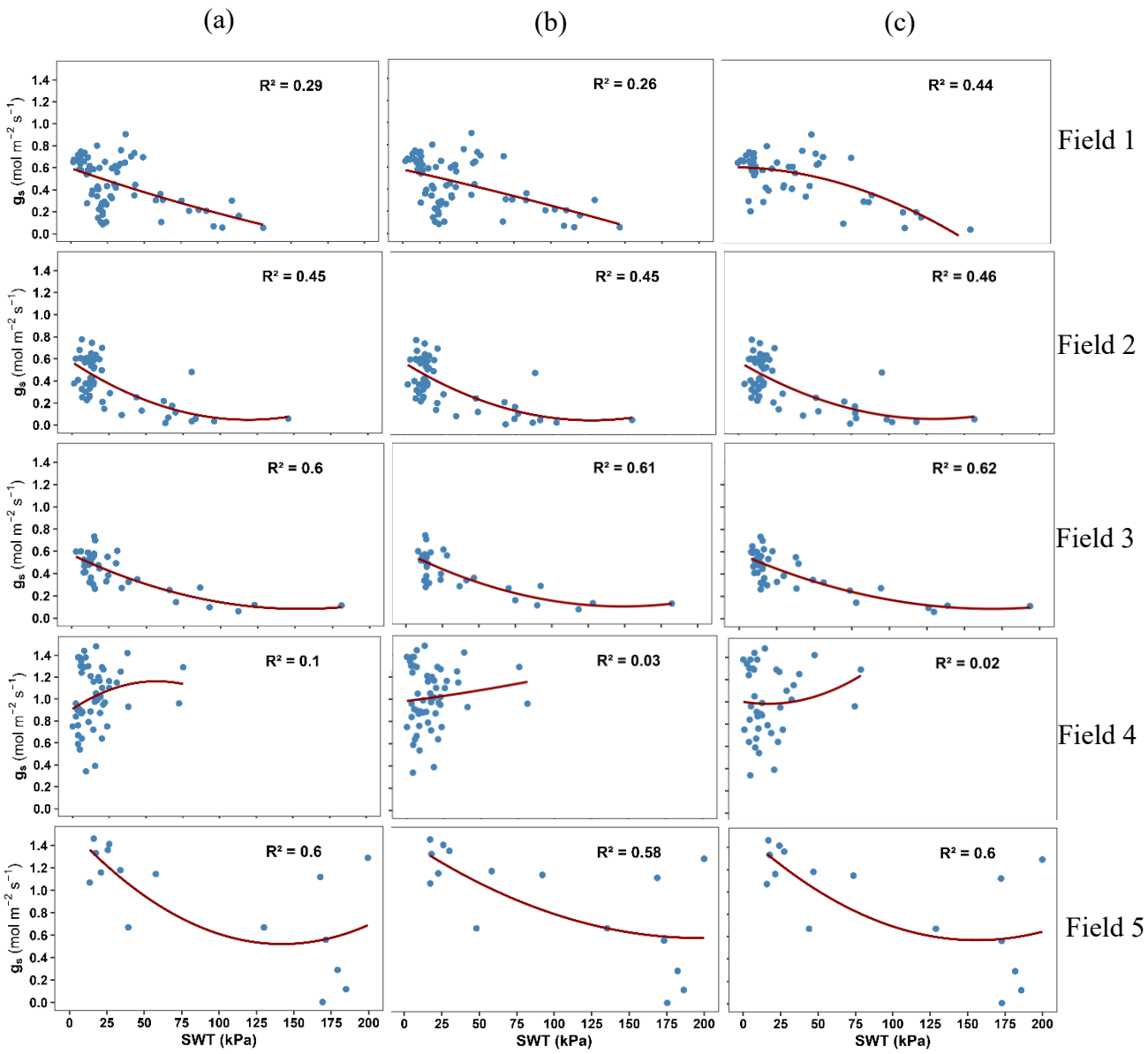

Figure 3.7. Relationship between the stomatal conductance (g_s) and average soil water tension (one day before the sampling day (a), midnight to 6 am of the sampling day (b), and the period of sampling (c).

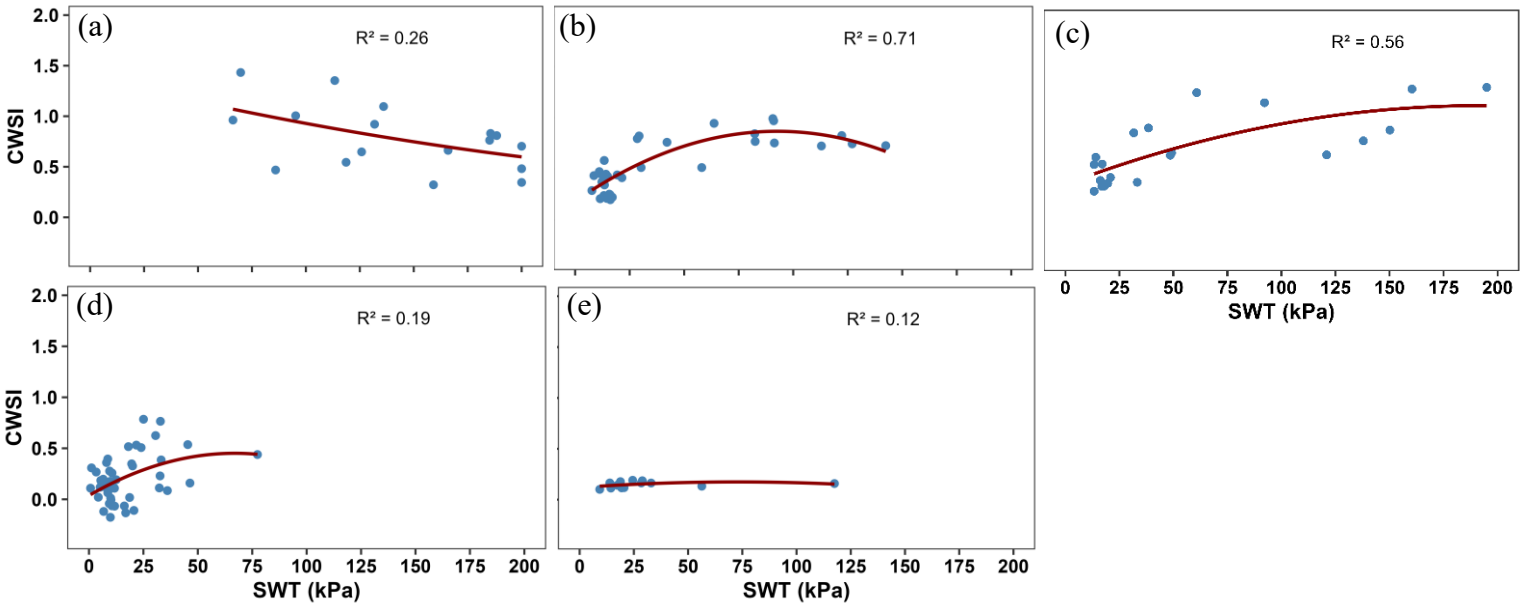

Figure 3.8. Relationships between the crop water stress index (CWSI) based on the theoretical energy balance equation and average soil water tension (SWT) during flight time for fields 1 (a), 2(b) and 3 (c) for 2023 and fields 4 (d) and 5 (e) in the 2024 growing season.

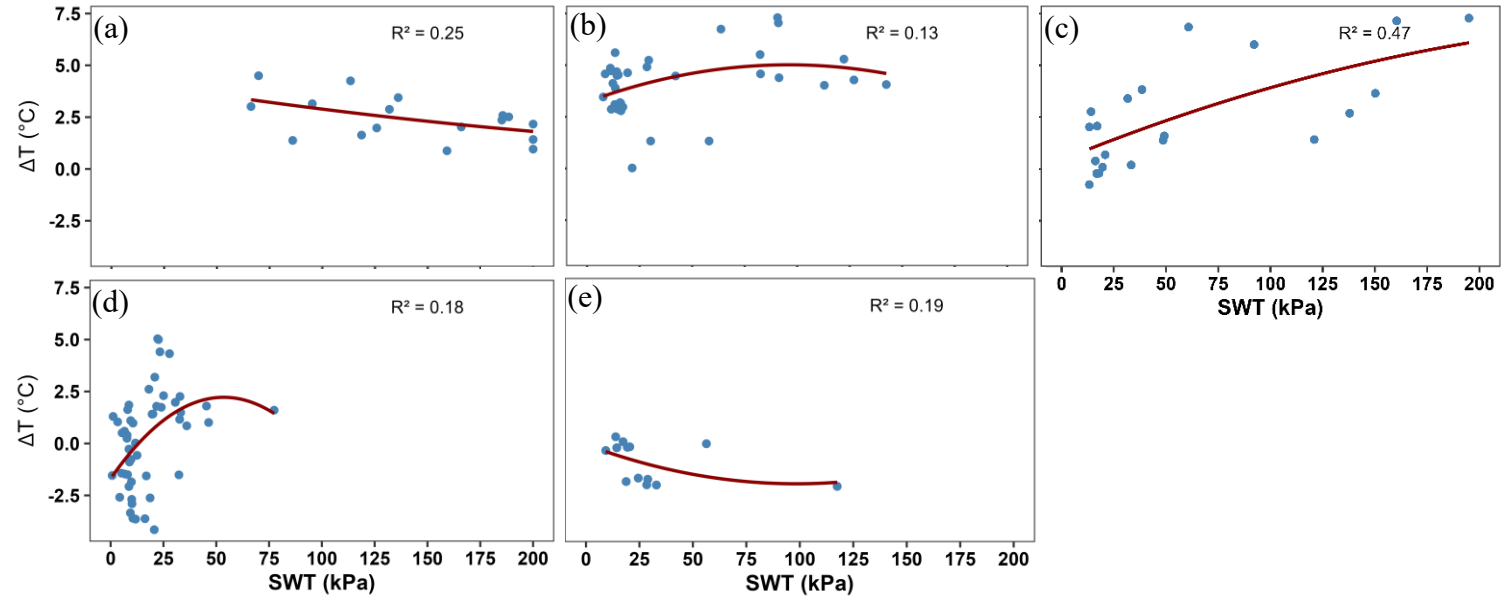

Figure 3.9. Relationships between the differential temperature (canopy temperature – air temperature, ΔT) and average soil water tension (SWT) during flight time for fields 1 (a), 2 (b) and 3 (c) in 2023 and fields 4 (d) and 5 (e) in the 2024 growing season.

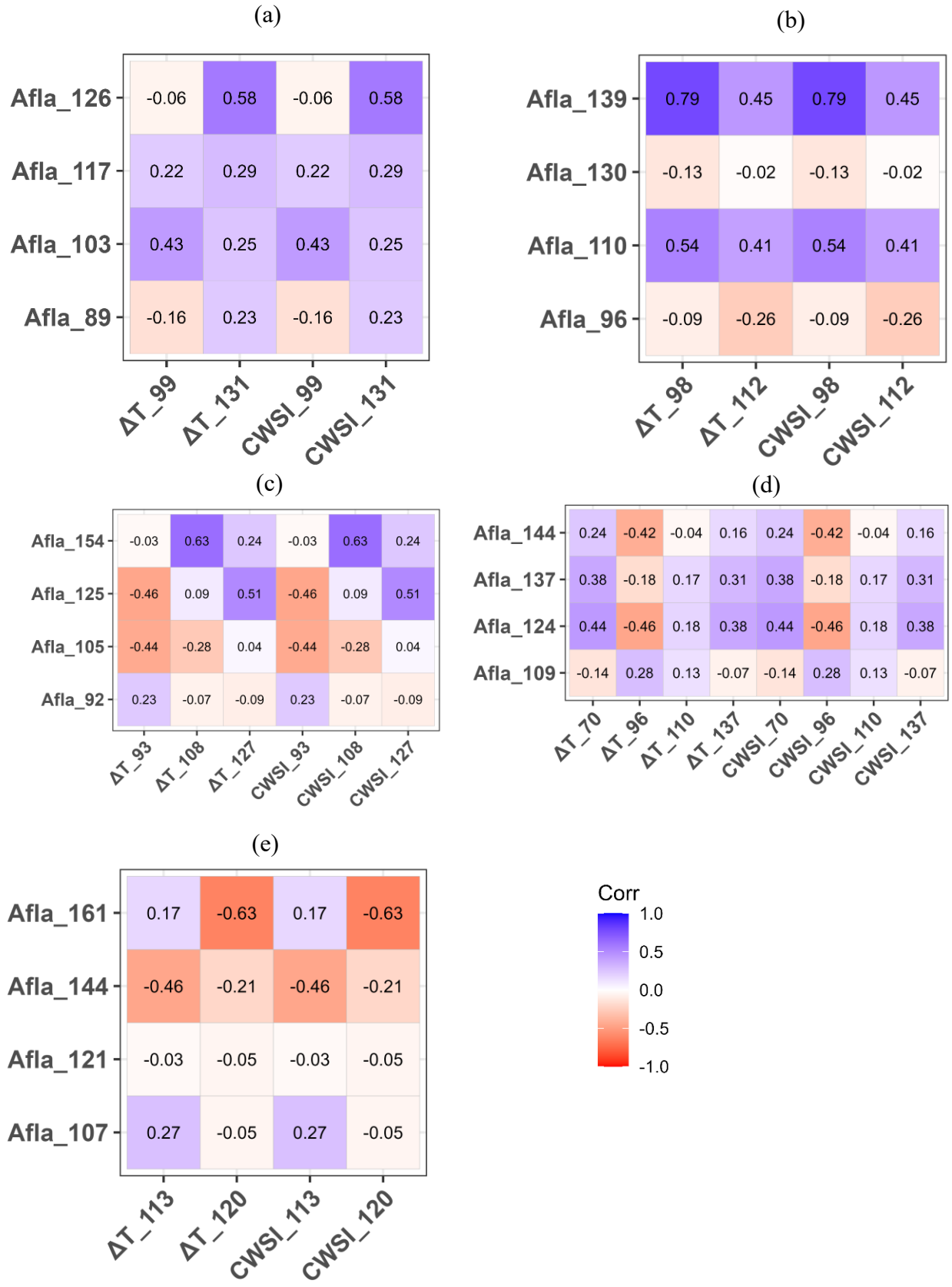

Figure 3.10. Correlation matrices showing the correlations among aflatoxin concentration, crop water stress index (CWSI) and canopy–air temperature differential (ΔT) across fields 1, 2 and 3 (a-c) in 2023, and 4 and 5 fields in 2024 (d,e). All data variables collected more than once during the season is represented by the variable name and days after planting (DAP) of when the data was collected.

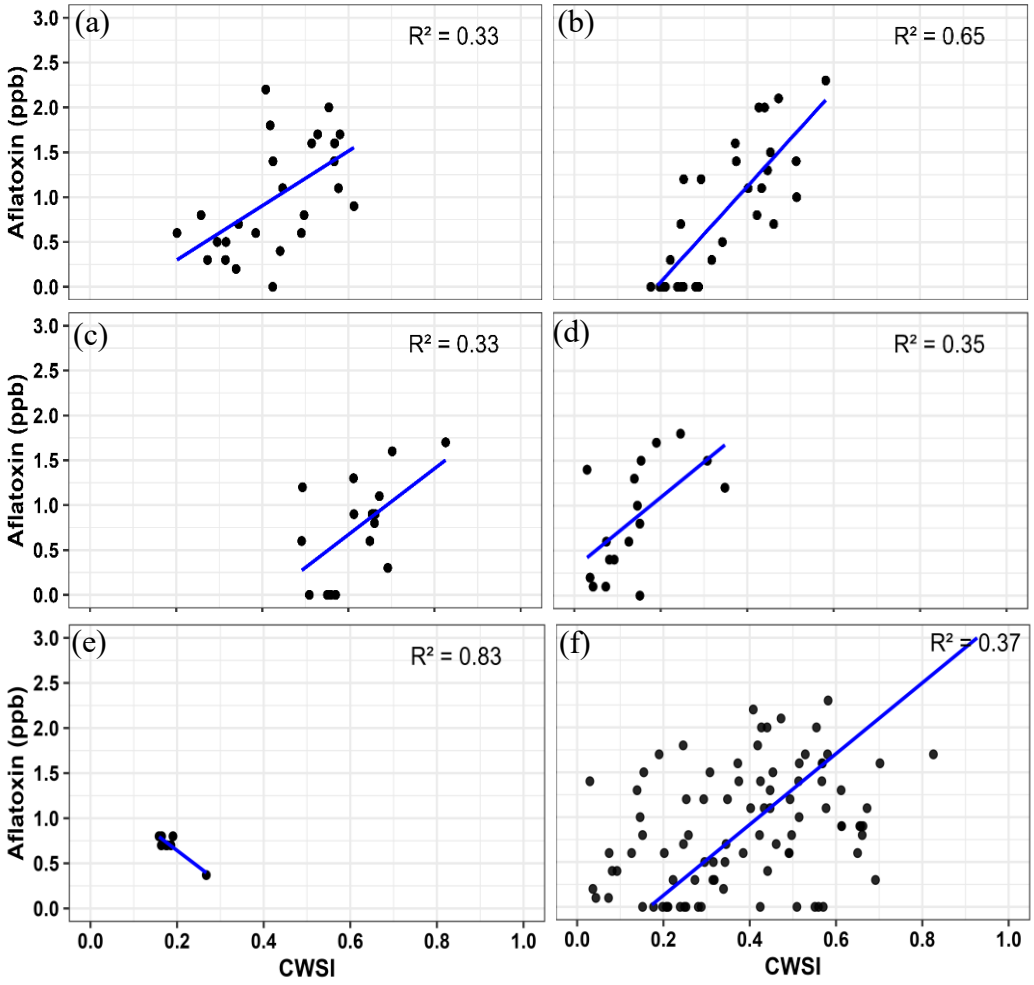

Figure 3.11. Relationship between crop water stress index (CWSI) and aflatoxin levels across fields. Panels (a–c) show field 1 (CWSI at 131 DAP and Aflatoxin level at 126 DAP), field 2 (CWSI at 98 DAP and aflatoxin level at 139 DAP), and field 3 (CWSI at 108 DAP and aflatoxin level at 154 DAP) during the 2023 growing season, while panels (d–e) correspond to field 4 (CWSI at 137 DAP and aflatoxin at 124 DAP) and field 5 (CWSI at 120 DAP and aflatoxin level at 161 DAP) during the 2024 growing season. Panel (f) shows data points from all fields in the 2023/24 growing seasons.

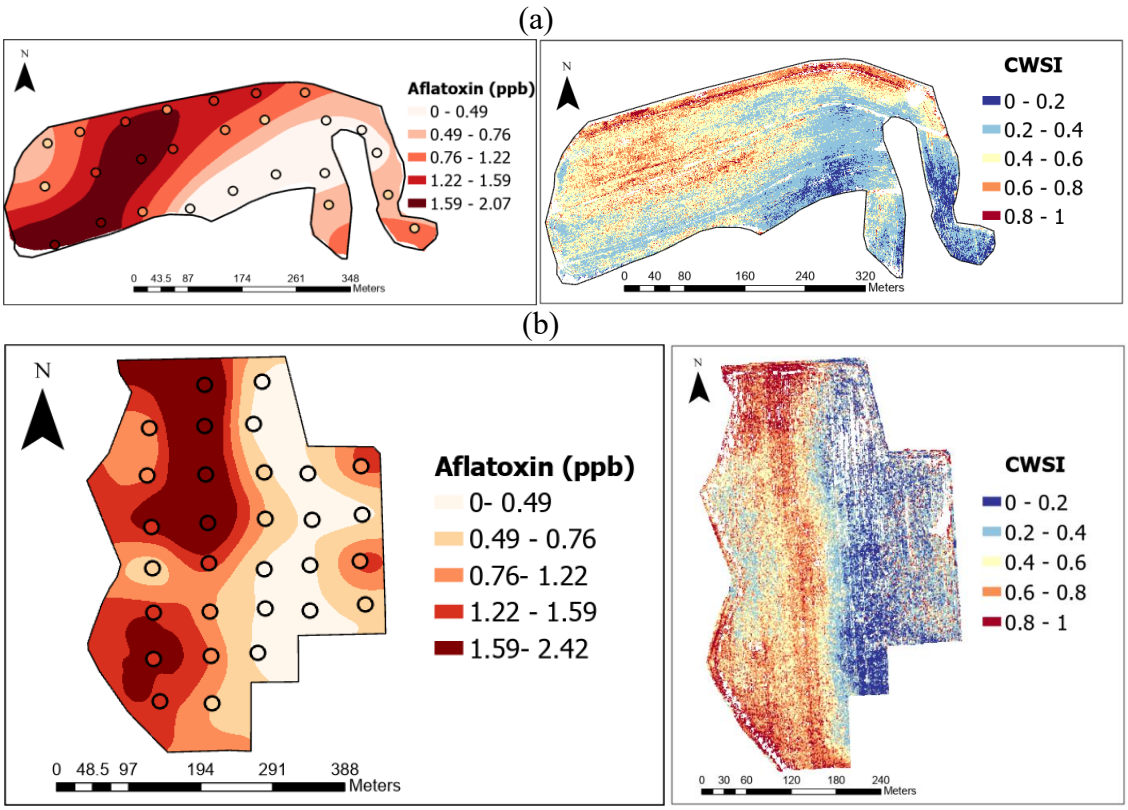

Figure 3.12. Spatial comparison between interpolated aflatoxin contamination risk and crop water stress index (CWSI) maps for Fields 1 (a), and 2 (b). Aflatoxin levels were interpolated using ordinary kriging. Circles represent the aflatoxin results from collected samples, used to create the interpolated maps.

CHAPTER 4

CONCLUSIONS

The main goal of this study was to evaluate how UAS-based thermal images can be used ultimately to better inform growers about crop water status variability and aid in the decision-making process for in-season management strategies. Two studies were conducted in 2025, in two experimental fields, and during 2023 and 2024 in commercial peanut fields in collaboration with growers. Remote sensing platforms can provide an advantage to common methods of crop water monitoring, which is the opportunity to collect data on a large scale, enabling the evaluation of spatial and temporal variability. Stomatal conductance (g_s) is regarded as one of the first plant defense mechanisms to water stress and has been used as a proxy to assess the water status in the field. Peanut plants exposed to drought or water stress close their stomata as a defense mechanism to reduce water loss through transpiration, leading to reduced stomatal conductance. The closure of stomata limits the transpiration cooling and raises the leaf temperature. Furthermore, stressed plants show increased leaf temperature because of the low transpiration.

In the study conducted in the 2025 growing season in Camilla, GA, the effects of irrigation treatments on leaf transpiration, g_s, and canopy temperature (Tc) in peanuts were evaluated. Canopy temperature extracted from the thermal images was used to develop empirical dry and wet baselines for peanuts to calculate crop water stress index (CWSI). Results showed that CWSI was significantly higher in dryland plots and on plots that used higher SWT values to trigger irrigation. Crop responses represented by g_s showed that conductance was significantly reduced in water-stressed plots as compared to other irrigated treatments. Regressions developed between CWSI and g_s showed a strong positive linear relationship in days, in which a higher variability in water stress was observed in the field. However, a comparison between the thermal camera and a high-

accuracy handheld thermal infrared sensor showed that the camera was overestimating temperatures by 1.5°C. As a result, thermal camera-derived CWSI was not as accurate due to a failure of the camera to accurately identify small changes in CWSI when low stress is present. These results are important to validate the use of UAV-based thermal sensors to detect in-season spatial and temporal peanut water stress variability, and to evidence limitations of this system. This study showed that UAV-based thermal cameras can effectively detect water stress when greater variability is present. However, it has accuracy limitations when well-watered conditions are observed across the field.

In the second study conducted in five different commercial peanut fields during the 2023 and 2024 growing seasons, the potential of UAV-based thermal images to assess aflatoxin contamination in peanuts was explored. Positive correlations were found between CWSI and aflatoxin levels, indicating the stress regions are more susceptible to fungus and aflatoxin contamination. Fields that experienced prolonged water deficit during pod development exhibited higher contamination risk, while uniformly wet fields showed no correlations between CWSI and aflatoxin concentrations. Results also showed that CWSI had higher correlations with aflatoxin levels collected at later stages of development, closer to harvest. Nonetheless, the 2023 and 2024 seasons were relatively wet, and only short drought periods were observed for some of the fields, which most likely led to very low aflatoxin contamination levels in these fields.

Overall, the study demonstrated the effectiveness and the limitations of UAS-based thermal sensing as a potential solution for efficient, non-destructive, and scalable methods for monitoring peanut water stress and identifying potential aflatoxin risk zones. The empirical baseline developed here lays the foundation for standardizing CWSI calibration under southeast U.S. growing conditions for peanuts. Using this remote sensing platform can aid farmers in taking more informed

irrigation decisions to meet crop water requirements and to plan for harvest logistics to avoid further contamination post-harvest, to potentially mitigate the risk of aflatoxin contamination development.